UNIVERSITY OF LIVERPOOL

Age Related Changes in Responses to Mechanical Loading in Mice

Thesis submitted in accordance with the requirements of the University of Liverpool for the degree of Doctor in Philosophy

By

Nihad Hameed Dawood

March 2022

Abstract

Bone is the basic unit of vertebrates' skeletal system which serves a variety of important functions, with age bone properties change. Bone modifications may include histological, physiological and genetic modifications that affect mechanical function. As a result of the ageing process the bones become weaker and more prone to fracture.

Osteoporosis is a progressive systemic skeletal disease characterized by low bone mass and micro architectural deterioration of bone tissue, with a consequent increase in bone fragility and susceptibility to fracture. Osteoporosis commonly occurs in humans (mostly women) over age 50, suggesting an age related mechanism is at play.

Previous studies demonstrated that, bone shows mechanical adaptation to loading, characterised by increased bone formation in response to mechanical loading. The exact underlying mechanisms are currently unclear. However osteocytes are the main mechanosensing cells in bone and therefore changes in osteocyte number or activity are highly likely to play a role in the age-related reduced anabolic response to loading.

Sclerostin, the bone morphogenetic protein antagonist which is secreted by osteocytes, acts as an extracellular inhibitor of canonical Wnt signalling pathway and the absence or decrease of sclerostin, revealed an increased in bone mass. Therefore, it is expected to be a key player in bone turnover.

Bone ageing is currently not fully understood, especially the specific changes in bone cell function and gene expression, and the link of these to the known decrease in adaptation to mechanical loading with ageing. To study age related changes in osteoblasts and osteocytes and their response to mechanical loading with ageing, two models were chosen, an *in vivo* model of mechanical loading for the knee and an *in vitro* model of mechanical stretch of primary mouse osteoblasts in two different age groups (young adult, 3 month old and aged adult, 15 month old mice).

The aim of this study is to investigate the effect of two parameters (age and load) on bone through assessing biochemical markers of circulating bone turnover (ELISA) after *in vivo* cyclical loading of mice tibias using 11N force, three times a week for two weeks. Bone volume, thickness and osteocyte numbers were assessed by micro CT image analysis, as well

as immunohistochemistry to quantify sclerostin expression in osteocytes using confocal microscopy. New bone formation was then assessed using fluorescent microscopy, specifically looking at calcein double labelled.

Finally, studying the genetic changes in the two age groups of mice in response to loading by the next generation gene sequencing (RNAseq) and quantitative measurement of polymerase chain reaction (qPCR) for relative expression of top significantly differentially expressed genes seen from the RNAseq study.

The main finding of this study is that aged mice did not respond to mechanical loading as seen in histological analysis. There was no bone formation after *in vivo* mechanical loading in mice tibias, ELISA results for biochemical marker sclerostin, osteocalcin, osteopontin, P1NP and CTX stayed the same between loaded and unloaded mice. Gene expression results showed no effect on stretched aged osteoblasts in *in vitro* loading either. While young mice showed a significant response to mechanical loading in all parameters studied. The most upregulated genes were connected to the transcriptional regulator ATRX gene which encodes the chromatin remodelling protein, and this is linked to the ubiquitin carboxyl-terminal hydrolase 34(Usp34) that removes conjugated ubiquitin from AXIN1 and AXIN2. It can also act as a regulator and activator to the Wnt signalling pathway, which is also upregulated in young osteoblasts. Additionally, the structural genes that encode for the tubulin genes and their products that participate in the formation of microtubules, the structural proteins that participate in cytoskeletal structure, were also upregulated.

Overall, young bone responds to mechanical loading more than aged bone. This is largely due to the reduced osteocyte number in aged bone, which is the main bone cell responsible for mechanosensing.

Acknowledgments

Firstly, I would like to thank the funders of this study, The Iraqi ministry of higher education and scientific research.

A great thank you to my primary supervisor Rob Van T' Hof as I have a substantial amount of appreciation for his teaching, support and guidance.

Significant thanks to my secondary supervisors Blandine Poulet and Anna Daroszewska.

Many appreciative thanks as well to Professor George Bou-Gharios and Dr. Aphrodite Vasilaki for their support and encouragement.

I would also like to thank the lab group members and my colleges for any assistance that they provided me with along the way.

Finally, I would like to give my considerable thanks and gratitude to all my family members; I could have never achieved any of this without their limitless love and support.

List of Figures

List of Tables

Abbreviations

3D	Three-dimensional
Ab	Antibody
ADA3	Alteration/deficiency in activation 3
ATP	Adenosine Triphosphate
AWERB	Animal Welfare and Ethical Review Body
BAM	Binary alignment map
Bglap	Bone gamma-carboxyglutamate protein
BLC	Bone lining cells
BMD	Bone mineral density
BMP	Bone morphogenetic protein
BMU	Basic multicellular unit
BMUs	Basic multicellular units
BRU	Bone remodelling unit
BRUs	Bone remodelling units
BSP-I/II	Bone sialoprotein 1 or 2
cDNA	Complementary DNA
cFMS	Colony-stimulating factor-1 receptor
CLS	Confocal laser scanning
Col1a1	Collagen type 1 alpha 1
CTX	C-terminal telopeptide or carboxy-terminal collagen crosslinks
DC-STAMP	Dendritic cell-specific transmembrane protein
DEXA	Dual-Energy X-ray Absorptiometry
DKK-1	Dikkop gene or protein
DMP1	Dentine matrix protein 1
ELISA	Enzyme-linked immunosorbent assay
FCGR2A	Low affinity immunoglobulin gamma Fc region receptor IIA
FCGR2B	Low affinity immunoglobulin gamma Fc region receptor IIB

FDA	The Food and Drug Administration
FGF23	Fibroblast growth factor 23
Gla OC	Gamma-carboxyglutamate osteocalcin
GO	Gene Ontology
HDFs	Human diploid fibroblasts
HRP	Horseradish peroxidase
IF	Immunofluorescence
IHC	Immunohistochemistry
MAR	Mineral apposition rate
M-CSF	Macrophage colony-stimulating factor
MEPE	Matrix extracellular phosphoglycoprotein
Micro-CT	Micro-computed tomography
MITF	Microphthalmia transcription factor
N-Bps	Nitrogenous-Bisphosphonate
NFATc1	Nuclear factor of activated T-cells, cytoplasmic 1
nN-Bps	Non-Nitrogenous-Bisphosphonate
NO	Nitric oxide
OPG	Osteoprotegerin
Ost	Osteoid
Osx	Osterix
PBM	Peak bone mass
PCP	Planar cell polarity
PHEX	Phosphate-regulating neutral endopeptidase
PML	Promyelocytic leukaemia
PtdIns	Phosphatidylinositol
PTH	Parathyroid hormone
RANKL	Receptor activator of nuclear factor kappa-B ligand
RER	Rough endoplasmic reticulum

RIN	RNA Integrity Number
RNA-seq	RNA sequencing
ROI	Reactive oxygen intermediates
ROS	Reactive oxygen species
SAHF	Senescence-associated heterochromatic foci
SAM	Sequence alignment map
SASP	Senescence associated secretory phenotype
SEM	Scanning electron microscopy
SERMs	Selective estrogen receptor modulators
Serpin	Serine proteinase inhibitor
SFRP	Secreted frizzled-related proteins
SMS	Senescence-messaging secretome
SOST	Sclerostin
TEM	Transmission electron microscopy
TMB	Tetramethylbenzidine
TNF-α	Tumour necrosis factor-α
TPA	Tissue plasminogen activator
TRAP	Tartrate-resistant acid phosphatase
uPA	urokinase
Usp34	Ubiquitin carboxyl-terminal hydrolase 34
µCT	Micro-computed tomography

Contents

Chapter 1. Introduction

1.1. Bone

Bone, a specialized and mineralized connective tissue, makes up, with cartilage, the skeletal system. Bone is the basic unit of vertebrates' skeletal system which constitutes approximately 15 % of the total body weight. Bone provides the framework for the body, supports mechanical movement, protects the dynamic internal organs such as the lungs and the brain, hosts hematopoietic cells within the bone marrow, stores the largest depot of minerals in the body (in total, 99 % of calcium, 85 % of phosphate and 50 % of magnesium are stored in the bones)(1), and maintains iron homeostasis(2), bone also serves an important endocrine function(3).

Morphologically, bones can be classified into flat (e.g. the cranial vault, the scapula and the vertebral lamina), short (e.g. tarsals, carpals and vertebral bodes) and long bones (e.g. femur, tibia and humerus)(4). Flat bones developed from intramembranous ossification while long bones mainly from endochondral ossification (Figure 1.1 A and B).

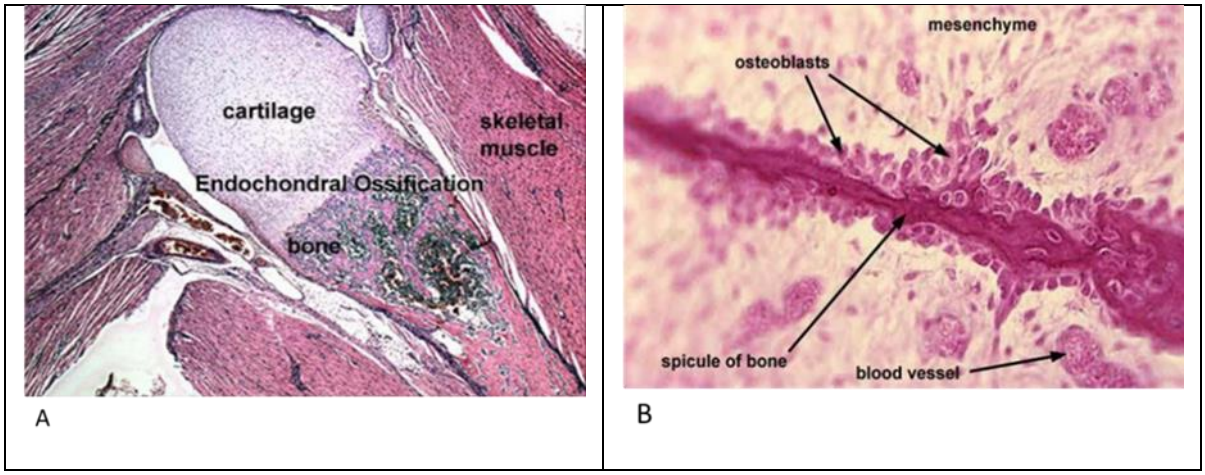

Figure 1.1. A. Endochondral ossification, B. Intramembranous ossification (De Neo, histology of bone and cartilage, 2011).

Anatomically, the long bone consists of two components: The cortical bone which is dense, solid, and surrounds the marrow space called shaft or diaphysis, and the trabecular or cancellous or spongy bone which is composed of trabecular plate network scattered in the

bone marrow section at each end of the shaft called the head or epiphysis. The transitional zone between the diaphysis and the epiphysis called the metaphysis(4). About 80% of the adult human skeleton weight consists of cortical bone(5).

Cortical bone has an outer periosteal and inner endosteal surfaces (Figure 1.2). The periosteum is a fibrous connective tissue sheath that surrounds the outer cortical surface of bone, except at joints where bone is lined by articular cartilage. It contains blood vessels, nerve fibres, osteoprogenetor cells, osteoblasts, and osteoclasts. It protects, nourishes, and aides in bone formation. It plays an important role in apposition growth and fracture repair. The endosteum is lining the inner surface of cortical and cancellous bone, it has a membranous structure and the blood vessel canals (Volkmann's canals) present in it(6).

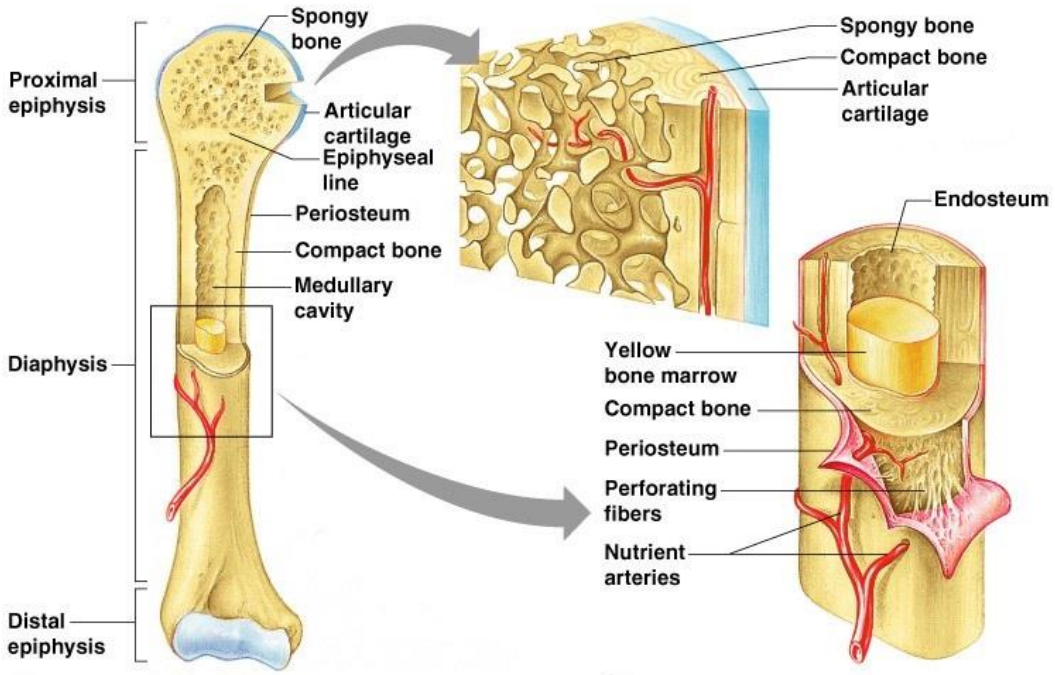

Figure 1.2. Structure of long bone. https://onlinesciencenotes.com/structure-functions-bones/

Histologically, bone can be classified based on the shape of collagen forming osteoid (osteoid is the early formed un-mineralized bone matrix that forms prior to the maturation of bone tissue) into two types, woven bone, which is characterized by a random organization of collagen fibres, and lamellar bone, which is characterized by a regular parallel arrangement of collagen into sheets (lamellae, see figure 1.3). Woven bone is weaker than lamellar bone due to the irregular orientations of collagen fibrils and the absence of lamellar pattern (Figure 1.4). Woven bone is formed when osteoblasts produce osteoid rapidly, mostly in all fetal bones and in fracture healing. Then the resultant woven bone is replaced by a process called remodelling by the deposition of more resilient lamellar bone. Practically all the bone in the healthy mature adult is lamellar bone(7).

Because of its mechanical function, bone requires a certain degree of strength and stiffness. Bone adapts to patterns of loading to avoid fractures caused by repetitive loading at physiologic levels because of its organization as a multiscale material. Following paragraphs contain more explanation for bone composition which gives it specialization.

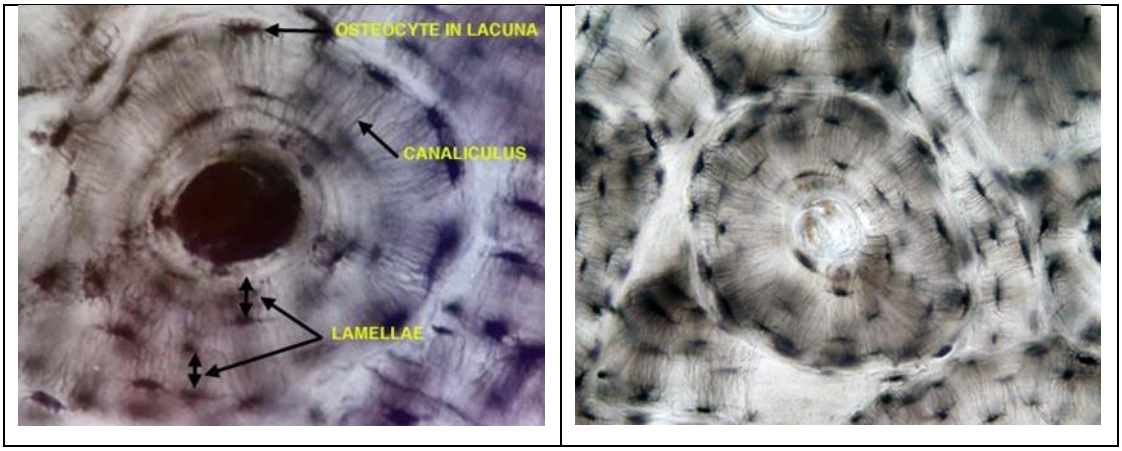

Figure 1.3. Lamellar bone in human showing lamellar sheets https://www.pinterest.com/pin/336503403383623742/

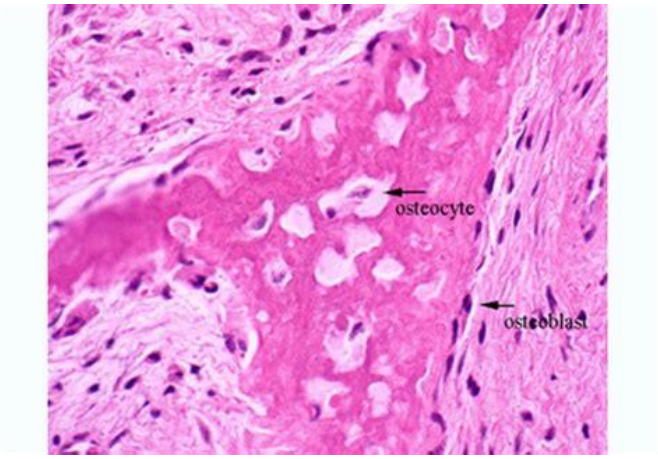

Figure 1.4. Woven bone in human showing lake of arrangement http://medicalschool.tumblr.com/post/13929724453/woven-bone-is-the-primitive-bone-first-laid-down

1.2. Bone Histology:

Bone is like other connective tissues that consists of cells and extracellular matrix. The cells unique to bone are osteoblasts, osteocytes, lining cells and osteoclasts.

1.2.1. Osteoblasts

Osteoblasts are mononuclear, and their shape varies from flat to cuboidal or columnar shape, reproducing their level of cellular activity, in later stages of maturity located along the bone surface, including 4–6 % of the total bone cells(8).

Osteoblasts are responsible for synthesizing the organic components of the bone matrix, including type I collagen, proteoglycans, and glycoproteins. Osteoblasts also synthesize the enzyme alkaline phosphatase, which is needed locally for the mineralization of osteoid(9). Two kinds of osteoblasts are formed differentiation of Osteoprogenitor cells, either mesenchymal osteoblasts, which synthesize woven bone in random orientation (figure 1.5.), or surface osteoblasts, which synthesize bone on surfaces in a well oriented lamellar arrangement (10).

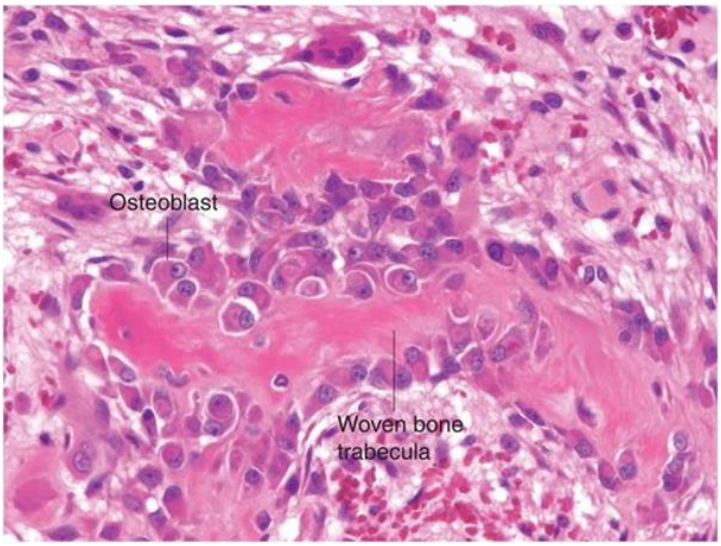

Figure 1.5. Osteoblasts, mononuclear and cuboidal shape on the surface of the woven bone https://radiologykey.com/the-skeleton-structure-growth-and-development-and-basis-of-skeletal-injury/

Osteoblasts are derived from mesenchymal stem cells (MSC) (Figure 1.6). That requires the expression of specific genes, and programmed steps, including the synthesis of bone morphogenetic proteins (BMPs) and members of the Wingless (Wnt) pathways(11).

Osteoblast progenitors expressing Runx2 and ColIA1 genes during osteoblast differentiation in the proliferation phase. In this phase, osteoblast progenitors show alkaline phosphatase (ALP) activity, and are considered pre osteoblasts (8). Pre osteoblasts change to mature osteoblasts (large and cuboidal) by increase the expression of Osterix and the secretion of bone matrix proteins such as osteocalcin, bone sialoprotein (BSP) I/II, and collagen type I (12).

Two main steps take place during the synthesis of bone matrix by osteoblasts: deposition of organic matrix and then its mineralization. In the first step, the osteoblasts secrete collagen proteins, mainly type I collagen, non-collagen proteins (osteocalcin, osteonectin, BSP II, and osteopontin), and proteoglycan including decorin and biglycan, which form the organic matrix. Thereafter, mineralization of bone matrix takes place into two phases: the vesicular and the fibrillar phases (13).

The vesicular phase starts when portions of vesicles with diameters ranging from 30 to 200 nm, called matrix vesicles, are released from the apical membrane area of the osteoblasts into the newly formed bone matrix in which they bind to proteoglycans and other organic

components. Because of its negative charge, the sulphated proteoglycans immobilize calcium ions that are stored within the matrix vesicles (14). Osteoblasts secrete enzymes that degrade the proteoglycans, to release the calcium ions from the proteoglycans, then these ions cross the Calcium channels existing in the matrix vesicles membrane. These channels are formed by proteins called annexins (13). Osteoblasts also secrete alkaline phosphatase (ALP) to degrade the phosphate-containing compounds and release phosphate ions inside the matrix vesicles. Then, the phosphate and calcium ions inside the vesicles combine, forming the hydroxyapatite crystals (15).

The fibrillar phase starts when the calcium and phosphate ions inside the matrix vesicles supersaturated leads to the breakdown of these structures and the hydroxyapatite crystals spread to the surrounding matrix (16). At this stage, the mature osteoblasts can undergo apoptosis or become osteocytes or bone lining cells, however, the mechanisms responsible for the osteoblasts fate are not known (17). Osteoblasts contact their neighboring osteoblasts cytoplasmically. Osteoblasts do not divide. They give rise to osteocytes, remain as osteoblasts, or return to the state of osteoprogenitor cells from which they derived.

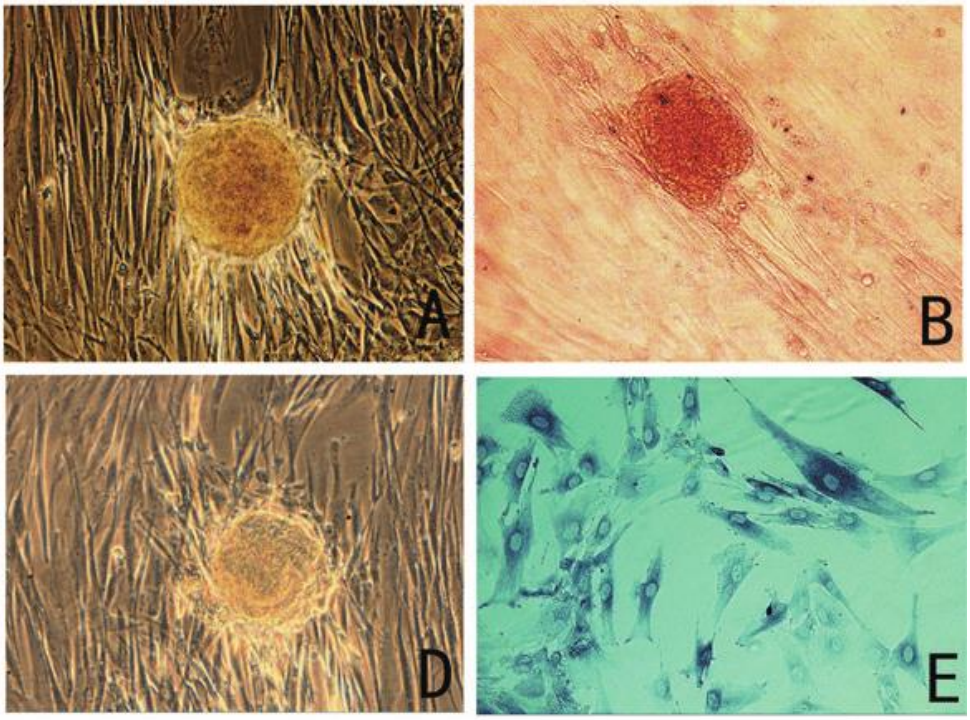

Figure 1.6. Differentiation of human umbilical cord – mesenchymal stem cells (HUC-MSCs) into osteoblasts in vitro. (A, D) Morphology of hUC-MSCs cultured in osteogenic medium for 21 days. (B, E) In vitro differentiation of hUC-MSCs into osteoblasts, were shown by positive alizarin red (B) and ALP staining (E) of calcified extracellular matrix. Scale bar: 100 mm. doi:10.1371/journal.pone.0064000.g006

https://www.researchgate.net/figure/Differentiation-of-hUC-MSCs-into-osteoblasts-in-vitro-A-D-Morphology-of-hUC-MSCs_fig26_236978569

1.2.2. Osteoclasts

Osteoclasts are large multinucleated cells, rest directly on a shallow bay called a resorption bay resulting from its activity on the resorbed bone tissue (Figure 1.7). Osteoclasts can be recognized as acidophilic large size cells which display a strong histochemical reaction for acid phosphatase due to containing of numerous lysosomes. One of these enzymes, the 35-kilodalton iron-containing tartrate-resistant acid phosphatase (TRAP), which is used clinically as a marker of osteoclast activity and differentiation(18).

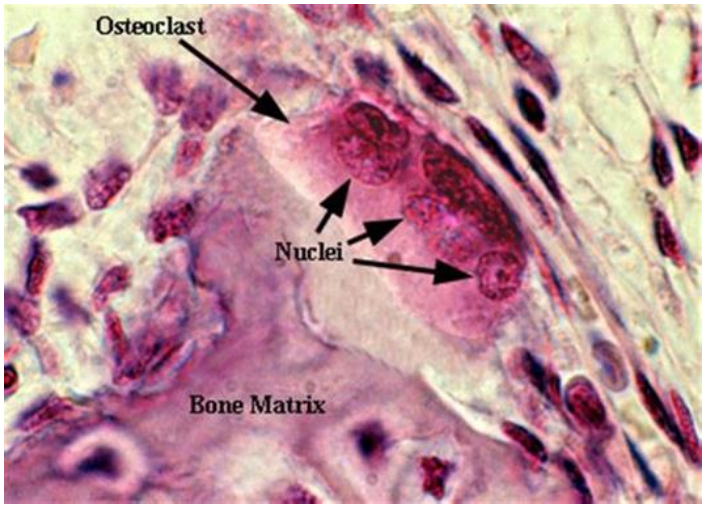

Figure 1.7. Osteoclast. Represent multinuclear cell larger than other cells.

http://www.pathologyoutlines.com/topic/bonemarrowosteoclasts.html

Osteoclasts originate from mononuclear cells of the hematopoietic stem cell lineage which terminally differentiated multinucleated cells (figure 1.8) under the influence of several factors. Among these factors the macrophage colony-stimulating factor (M-CSF), secreted by Osteoprogenitor mesenchymal cells and Osteoblasts(19), and RANK ligand, secreted by osteoblasts, osteocytes, and stromal cells(20). These factors together promote the activation of transcription factors and gene expression in osteoclasts. M-CSF binds to its receptor (Colony-stimulating factor-1 receptor (cFMS)) present in osteoclast precursors, which stimulates their proliferation and inhibits their apoptosis(21).

The receptor activator of nuclear factor kappa-B ligand (RANKL) is a key factor for osteoclastogenesis and is expressed by osteoblasts, osteocytes, and stromal cells. When it binds to its receptor RANK in osteoclast precursors, osteoclast formation is induced(22). On the other hand, another factor called osteoprotegerin (OPG), which is produced by a wide range of cells including osteoblasts, stromal cells, and gingival and periodontal fibroblasts, binds to RANKL, preventing the RANK/RANKL interaction and, consequently, inhibiting the osteoclastogenesis(23). Thus, the RANKL/RANK/OPG system is a key mediator of osteoclastogenesis.

The RANKL/RANK interaction also promotes the expression of other osteoclastogenic factors such as NFATc1 and Dendrocyte Expressed Seven Transmembrane Protein (DC-STAMP). By

interacting with the transcription factors PU.1, cFos, and MITF, NFATc1 regulates osteoclast specific genes including TRAP and cathepsin K, which are crucial for osteoclast activity(24). Under the influence of the RANKL/RANK interaction, NFATc1 (NFATc1 gene encodes Nuclear factor of activated T-cells, cytoplasmic 1 protein) also induces the expression of DC-STAMP, which is crucial for the fusion of osteoclast precursors(25). During bone remodelling osteoclasts polarize; then, four types of osteoclast membrane domains can be detected: the sealing zone and ruffled border that are in contact with the bone matrix, as well as the basolateral and functional secretory domains, which are not in contact with the bone matrix(26,27).

Polarization of osteoclasts during bone resorption involves rearrangement of the actin cytoskeleton, in which an F-actin ring that comprises a dense continuous zone of highly dynamic podosome is formed and consequently an area of membrane that develop into the ruffled border is isolated. Interestingly, these domains are only formed when osteoclasts are in contact with extracellular mineralized matrix, The attachment process of the osteoclast podosomes to the bone surface mediated via integrin, as well as the CD44(28,29).

Ultra-structurally, the ruffled border is a membrane domain formed by microvilli, which is isolated from the surrounded tissue by the clear zone or sealing zone. The clear zone is an area empty of organelles located in the periphery of the osteoclast adjacent to the bone matrix(29). This sealing zone is formed by an actin ring and some other proteins, including actin, talin, vinculin, paxillin, tensin, and actin-associated proteins such as α-actinin, fimbrin, gelsolin, and dynamin. The -integrin binds to non-collagenous bone matrix containing-RGD sequence(consists of Arginine, Glycine, and Aspartate) such as bone sialoprotein, osteopontin, and vitronectin, forming a peripheral sealing that restricts the central region, where the ruffled border is situated (29).

The osteoclast activity depends on the ruffled border preservation, which formed due to powerful transferring lysosomes and endosomes. The ruffled border have a vascular-type H^+-ATPase (V-ATPase), which helps to acidify the resorption bay and enables hydroxyapatite crystals dissolution(29). In this region, protons and enzymes, such as tartrate-resistant acid phosphatase (TRAP), cathepsin K, and matrix metalloproteinase-9 (MMP-9) are transported into a compartment called How ship lacuna leading to bone degradation. The products of this

degradation are then endocytosed across the ruffled border and transcytosed to the functional secretory domain at the plasma membrane (27).

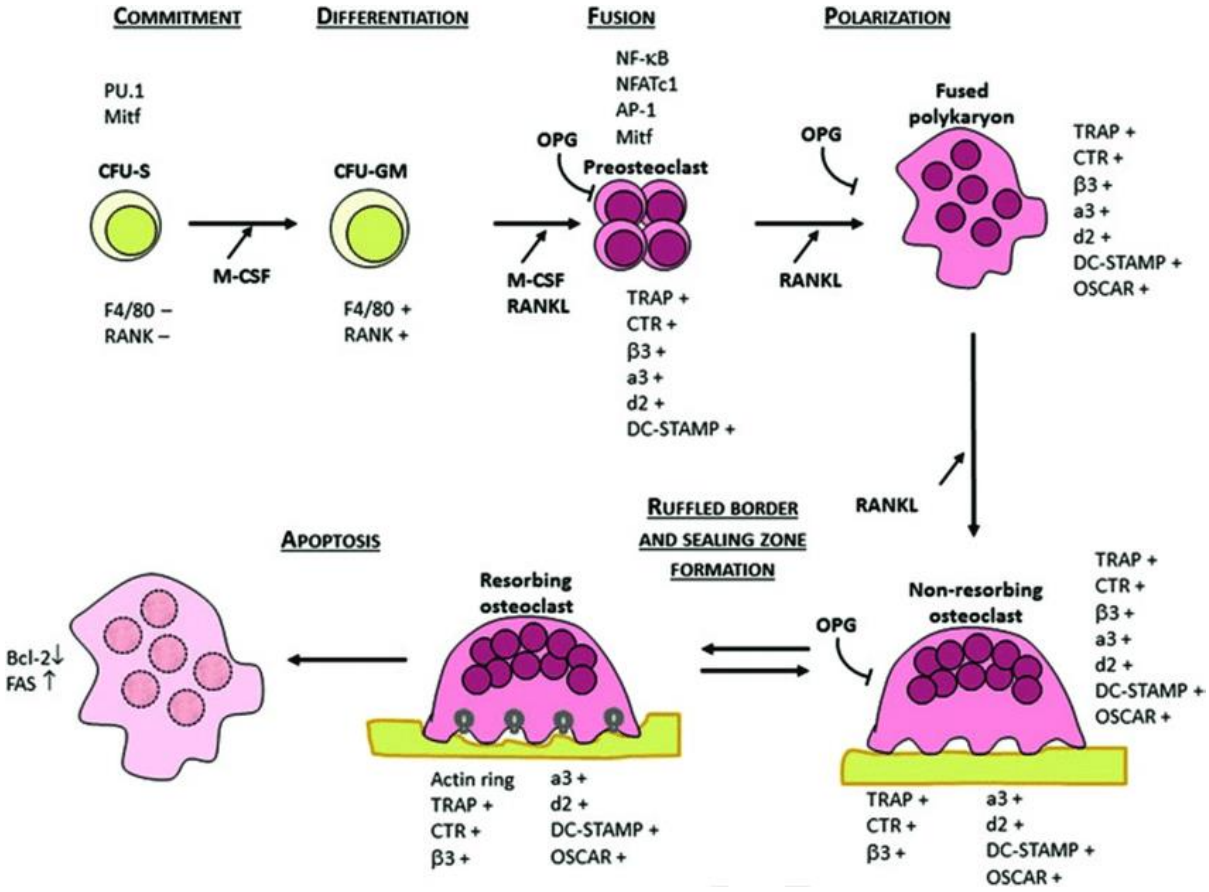

Figure 1.8. Osteoclastogenesis. (Adapted from Boyle et al. [69]). In the presence of M-CSF and RANKL, osteoclast precursors undergo differentiation and fusion. Transcription factors are listed above the cells; key functional proteins are listed below the cells. To regulate osteoclast formation and function, osteoblasts and stromal cells secrete OPG, a decoy receptor for RANKL.

https://www.researchgate.net/profile/Irina_Voronov/publication/328123188/figure/download/fig1/AS:761453405544449@1558556047276/Osteoclastogenesis-adapted-from-Boyle-et-al-69-In-the-presence-of-M-CSF-and-RANKL.png

Abnormal increase in osteoclast formation and activity leads to some bone diseases such as osteoporosis, where resorption exceeds formation causing decreased bone density and

increased bone fractures (30). In some pathologic conditions including bone metastases and inflammatory arthritis, abnormal osteoclast activation results in periarticular erosions and painful osteolytic lesions, respectively.

On the other hand, in osteopetrosis, which is a rare bone disease, genetic mutations that affect formation and resorption functions in osteoclasts lead to decreased bone resorption, resulting in a disproportionate accumulation of bone mass(30). These diseases demonstrate the importance of the normal bone remodelling process for the maintenance of bone homeostasis.

Furthermore, there is evidence that osteoclasts display several other functions. For example, it has been shown that osteoclasts produce factors called clastokines that control osteoblast during the bone remodelling cycle. Other recent evidence is that osteoclasts may also directly regulate the hematopoietic stem cell niche(30). These findings indicate that osteoclasts are not only bone resorbing cells, but also a source of cytokines that influence the activity of other cells.

1.2.3. Osteocytes

Osteocytes, comprise 90–95% of the total bone cells, are the most abundant and long-lived cells, with up to 25 years lifespan(30). Unlike osteoblasts and osteoclasts, which have been defined by their own functions during bone formation and bone resorption, osteocytes were formerly defined by their morphology and location. For years, due to difficulties in isolating osteocytes from bone matrix led to the inaccurate view that these cells would be inactive cells, and their functions were misunderstood(31). The development of new technologies such as the identification of osteocyte-specific markers, new animal models, development of techniques for bone cell isolation and culture, and the establishment of phenotypically stable cell lines led to the improvement of the understanding of osteocyte biology. In fact, it has been recognized that these cells play several important functions in bone(30).

The osteocytes are located within lacunae surrounded by mineralized bone matrix, wherein they show a dendritic morphology(31), (Figures A and B). The morphology of embedded osteocytes differs depending on the bone type. For instance, osteocytes from trabecular bone

are more rounded than osteocytes from cortical bone, which display an elongated morphology(32).

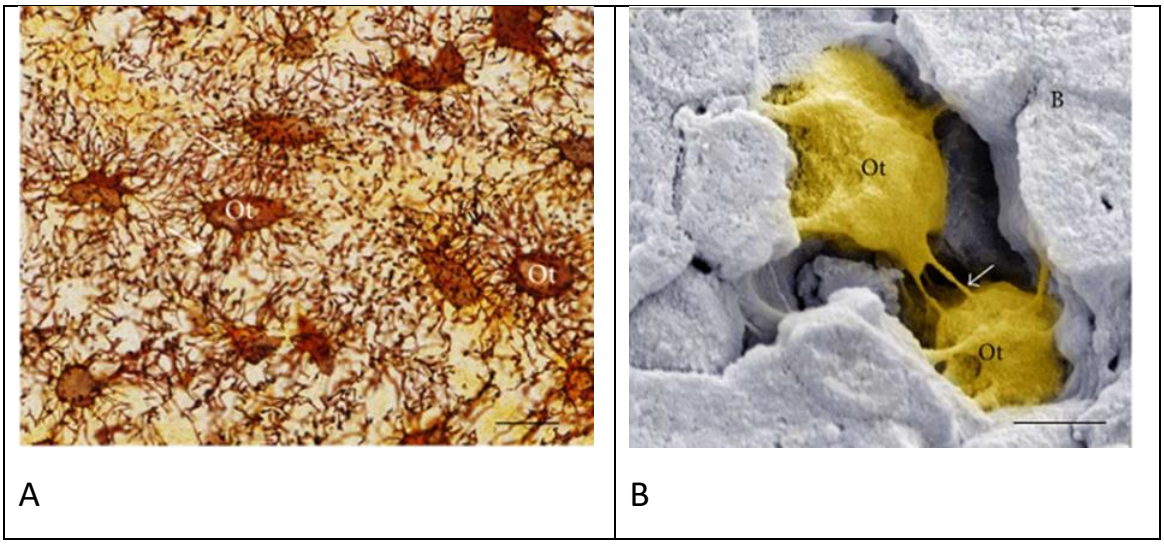

Figure 1.9. Osteocytes: Light (A) and electron (B) micrographs of slices of alveolar bone rats. (A) Section subjected to the silver impregnation method. Note the cytoplasmic processes (arrows) of the osteocytes (Ot) connecting with each other. Scale bar: 15 µm. (B) Scanning electron micrograph showing two osteocytes (Ot) surrounded by bone matrix (B). Note that the cytoplasmic processes (arrows) are observed between the osteocytes (Ot) forming an interconnected network. Scale bar: 2 µm (33).

Osteocytes are derived from MSCs lineage through osteoblast differentiation (as mentioned in the last paragraph of section 2.1.1). In this process, four recognizable stages have been suggested: osteoid-osteocyte (the surface osteoblasts), preosteocyte (the embedding osteoid osteocyte), young osteocyte (early mineralizing osteocytes), and mature osteocyte(17). At the end of a bone formation cycle, a subpopulation of osteoblasts becomes osteocytes incorporated into the bone matrix. This process is accompanied by conspicuous morphological and ultrastructural changes, including the reduction of the round osteoblast size. The number of organelles such as rough endoplasmic reticulum and

Golgi apparatus decreases, and the nucleus-to-cytoplasm ratio increases, which correspond to a decrease in the protein synthesis and secretion(34).

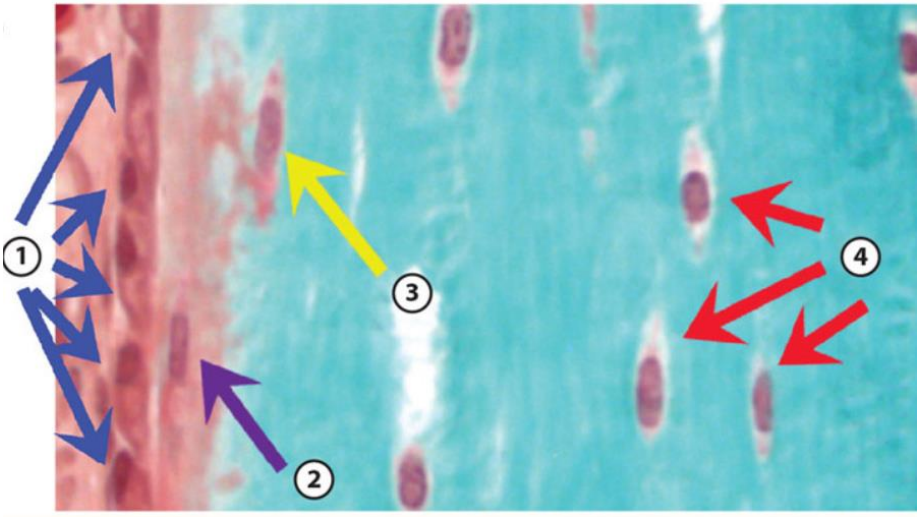

Figure1.10. The Goldner-stained bone section shows marrow, the surface osteoblasts (①), the embedding osteoid osteocyte (②), early mineralizing osteocytes (③), and mature osteocytes (④) (35).

During osteoblast/osteocyte transition, cytoplasmic process starts to emerge before the osteocytes have been encased into the bone matrix (8). The mechanisms involved in the development of osteocyte cytoplasmic processes are not well understood. However, the protein E11/gp38, also called podoplanin may have an important role. E11/gp38 is highly expressed in embedding or recently embedded osteocytes, similarly to other cell types with dendritic morphology such as podocytes, type II lung alveolar cells, and cells of the choroid plexus (36).

It has been suggested that E11/gp38 uses energy from GTPase activity to interact with cytoskeletal components and molecules involved in cell motility, whereby regulate actin cytoskeleton dynamics (37,38). Accordingly, inhibition of E11/gp38 expression in osteocyte-like MLO-Y4 cells has been shown to block dendrite elongation, suggesting that E11/gp38 is implicated in dendrite formation in osteocytes (36). A number of markers have been identified that are differentially expressed during osteocyte differentiation process such as Cbfa1/Runx2, Osx, Alp, Col1a1, and Bglap). Once the stage of mature osteocyte totally entrapped within mineralized bone matrix is accomplished, several of the previously expressed osteoblast markers such as OCN, BSPII, collagen type I, and ALP are downregulated.

On the other hand, osteocyte markers including dentine matrix protein 1 (DMP1), Phosphate-regulating neutral endopeptidase (PHEX) and E11 are highly expressed for early osteocyte and RANKL, Sclerostin (SOST), fibroblast growth factor 23 (FGF23), and matrix extracellular phosphoglycoprotein (MEPE) for mature osteocytes (35,39,40).

Whereas the osteocyte cell body is located inside the lacuna, its cytoplasmic processes (up to 50 per each cell) cross tiny tunnels that originate from the lacuna space called canaliculi, forming the osteocyte lacuna-canalicular system (41) (Figures 1.9 A and B). These cytoplasmic processes are connected to other neighbouring osteocytes processes by gap junctions, as well as to cytoplasmic processes of osteoblasts and bone lining cells on the bone surface, facilitating the intercellular transport of small signalling molecules such as prostaglandins and nitric oxide among these cells. In addition, the osteocyte lacuna-canalicular system is in close proximity to the vascular supply, whereby oxygen and nutrients can reach osteocytes(42).

It has been estimated that osteocyte surface is 400-fold larger than that of the all Haversian and Volkmann systems and more than 100-fold larger than the trabecular bone surface (43). The cell-cell communication is also achieved by interstitial fluid that flows between the osteocytes processes and canaliculi (43). By the lacunocanalicular system, the osteocytes act as mechanosensors as their interconnected network has the ability to detect mechanical pressures and loads, thus it can help the adaptation of bone to daily mechanical forces (31). By this way, the osteocytes seem to act as orchestrators of bone remodeling, through regulation of osteoblast and osteoclast activities (44). Moreover, osteocyte apoptosis has been recognized as a chemotactic signal to osteoclastic bone resorption(45–48). In agreement, it has been shown that during bone resorption, apoptotic osteocytes are surrounded by osteoclasts (49–51).

The mechanosensitive function of osteocytes is talented due to the strategic location of these cells within bone matrix. Thus, the shape and spatial arrangement of the osteocytes are in agreement with their sensing and signal transport functions, sponsoring the translation of mechanical stimuli into biochemical signals, a phenomenon that is called piezoelectric effect(52). The mechanisms and components by which osteocytes convert mechanical stimuli to biochemical signals are not well known. However, two mechanisms have been proposed. One of them is that there is a protein complex formed by a cilium and its associated proteins PolyCystins 1 and 2, which has been suggested to be crucial for osteocyte mechanosensing

and for osteoblast/osteocyte-mediated bone formation (53). The second mechanism involves osteocyte cytoskeleton components, including focal adhesion protein complex and its multiple actin-associated proteins such as paxillin, vinculin, talin, and zyxin (54). Upon mechanical stimulation, osteocytes produce several secondary messengers, for example, Adenosine triphosphate (ATP), nitric oxide (NO), Ca^{2+}, and prostaglandins (PGE_2 and PGI_2,) which influence bone physiology (55,56). Independently of the mechanism involved, it is important to mention that the mechanosensitive function of osteocytes is possible due to the intricate canalicular network, which permits the communication among bone cells.

As osteocytes are multifunctional, critically essential cells, the major aim in healthcare research is to keep osteocytes alive and healthy, especially with aging. With aging, osteocyte death is accelerated, mainly through apoptosis leaving empty lacunae that can fill in with mineral, a process called micropetrosis. Micropetrosis may work as a compensatory mechanism in aged bone by removing the empty lacunae which can play as a stress concentrator if left open. Osteocytes can also undergo programmed cell death, especially in the existence of micro damage, which stimulates the release of chemical signals for osteoclasts to remodel the damaged bone (57).

1.2.4. Bone Lining Cells

Bone lining cells are inactive flat-shaped osteoblasts that cover the bone surfaces, where neither bone resorption nor bone formation is occur. These cells have a thin and flat shape nucleus, its cytoplasm shows few cytoplasmic organelles such as rough endoplasmic reticulum and Golgi apparatus (58) (Figure 1.10). Some of these cells show processes extending into canaliculi, and gap junctions are also detected between adjacent bone lining cells and between these cells and osteocytes (59).

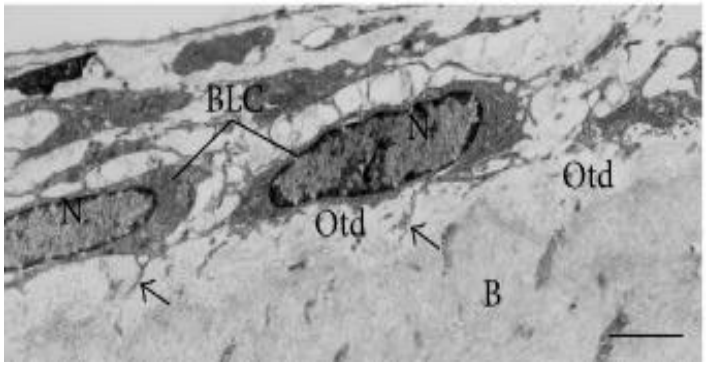

Figure 1.11. Bone lining cells (BLC) showing limited cytoplasm are situated on the osteoid surface (Otd). BLC extend some thin cytoplasmic projections (arrows) towards the osteoid (Otd). Scale bar: 2 µm. N: nucleus. (33).

The secretory activity of bone lining cells depends on the bone physiological status, thus their secretory activity may reacquire to enhance their size and become cuboidal shape(59). Bone lining cells functions are not completely understood, but it has been shown that these cells prevent the direct interaction between osteoclasts and bone matrix, when bone resorption should not happen, and also participate in osteoclast differentiation, by producing OPG and the RANKL (60,61). Moreover, the bone lining cells is one of the important component of the bone multicellular units (BMU) that present during the bone remodelling cycle (62).

1.2.5. Bone matrix:

The mature bone matrix distinguishes bone from other connective tissues by its mineralisation which produces an extremely hard tissue capable of providing support and protection. The mineral is calcium phosphate in the form of hydroxyapatite crystals [Ca10 (PO4)6(OH) 2].

In addition to the support and protection function, bone plays an important role in the homeostatic regulation of blood calcium levels. By phosphate and calcium mobilization from the matrix to the blood to maintain the right needed levels(63).

The main function of extracellular matrix is not only occupying the cells which are responsible for its synthesis and maintenance, but it has also an influence on the cellular functions.

The interaction between cells and matrix mediated by specific cell receptors and cell binding epitopes that play an important rule to regulate or promote cellular differentiation and gene

expression levels. An additional influence of the extracellular matrix on morphogenesis and cellular metabolism can be recognised by the storage and release of growth factors which is modulated by their binding to specific matrix components(64).

The bone matrix composed of a scaffold of interwoven collagen fibres within hydroxyapatite crystals, associated with it other non-collagenous proteins.

The major structural component of bone matrix is collagen which composed about 90% of the total weight of the bone matrix proteins, mostly collagen type I (about 80% of the collagen fibres) then type V collagen and a little amounts of other types such as type III, XI, and XIII collagens(22).

Each collagen fibre consist of collagen fibrils in variable dimeters and sizes depend on different location and stage of development. The collagen molecule measures about 300 nm long and 1.5 nm thick and has a head and a tail. Within each fibril, the collagen molecules line up head to tail in overlapping rows with a gap between the molecules in each row and a one-quarter-molecule stagger between adjacent rows. The strength of the fibril is created by the covalent bonds between the collagen molecules of adjacent rows (63).

Collagen type I is a large molecule (MW >300 000 Da) with a trimeric helical structure. Type I collagen is initially synthesized in the rough endoplasmic reticulum (RER) as a precursor molecule (type I procollagen) that combines two proα1 (I) and one proα2 (I) peptide chains (encoded by COL1A1 and COL1A2 genes, respectively) in a triple helix of 1014 amino acids composed of un-interrupted Gly-X-Y tripeptide replicates (Gly is glycine and X and Y are proline or lysine), bordered by propeptides at both N- and C-terminal ends. During and after translation, the three chains undergo extensive modification. All Y-position proline residues convert to 4-hydroxyproline by Prolyl-4-hydroxylase, this modification is essential for thermal stability of the trimeric composition (the individual chains unfold from the stable triple helix melt at about 27°C, whereas with hydroxylation, the melting temperature is about 42°C). Some Y-position lysine residues within the triple helical domain are hydroxylated by the enzyme lysyl hydroxylase-1, and glucose and galactose groups added by glycosyltransferases. Hydroxylation of these triple helical residues is to form stable intermolecular complex that provide the flexible strength in tissues(5).

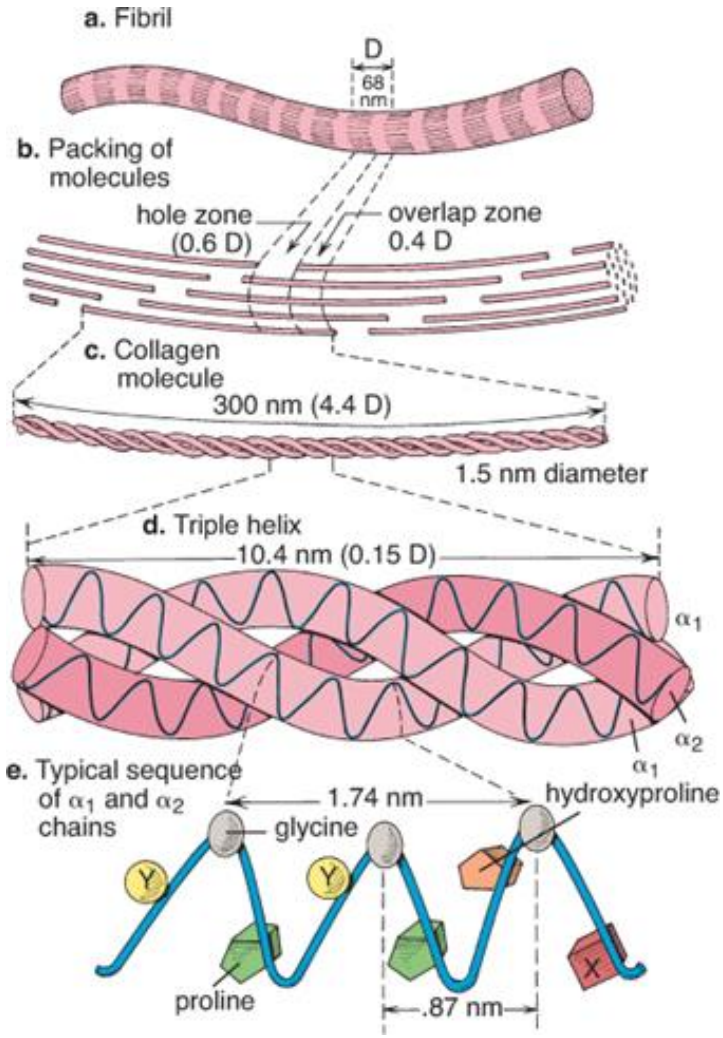

Figure 1.12. Diagram showing the molecular character of a type 1 collagen fibril in increasing order of structure. **a.** A collagen fibril displays periodic banding with a distance (D) of 68 nm between repeating bands. **b.** Each fibril is composed of staggered collagen molecules. **c.** Each molecule is about 300 nm long and 1.5 nm in diameter. **d.** The collagen molecule is a triple helix. **e.** The triple helix consists of three α chains. Every third amino acid of α chain is a glycine. The X position following glycine is frequently a proline, and the Y position preceding the glycine is frequently a hydroxyproline.(63).

The trimeric three chains interacting through the carboxyl-terminal propeptide regions of each chain. These regions start to fold and begin to develop the formation of the triple helix while the whole chain still unfolded. Many enzymes and molecular chaperones involved the folding and trimerization process, such as peptidyl disulfide isomerase (PDI), which is part of

the prolyl 4-hydroxylase complex also, and prolyl peptidyl cis-trans isomerase B (which called cyclophilin B). This protein assist the folding around prolyl residues, same as in the carboxyl-terminal propeptide adjacent to cysteine residues, and as part of a complex that includes two additional proteins, cartilage-related protein and prolyl 3-hydroxylase, to modify certain triple helical prolines.

Protein-disulphide isomerase helps to secure the three chains in a trimer by the disulphide bonds between the carboxyl-terminal regions in the chains. Lysyl hydroxylase, hydroxylates lysine residues outside the major triple helical domain to form the mature intermolecular crosslinks. These complex modifications, which are necessary for correct folding, declaring thermal stability of the triple helix and crosslink formation between collagen molecules when they are secreted into the matrix. Procollagen trimers are then transported via the Golgi network and packaged into membrane-bound organelles where lateral aggregation, the initial phase of fibril formation, occurs. As secretion occurs, the procollagen molecules are further processed into mature type I collagen molecules by proteolytic cleavage of the N- and C-terminal propeptides (by the enzymes ADAMTS-2 (a disintegrin and metalloproteinase with thrombospondin motifs 2) and BMP1, respectively). Finally, the trimers are assembled into collagen fibrils and fibres and attached in those positions by intermolecular lysine-derived crosslinks in a process that is begun by modification of specific residues by lysyl oxidase. These cross-links are initially reducible, but as tissue maturation proceeds, they are converted into non-reducible compounds including hydroxylysylpyridinoline (derived from three hydroxylysine residues) and the less abundant lysylpyridinoline (derived from two hydroxylysine residues and one lysine residue). The latter (also known as deoxypyridinoline) is present mostly in bone tissue and dentine, where it accounts 21% of the total mature cross-links(5).

It has been identified that ageing affects the sequence position and abundance of multiple post-translational modifications in the collagen type 1 in mouse bone. In aged mice there is an increase in local negative charge at the surface of the collagen I triple helix around a deamidation site, agitation of water interactions with collagen I backbone, and desirability of water molecules to the side chains. These changes may affect the stability of the triple helix, which in turn retreating its ability to opposite fracture resistance to the bone(65).

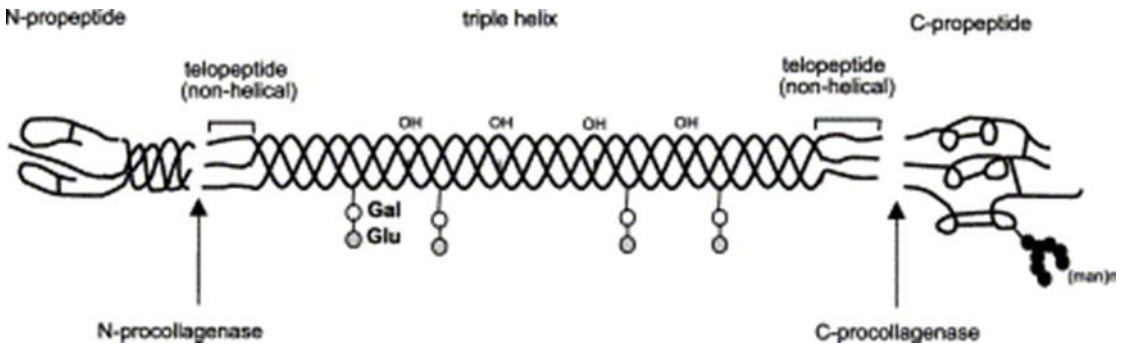

Figure 1.13. Molecular structure of type I collagen molecule showing the cleavage sites for N- and C-procollagenases. (64)

The matrix non-collagenous proteins (the ground substance of bone) constituting 10% of the total weight of bone matrix proteins, they are essential to bone development, growth, remodelling, and repair. The four main groups of non-collagenous proteins found in the bone matrix are the following:

- **Proteoglycan macromolecules:** Proteoglycans responsible for the strength of bone. They are also responsible for binding growth factors, and in some conditions, they may inhibit mineralization. Proteoclycans contain a core of protein with attached side chains of glycosaminoglycans (hyaluronan, chondroitin sulfate, and keratan sulfate, see figure 1.13). Some proteoglycans, such as keratan sulfate, contain osteoadherin, a bone-specific protein that binds to hydroxyapatite crystals strongly(66).

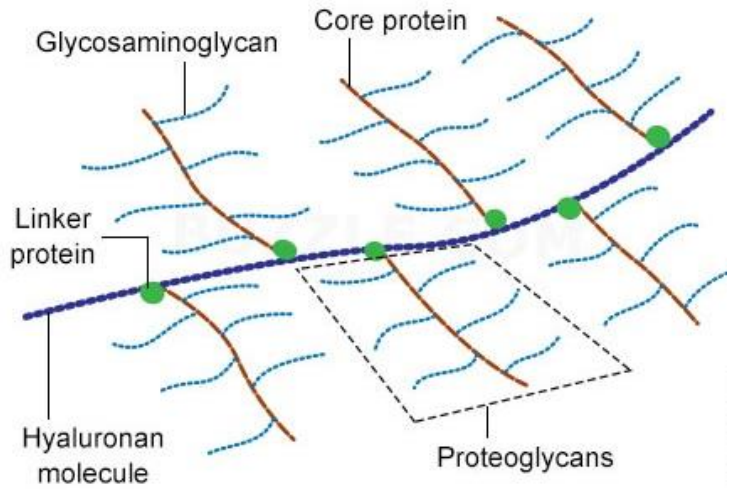

Figure 1.14. Proteoglycans structure https://th.bing.com/th/id/R847bacec60f3df8cc2f5522189d1d7c5?rik=EU%2bFRRSrPQxRDQ&riu=http%3a%2f%2fwww.buzzle.com%2fimages%2fbuzzle%2fstructure-of-proteoglycans.jpg&ehk=KqfUrnkIMlNqWZWoDe9PJVFKyiZ%2b5tS0ZjpuMLYFfJs%3d&risl=&pid=ImgRaw

- **Multiadhesive glycoproteins:** Glycoproteins are responsible for attachment of collagen fibres and bone cells to the mineralized ground substance. The important glycoproteins are: Osteonectin which works as a glue between the collagen and hydroxyapatite crystals; podoplanin (E11) which produced by osteocytes in response to mechanical stress; dentin matrix protein (DMP) which is essential for bone matrix mineralization; BSP-1, e.g. osteopontin, which facilitates attachment of bone cells to the matrix; and BSP-2, which facilitates attachment of bone cells and helps in calcium phosphate formation during the mineralization process(63).

- **Bone-specific, vitamin K–dependent proteins:** assist in variable functions, they include osteocalcin, which captures calcium ions from the circulation and incorporate them in the hydroxyapatite crystals, and stimulates osteoclasts in bone remodelling; protein S, which assists in the removal of cells undergoing apoptosis; and matrix Gla-protein (MGP), which participates in the development of vascular calcifications(67).

- **Growth factors** and **cytokines:** small regulatory proteins, they include: insulin-like growth factors (IGFs), tumour necrosis factor α (TNF-α), transforming growth factor β (TGF-β), platelet-derived growth factors (PDGFs), BMPs, Sclerostin (a BMP antagonist, BMPs induce the differentiation of mesenchymal cells into osteoblasts), and interleukins (IL-1, IL-6)(63).

1.3. Bone Modelling and Remodelling

Bone modelling occurs at low pace throughout life. Modelling process includes bone resorption and formation in an uncoupled manner and on separate surfaces. While, bone remodelling includes both bone resorption and formation activities in coupled and balanced within each BMU.

BMUs or bone remodelling units (BRUs) are composed of both osteoclast and osteoblast lineages, which are active at specific times during the remodelling cycle. These packages of cells are located along the bone surface, mostly at the interface with the hematopoietic bone marrow (endosteum) and at the surface of bones (periosteum) Figure 1.6. BMUs are initiated through the activation of bone resorption, which is followed by bone formation. Within each BMU, activities are "coupled" if bone formation follows bone resorption, and activities are "balanced" if the amount of bone formed by osteoblasts equals the amount of bone that was previously resorbed by osteoclasts. Stimulating bone remodelling increases bone turnover through an increase in the number of BMUs per bone surface area, also called activation frequency. In osteoporosis, within a BMU both coupled but unbalanced or uncoupled bone remodelling can cause severe alterations in bone mass, which will increase in severity proportionally to the activation frequency(68).

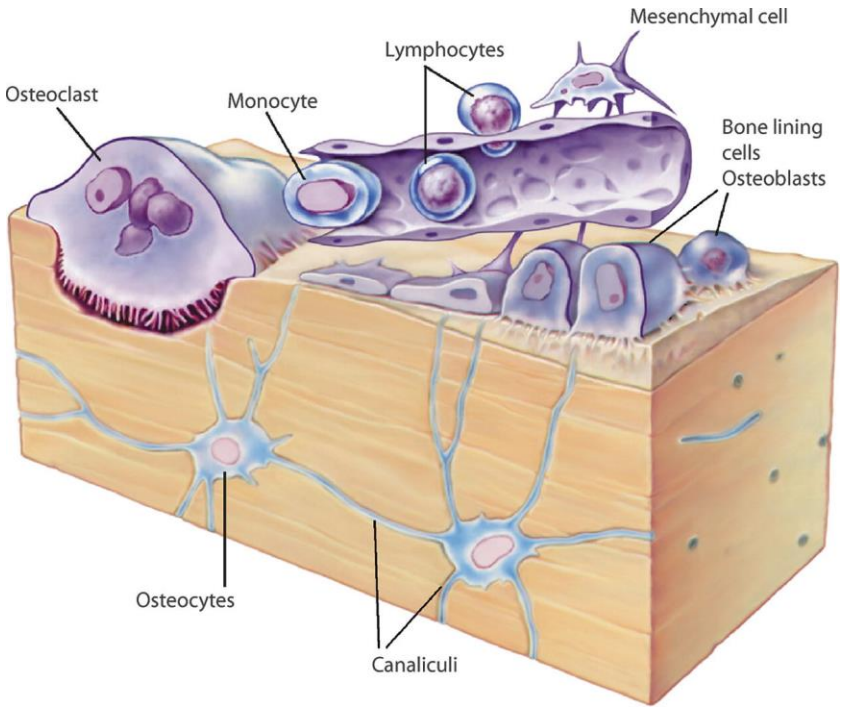

Figure 1.15. Bone remodelling unit (BRU), consisting osteoclasts, osteoblasts, osteocytes and endosteal lining cells as well as various progenitor cells (69).

There are two to five million BRU of the skeletal system, which are required for the maintenance of the bones. The total quantity of the bone decreases if more bone is resorbed than is produced over the years. It has been estimated that osteoporosis develops when for every 30 units of bone resorbed, only 29 are produced. This unbalance may cause by high turnover (increased osteoclastic activity without increased osteoblastic activity). Or by low turnover (normal osteoclastic activity but decreased osteoblastic activity). Or by decreased both osteoclastic and osteoblastic activities(69).

One remodelling cycle takes approximately 120 days, and it has been divided into 6 phases:

1. Quiescence phase*:* a layer of flat lining cells over a thin collagenous membrane covers the surface of the bone.

2. Activation phase: the quiescent or calm bone surface is prepared for resorption. This involves disclaimer of the endosteal lining cells and removal of the thin collagenous membrane covering the bone surface by matrix metalloproteinases which produced

by osteoblasts. The activation site may be enhanced by mechanical stresses transferred to the endosteal lining cells via the osteocytic-canalicular network

3. Resorption phase: including the recruitment and fusion of osteoclastic precursors, preparation of osteoclasts for resorption and development of the ruffled membrane; osteoclasts resorb the bone, which leads to the formation of pits; osteoclasts migrate slowly or undergo apoptosis.

4. Reversal phase: osteoblast progenitors are fascinated to the resorption pit, while monocytes and endosteal lining cells prepare the surface of the resorption pit for new bone production by removal of the wastes left by the osteoclasts.

5. Formation phase: A. early formation face: production of osteoid by active osteoblasts. B. Late formation face: mineralisation of osteoid.

6. Quiescence phase: the osteoblasts turn into the flat endosteal lining cells or into osteocytes trapped in the newly formed bone matrix.

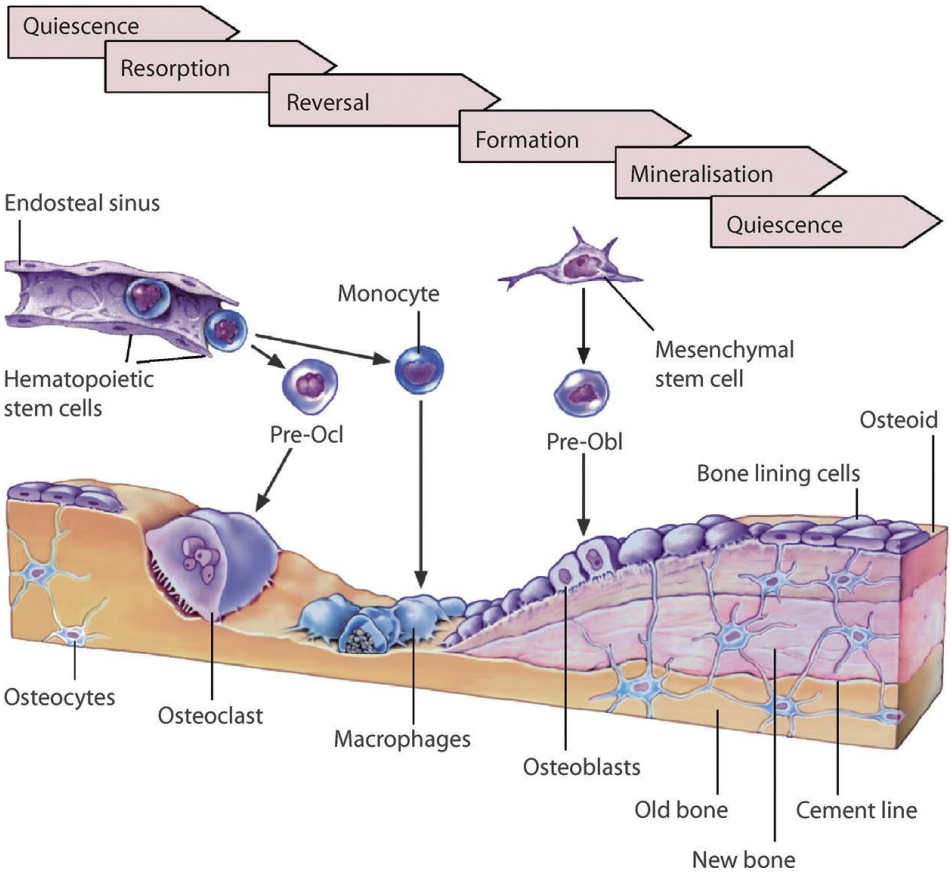

Figure 1.16. Bone remodelling steps in adult's trabecular bone (69).

In bone remodelling, cells contribute differently, according to their differentiation stage. Specifically, immature Osteoblasts can regulate osteoclastogenesis, while only mature osteoblasts are capable to synthesise bone matrix. The canonical Wnt/β-catenin pathway is crucial for bone formation. During Wnt signaling activation, Wnt proteins bind to Frizzled receptor and low-density lipoprotein receptor-related proteins five and six (LRP5, LRP6). The consequent hypophosphorylated state of β-catenin prevents its degradation, and it results in the upregulation of transcription factors crucial for osteoblast differentiation(70). The Wnt signal is controlled by several antagonists, such as Sclerostin (SOST), Dickkopf-1 (Dkk-1), and secreted frizzled-related proteins (sFRP), which inhibit wnt signalling and therefore osteoblastogenesis and bone formation (71).

Osteoclastogenesis (see paragraph 1.2.2) is mainly controlled by two factors: the macrophage-colony stimulating factor (M-CSF), and the RANKL which need to bind to their own receptors, c-fms and RANK on osteoclast precursors to start the osteoclastogenesis. The RANKL-RANK binding can be antagonized by OPG, a soluble RANKL receptor secreted by osteoblasts and bone marrow stromal cells, by binding to RANK and prevents the osteoclastogenic effect of RANKL(72).

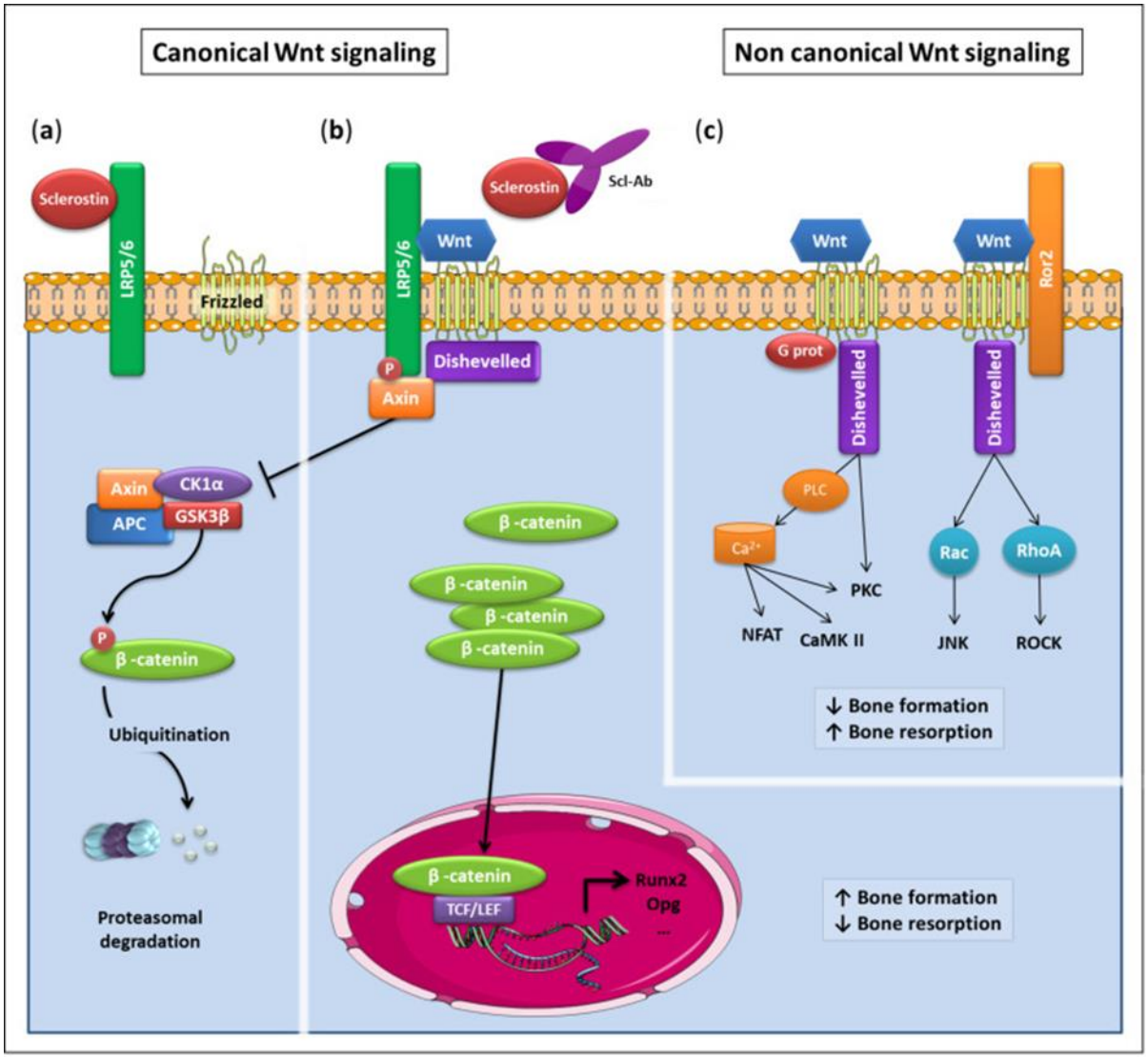

Figure 1.17. Canonical and non-canonical Wnt signalling pathways. (a) Wnt signalling OFF: If there is no Wnt ligand, or if sclerostin prevents its binding to the receptor complex, the destruction complex Axin-APC-CK1-GSK3 phosphorylates-catenin, targeting it for ubiquitination and degradation by the proteasome. (b) Wnt signaling ON: Canonical Wnt signaling is activated by Wnt ligands binding to Frizzled receptors and LRP5/6 co-receptors, resulting in the recruitment of axin and disheveled by the receptor complex and leading to GSK3 inhibition, the mechanism of which is still debated. β-catenin accumulates, trans locates into the nucleus and associates with transcription factors to induces the expression of target genes. Scl-Ab blocks the action of sclerostin, preventing its binding to Lrp5/6 and therefore canonical Wnt signaling inhibition. (c) Non-canonical Wnt signaling can also be activated by binding of Wnt ligands to Frizzled receptors. In the Wnt/Ca2+ pathway, increased intracellular calcium concentration, possibly via G proteins and PLC, activates CaMKII, PKC and NFAT. In

the Wnt/planar cell polarity (PCP) pathway, small G proteins such as Rac and Rho are activated, resulting in JUNK and ROCK activity. APC: APC adenomatous polyposis coli; CaMKII: calmodulin-dependent protein kinase type 2; CK1: Casein kinase 1; GSK3: Glycogen synthase kinase 3; JUNK: Jun kinase; LRP: Low-density lipoprotein receptor-related protein; NFAT: Nuclear factor of activated T cells; PKC: Protein kinase C; PLC: phospholipase C; ROCK: RHO-associated kinase; ROR: Receptor-tyrosine-kinase-like orphan receptor; Scl-Ab: Anti-sclerostin antibody (73).

1.4. Sclerostin

Sclerostin is a key regulator of bone homeostasis; encoded by the SOST gene. Sclerostin is a secreted glycoprotein with a C-terminal cysteine knot-like domain and sequence similarity to the DAN family of bone morphogenetic protein (BMP) antagonists produced mainly by osteocytes and inhibits bone formation by osteoblasts that induced by BMPs (74)(74,75). SOST can bind to both LRP5 and LRP6 and inhibits the canonical Wnt *ß*-catenin pathway, recent studies have shown that loss of function mutations in the SOST gene cause the progressive skeletal overgrowth disorders, sclerosteosis and Van Buchem diseases. The overgrowth is the result of hyperactive Wnt signalling (76,77). Although originally SOST was believed to only act on osteoblasts, recent research has shown effects in cardiovascular disease, diabetes and obesity(78), indicating that sclerostin may have endocrine functions.

1.5. Osteoporosis

The balance between bone resorption and bone formation which guarantees the strength and integrity of the skeleton can be altered by several physiological disorders and lead to an altered peak bone mass (PBM) and therefore bone loss, subsequent to an increased risk of osteoporosis and fractures (79)

Literature data have demonstrated an involvement of RANKL, OPG, sclerostin and DKK-1, in congenital and developed pediatric diseases (80).

Metabolic bone diseases, such as osteoporosis and osteopetrosis, affect the bone remodelling process. They can alter bone balance ether positively or negatively, causing either excessive bone formation or bone resorption, respectively. Osteopetrosis is a rare

disease that causes a positive bone balance results in increased bone mass caused by a dysfunction in the ability of osteoclasts to acidify there resorption pits, resulting in inappropriate resorption with continued bone formation consequences in thicker and harder bones that are more liable to fracture (81–83). The most predominant metabolic bone disorders are osteopenia and osteoporosis, both of which refer to a loss of bone mineral density (BMD). Generally, osteoporosis has been defined as a progressive systemic skeletal disease characterized by low bone mass and micro architectural deterioration of bone tissue, with a consequent increase in bone fragility and susceptibility to fracture (84). The World Health Organisation classified patients with BMD between 1 and 2.5 standard deviations below the mean of healthy young adults as osteopenic, lower than 2.5 is diagnosed as osteoporotic (77). Osteoporosis classified as primary type 1, primary type 2 or secondary. Type 1 is the most common and is mostly termed as postmenopausal osteoporosis as it is associated with oestrogen deficiency that results of postmenopausal which causes increased RANKL and decreased OPG production and reduced osteoclast apoptosis (85–87). Type II is also identified as senile or age-related osteoporosis and may occur in both men and women with age. Secondary osteoporosis can cause as a consequence of an adverse reaction to a medical condition or a physical activity change, such as glucocorticoid and immobilisation-induced osteoporosis (88) or inflammation-induced bone loss as in periodontitis or rheumatoid arthritis, RANKL overexpressed by immune cells (89,90). As osteoporosis causes bone mass loss and consequents bone strength reduction, resulting in an increase in fragility and susceptibility to fracture, now 50% of women and 20% of men over the age of fifty having fragility fracture, and about 158 million people over the age of 50 are predictable to have osteoporotic fracture worldwide. This number expected to double by 2040 (91). Hip fracture is the most common fracture which occurs in elderly women with osteoporosis after a fall from standing position, and the most common surgery in orthopaedic is the one that involves hip fracture (92). The national hip fracture debate in 2019 reported that numbers of hip fractures are increasing during winter months and contribute to increased hip fracture patient mortality at this time (93).

Thus, osteoporosis is an impact in poor quality of life, as it causes significant functional impairment leading to prolonged immobilisation and limitations in daily living activities causing a reduction of health-related quality of life (94). Figure 1.13 illustrates the significance

of hip fractures morbidity, with a mortality more than 20% that extends well beyond 12 months following fracture, in one year, and large percentage of patients have outstanding functional deficits in essential and instrumental activities of daily living (95).

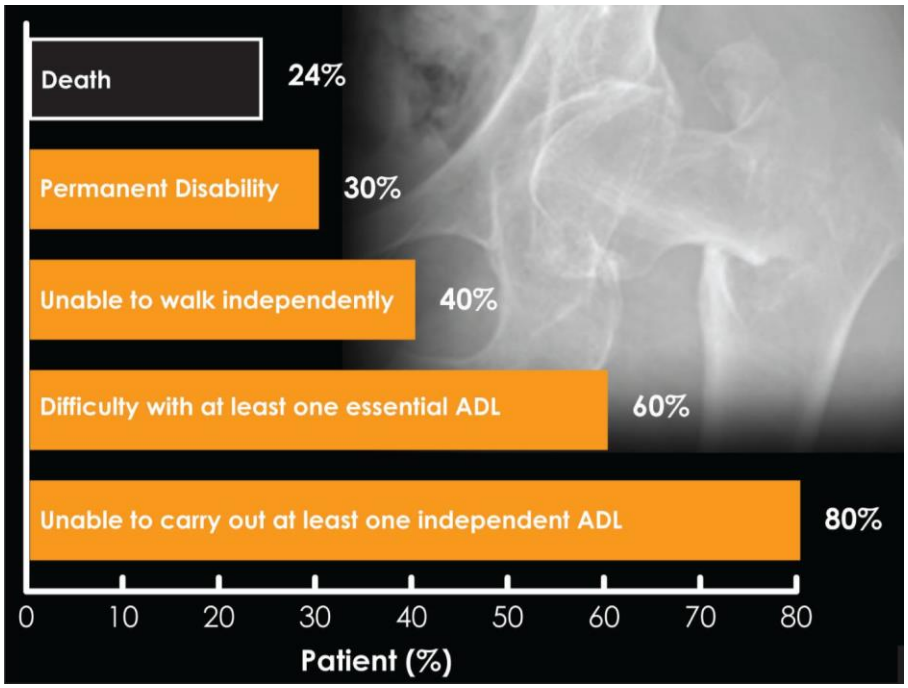

Figure 1.18. One-year hip fracture mortality and morbidity. Hip fractures have a significant morbidity, with a mortality more than 20% that extends well beyond 12 months following fracture.
dailhttps://m2.healio.com/~/media/journals/ortho/2012/9_september/10_3928_01477447_20120822_12/fig6.jpg (80).

In summary, the possible risk factors for osteoporosis can be identified as modifiable factors, including diet and lifestyle factors, and non-modifiable factors such as gender, age, genetic factors, and history of prior fractures, diseases and pharmacological treatments. The modifiable factors, such as a balanced diet and exercise, have an important role already in childhood. In particular, regular physical activity has a key role in bone strengthening, not only in healthy children, but also in those suffering from chronic diseases (96,97).

1.5.1. Osteoporosis treatment

Treatment of osteoporosis includes a number of strategies, all of which are aimed at prevention or reduction of fractures. They can be divided into pharmacological treatment, calcium and vitamin D supplementation and lifestyle modifications. Pharmacological therapeutic options can be classified according to the mechanism of action by which Antiresorptive, such as Bisphosphonates and selective estrogen receptor modulators (SERMs) (98), since their main role is to block osteoclast activity and their effects are aimed to block either further decrease of bone density or deterioration of skeletal microarchitecture. In contrast, parathyroid hormone treatment such as teriparatide, is osteoanabolic therapy that restores bone microarchitecture with increase in cortical bone thickness (98).

Bisphosphonates are the first-choice treatment of osteoporosis, bisphosphonates (BPs) are effective anti resorptive agents presently available that can reduce the risk of hip, vertebral, and wrist fractures by 35-65% after long term treatment (3-5 years). The most commonly prescribed bisphosphonates for postmenopausal osteoporosis are alendronate and zoledronate (99). Bisphosphonates are synthetic, non-hydrolysable analogues of pyrophosphate which bind to hydroxyapatite crystals, the specificity of this drugs comes from the two phosphonate groups that work together to bind calcium ions preferentially to the Bisphosphonate molecules. Therefore bisphosphonates accumulate in high concentrations in bone tissue and attach to osteoclasts to disrupt the intracellular enzymatic functions needed for bone resorption. Subsequent to this strong inhibition of osteoclast activity, bone resorption is almost completely blocked at the level of BMU, with a consequent blockade of bone remodelling (100,101).

There are two different classes of BPs: non-nitrogenous-BPs (nN-Bps) and Nitrogenous-BPs (N-Bps). The nN-BPs, such as clodronic acid, are converted intracellularly to methylene-containing analogues of ATP, its accumulation in osteoclasts in vitro inhibits bone resorption by inducing osteoclast apoptosis. On the conflicting, the N-BPs such as Zoledronate, Alendronate, Ibandronate and Risedronate are not metabolized into toxic intracellular analogues of ATP, but act by inhibiting farnesyl-diphosphate-synthase, a key enzyme of the HMG CoA-reductase (mevalonate) pathway. The inhibition of protein prenylation may affect many proteins in the osteoclast, resulting to affect osteoclastogenesis, cell survival, and cytoskeletal dynamics. Generally, the addition of nitrogen group in the molecules modifies

their potency, N-BPs are more powerful than nN-BPs at inhibiting bone resorption in vivo (102).

Selective estrogen receptor modulators (SERMs), are a class of drugs that act on the estrogen receptor (ER). They are non-steroid compounds and have tertiary structures that can bind to the estrogen receptor. These compounds have either selective agonist or antagonist effects, depending on the target tissue, thereby permitting the possibility to selectively inhibit or stimulate estrogen-like action in various tissues (103).

Raloxifene is a second generation of SERMs currently in use for osteoporosis, and was developed for prevention and treatment of postmenopausal osteoporosis. As bone cells express two estrogen receptors, α and β. Raloxifene is similar to estrogen in interacting with the ligand-binding domain, with minor conformational differences, when it binds to the ERs, start to activate ER dimerization and a specific conformational change. This change facilitates binding of coregulatory proteins that modify and activate its transcriptional activity on specific response elements in the promoter regions of target genes.

RAL, acting on bone as estrogen, by a direct ER- dependent mechanism, decreases osteoclast differentiation from hematopoietic precursors, without increasing cell apoptosis. RAL appears to act by two different and independent mechanisms: a direct action on osteoclasts, but also an osteoblast-mediated mechanism. Data demonstrated that RAL inhibits the release of interleukin-6 and tumour necrosis factor-α (TNF-α) from osteoblasts. These two cytokines can enhance the effect of RANKL on osteoclast differentiation. In addition, RAL increases the osteoblast-specific transcription factor Cbfa1/Runx2 and α2 procollagen type I chain mRNAs which suggests that this SERM can modulate osteoblast activity. Therefore RAL acts on both bone formation and bone resorption, not entirely blocking bone remodelling like bisphosphonates do, but modulating bone remodelling similar to the actions of estrogens on bone before the menopause (104). Recent studies have demonstrated that RAL treatment is able to decrease circulating cytokines levels in postmenopausal osteoporotic women, suggesting that this molecule could modulate bone turnover by controlling cytokines levels after menopause (105).

Teriparatide is the most common bone anabolic osteoporosis medication. Results of clinical trials, to evaluate the role of recombinant human parathyroid hormone in postmenopausal

women affected by severe osteoporosis, showed that parathyroid hormone (PTH) is highly effective at increasing BMD in the spine and throughout the skeleton. It works by stimulating bone turnover with new bone formation on trabecular, endocortical, and periosteal bone surfaces. Although PTH also stimulates bone resorption, it stimulates osteoblastic bone formation more than osteoclastic bone resorption, leading to a net increase in bone volume (106). PTH enhances bone strength by restoring bone architecture in both cancellous and cortical bone, expanding bone size as well as improving BMD(107). Clinical treatment with teriparatide for postmenopausal women showed significant increase in bone mass at the lumbar spine (9.7%), total hip (2.6%), total body bone mineral density, as well as a significant 65% reduction in vertebral fractures and a 53% reduction in nonvertebral fractures in treated patients (108). Although, PTH maintains the same efficacy obtained in osteoporotic untreated or previously treated women with anti-resorptive therapy (109) there is a suggestion that prior treatment may rounded some of the skeletal response to PTH (110). However, BMD increases significantly; bone turnover is radically stimulated. Therefore, all patients, after the PTH course, should be given a potent antiresorptive agent to maintain the PTH-induced increased bone mass and antifracture efficacy. The Food and Drug Administration (FDA) has approved the use of teriparatide for 2 years in postmenopausal women and men at high risk for fracture. The most common side effects associated with teriparatide include dizziness and leg cramps(111).

During 2000s, pharmaceutical active sclerostin programs started to bring to market the first non-PTHR1-based anabolic therapy. Recently, the sclerostin antibody (romosozumab) was approved for clinical use in the United States as a therapy for the treatment of postmenopausal women with osteoporosis at high risk of fracture. Treatment with sclerostin monoclonal antibodies showed effective osteoanabolic responses in mice, rats, and monkeys, in preclinical studies (112). Romosozumab therapy showed significant reductions in vertebral fractures at 1 and 2 years treatment for large international population of women in phase III studies (113) . NICE is now considering the role of Romosozumab, the new monoclonal antibody that binds to and blocks sclerostin (114)(a protein secreted by osteocytes that inhibits the Wnt signalling pathway and promotes decreased bone formation) (see paragraph 4 of 3. Bone modelling and remodelling), thus inhibition of sclerostin modifies cellular activity and pathways, resulting in increased production of bone matrix and reduced bone resorption,

increasing trabecular and cortical bone mass(115). Despite its clinical efficacy and selectivity to bone, as romosozumab induces the uncoupling of bone remodeling, leading to both an increase in bone formation and a decrease in bone resorption during the first months of treatment, some concern were raised about side effects including increased risk for cardiovascular disease(73).

In addition to the anti-sclerostin antibody that targets and neutralizes the osteocyte specific factor sclerostin, there are other therapeutic antibodies offered that target other osteocyte factors. They are including anti-FGF23, burosumab, and anti-RANKL, denosumab. The mechanisms for regulating FGF23 production are complex, as In addition to the anti-FGF-23 antibody, there is another possible therapeutics include FGF receptor inhibitors (116).

Studies have linked high levels of circulating FGF23 to an increased risk of heart disease, vascular calcification, and increased fat mass (116).

Current treatment is not enough.

Even though anti-resorptive drugs such as bisphosphonates have been available for more than 30 years, the incidence of osteoporotic fractures has decreased only marginally (in the US by about 15% in women between 1986 and 2005, unchanged in men(117)), and current treatment only reduces fracture incidence by 20-60% (118,119). Anti-resorptive drugs lead to the suppression of new bone formation and are incapable of restoring normal bone. Moreover, anti-resorptive drugs are associated with serious side effects such as atypical femoral fractures and osteonecrosis of the jaw. Because of these side effects they can only be used for a limited amount of time (currently up to 5 years). Furthermore, compliance is poor with just 20% of patients still taking bisphosphonates after 3 years (120). The only two anabolic agents currently licensed, teriparatide and anti-sclerostin (romosozumab), are reserved for severe osteoporosis and can only be given for up to 2 years for teriparatide and 1 year for romosozumab (121). Due to the ageing of the population, the number of admissions for osteoporotic fractures is actually still rising (122). Therefore, age-related bone fragility is an on-going health problem. Apart from the effects of the menopause, the mechanisms underlying age-related bone fragility are still poorly understood. Therefore, further research is required to identify additional and targeted prevention and treatment strategies to achieve healthy bone ageing.

1.6. Ageing and bone

The general mechanism of ageing in variable biological systems is a stochastic damage inflicted to biological macromolecules that drive the force for the ageing process. The damage is resulting from small reactive molecules, such as reactive oxygen intermediates (ROI), that are produced during normal cellular metabolism and are associated with essential and important cellular functions (123). These macromolecules include proteins, lipids and DNA. Cellular dysfunction resulting from macromolecular damage can cause genomic instability, inappropriate cell differentiation or cell death and even replacement of the dead cell by another via cell proliferation. This can lead to loss of parenchymal cell mass and functional impairment of tissues, which are typical features of ageing of tissues and organs (124).

1.6.1. Epigenetic changes

What are epigenetic modifications? They are modifications to both nucleotides in the DNA methylation, as well as modifications to histones. These changes lead to changes in transcription, and therefore to cell, function (125). Another epigenetic change occurs, is the modification of micro RNA expression, again leading to changes in expression of target mRNAs.

1.6.2. Cell senescence

Cell senescence is often defined as a state of “irreversible” or “permanent” cell cycle arrest, in contrasting to the voluntarily reversible inactive state. The senescence phenotype was originally identified in genetically normal, primary, human diploid fibroblasts (HDFs), which rejected to proliferate indefinitely in culture (126). Cells respond to cytotoxic stimuli differently depending upon the cell type and the strength of the stress. HDFs are relatively resistant to apoptosis, and are highly liable to senescence. The senescence process is much longer than apoptosis, may be due to the way signals transportation. In apoptosis, a variety of triggers can converge to the executioner caspases through a common mechanism (127).

Cell quiescence as well is a reversible cell cycle arrest, which is induced by the absence of mitogens or growth factors, nutrient starvation, or increasing cell density in contrast to senescence. Lymphocytes, whose activation is part of the immune response, adult stem cells, or dermal fibroblasts, which actively participate in wound healing are typical examples of quiescent cells (128). Quiescence is considered by low protein synthesis and metabolism,

cellular growth deficiency, and, the lack of global heterochromatin structures such as promyelocytic leukemia (PML) protein (129) or senescence-associated heterochromatic foci (SAHF) (130). Recent studies showed that fibroblasts reduced quiescent by contact inhibition exhibit comparable metabolic activity to actively proliferating cells. In addition to stimulate recycling of damaged macromolecules via autophagy, high metabolic activity might serve for biosynthesis and secretion of extracellular matrix proteins (131). Outstandingly, quiescent cells upregulate genes, such as HES1, that inhibit senescence and apoptosis while expression of genes involved in cell division downregulated (132).

The senescence process can be observed as a composition of a series of signaling transductions, rather than the single signal in apoptosis, such as senescence associated heterochromatic foci (SAHFs) and epigenetic gene regulation, the DNA damage response, senescence associated secretory phenotype (SASP)/Senescence-messaging secretome (SMS), and macro autophagy (130,133). Due to the highly heterogeneous nature of the senescence phenotype, it is not possible to identify a universal marker for senescence that applies in all cases. However, the use of a combination of various markers often associated with effector programs of senescence has successfully contributed to extending the concept of senescence outside the HDF system: a similar phenotype can be induced by various cellular stresses in different types of somatic cells, as well as different tissues in animals (134,135). Importantly, the effector mechanisms and markers used in these studies were mostly identified in experiments using HDFs, and thus, HDFs are still the best-characterized model system for this topic. However the term “senescence” used to specifically describe the cellular phenotype, distinct from “aging” at the organism level(135). results detected senescent cells in several premalignant or benign conditions and showed that the senescence program effectively prevents tumorigenesis (136,137) , thus senescence has placed as a tumour suppressor as apoptosis.

1.6.3. Inflammation

The presence of senescent cells has mostly been associated with aging, chronic senescent cell accumulation due to higher production and/or inefficient clearance with aging in humans and mice, contributes to the development of age-associated pathologies (138). Age-related accumulation of senescent cells has been credited to diminished immune surveillance (139). Regardless of how cellular senescence is induced, a serious feature of senescent cells is the

acquirement of the senescence-associated secretory phenotype SASP, which is a dysfunctional mixture of proinflammatory cytokines and matrix degrading proteases that communally modify the local environment (140), these secreted factors can negatively influence the function of adjacent cells (141). Thus, age-dependent accumulation of senescent cells promotes damaging effects in part by acting as a permanent source of proinflammatory mediators, enabling a continued infiltration of immune cells, which in turn have a significant effects on bone cells.

With age bone properties change, bone modifications may include the mechanical function, shape of bones, bone cells, the matrix they produce, and the mineral that is deposited on this matrix (142). As a result of the ageing process the bones become weaker and more prone to fracture (143).

Bone ageing is currently not fully understood, especially the specific changes in bone cell function and gene expression, and the link of these to the known decrease in adaptation to mechanical loading with ageing. In addition, it is currently not known whether the aged bone cells secrete factors which may affect other organs.

1.7. Mechanical loading and bone

The effect of mechanical loading on bone has been studied since the nineteenth century. These studies have primarily used animal models of mechanical loading subsequently, bone adaptation is a highly complex process that is difficult to fully escalate.

In 1892, Julius Wolff the anatomist and orthopaedic surgeon hypothesized that bone adapted to its mechanical environment according to strict mathematical laws. Now, this principle known as Wolff's Law, established on anatomical dissection studies which revealed increased bone mass in areas that expected to be highly mechanically stressed and low bone mass with low stresses. Furthermore, Wolff with his colleagues Meyer and Culmann, observed that trabeculae in the femoral head and neck were orientated to reduce bending stresses when was loaded. These observations allowed Wolff to state his "Law" as "*Every change in form or function of bone or of their function alone is followed by certain definite changes in their internal architecture, and equally definite alteration in their external conformation, in accordance with mathematical laws*" (144).

Architectural bone changes were hypothesized to occur due to a dynamic adaptive process in response to changes in the mechanical stimulus derived from load-bearing. This theory was further developed by Harold Frost in 1960 whose thoughts form the basis of the current theory of bone adaptation (145). Frost recognized that the most likely loading-derived stimulus for bone cells would be the strains developed in the bone tissue as a result of loading. His mechanostat theory suggests a negative feedback system, represented as, the local mechanical strain, caused by functional mechanical loading, result in a structurally appropriate bone mass and architecture. Thus, in bone areas with mechanical strains higher than the set point, result in bone formation which make a stiffer bone construct. In opposition, bones with strains lower than the set point, would result in bone resorption, then decrease in bone mass (145). It is an important component of this theory that the mechanostat is a local phenomenon with local changes in strain adjusting local bone mass through local bone formation or resorption. However, it is noticed that the mechanostat drives in a wider physiological situation and the ability to create and maintain structural competency may significantly modified by systemic circumstances (146,147).

General findings gained from *in vivo* animal loading models

- Bone remodelling is affected by dynamic loads but not by static (148).
- Bone formation correlated with the peak strain magnitude of loading (149–151)
- Stimulus strains can determined by the origin of loading, experiments showed that a progressively increasing osteogenic can be a response to progressively increasing loads(152).
- Increasing strain rate during loading and unloading stimulates bone formation (153).
- Small numbers of loading cycles are required to stimulate bone formation and maximizing the number dose not lead to a maximal stimulation (154).
- Inserting rest between loading cycles increases bone formation (155).

1.8. Aims

The mechanisms underlying the decrease in the bone anabolic effect of mechanical loading with ageing are still mostly unknown. The main cells effecting this anabolic response are the bone forming osteoblasts and the mechanosensing osteocytes.

Therefore, the main aim of this thesis was to:

Study age related changes in osteoblasts and osteocytes and their response to mechanical loading.

Study a comparison between young and aged mice through studying the difference in their response to the mechanical loading.

The models chosen to do this were the mouse *in vivo* model of mechanical loading of the knee as described in (156), and the *in vitro* model of mechanical stretch for the primary mouse osteoblasts. The main objectives to achieve this were:

1. Study the effects of loading on circulating bone turnover factors produced by bone cells in young and aged mice.
2. Analyse the effect of ageing on the bone anabolic response to loading in vivo using histomorphometry and Micro-computed tomography (µCT) analysis for young and aged mice bone tissue.
3. Analyse the effects of loading and age on the distribution of osteocytes through µCT analysis for young and aged mice loaded and non-loaded bones.
4. Analyse the effect of ageing and loading on sclerostin expressed by osteocytes through florescent immunostaining image analysis by confocal microscope.
5. Study the changes in gene expression patterns in osteoblasts and osteocytes after mechanical loading in young and aged mice by studying the next generation gene sequencing.

Chapter 2. Materials and Methods

2.1. Experimental Animals:

Female C57BL6 mice of two different ages, young (3months old) and aged (15monthes old)) were obtained from Charles River Ltd, United Kingdom. Animals were housed in a pathogen-free facility, at the Biomedical Services Unit, University of Liverpool. All procedures were in accordance with the Animals Scientific Procedures Act 1986 and the EU Directive 2010/63/EU and after the local ethical review and approval by Liverpool University's Animal Welfare and Ethical Review Body (AWERB).

We used C57 Black 6, the common inbred strain of the laboratory mouse and the most widely used mouse strain, due to the availability, easy breeding, and sturdiness (157).

Each age group was separated into two groups, one for *in vivo* loading and the other one for the *in vitro* loading (n=6 for each group).

2.2. *In vivo* loading

Animals (young N=6, aged N=6) were anaesthetised using isoflurane and the right tibia loaded mechanically by applying axial compressive loads from a servo-hydraulic materials testing machine (Model HC10, Dartec, UK) via custom-made padded cups which hold knee and ankle joints flexed and the tibia vertically (158). The loading occurs by pressing the upper cup on the knee using a loading pattern consisting of a trapezoidal wave for 40 cycles with peak 11 N loads for 0.05 s, rise and fall times 0.025 s each and baseline hold time of 9.9 s at 2 N. Right knees were loaded 3 times per week for 2 weeks. The left tibia was used as a non-loaded control. To assess bone formation, each mouse was injected with calcein (200µl IP injection at 2mg/ml) three days before the final loading, and on the last day of loading, then culled 2 days later. Right and left tibias were obtained for quantitative and qualitative bone measurements with micro-computed tomography scan (micro-CT) and immunohistochemistry.

Another two young and aged mouse groups (N=4 for each age) were loaded using the same protocol, but without calcein injection. Right and left tibias were dissected after culling and RNA extracted for qPCR analysis.

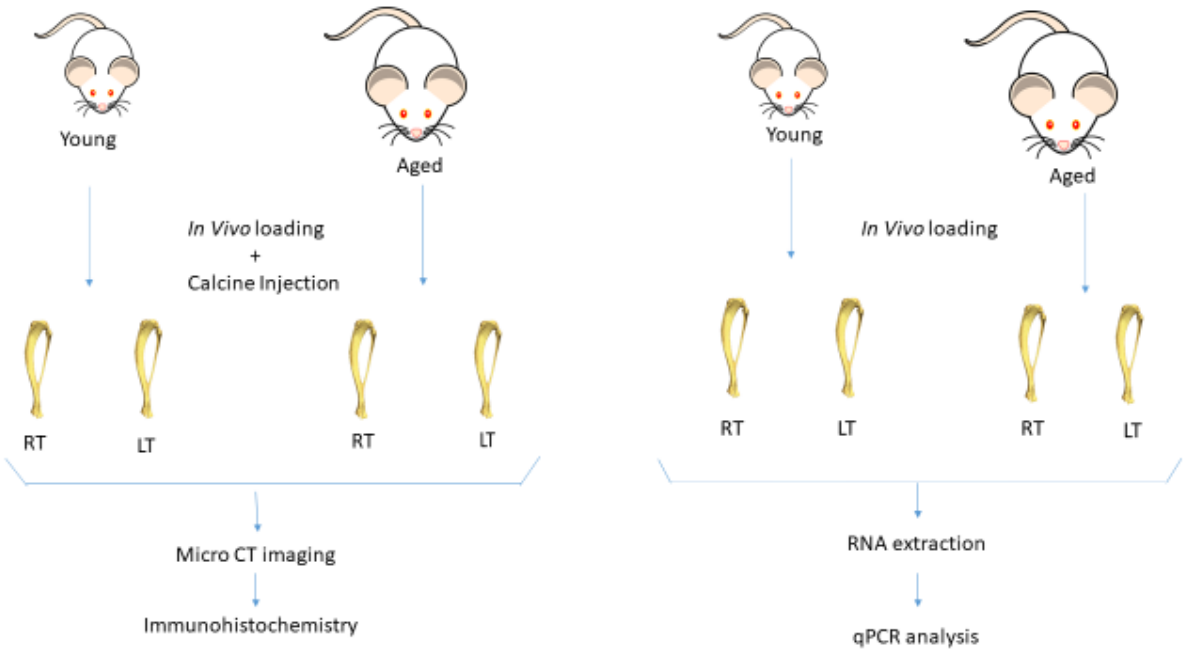

Figure 2.1. Schematic overview of the experimental design for the *in vivo* mechanical loading model for young adult and aged adult mice. RT: Right Tibia, LT: Left Tibia. S

2.2.1. Animal dissection

Two groups of young in-vivo loaded mice (n=6) and aged in-vivo loaded mice (n=6) with calcein injection were culled with CO_2, blood was obtained by cardiac puncture and collected in a covered test tube and left to clot by leaving it undisturbed at room temperature for 15-30 minutes. Left and right lower limbs were removed using scissors, and tibias and femurs separated. All soft tissue was removed from bones by scraping the bones with a scalpel then fixed overnight in paraformaldehyde (4% in PBS) and stored in 70% ethanol until used for µCT scanning and subsequent immunohistochemistry. The clotted blood was centrifuged at 1,600 x g for 10 minutes in a refrigerated centrifuge and the resulting serum supernatant was immediately transferred into a clean polypropylene tube using pipette. The samples were maintained at 2–8°C while handling then stored at –20°C until use in the Enzyme-linked immunosorbent assays (ELISA).

Two other groups of young in-vivo loaded mice (n=6) and aged in-vivo loaded mice (n=6) with no calcine injection were culled using CO_2, blood was obtained by cardiac puncture

immediately as described above. Left and right lower limbs have been released, tibias and femurs have been separated. All soft tissue was removed from bones by scraping the bones with the scalpel. Next, the epiphyses and diaphysis were cut off and the bone shaft opened using a 27 gauge hypodermic needle. Bone shafts were put in to a 500µl Eppendorf containing a hole in the bottom of the tube. This small Eppendorf was contained in a 1.5ml Eppendorf. Then Eppendorf's were centrifuged at 800xg for 3 minutes at room temperature to remove the bone marrow. After flushing out bone marrow from the tibias, the clean bones were cut into small fragments with the aid of a scalpel. The fragments were then transferred to a T25 flask containing 5ml of 1mg/ml collagenase in Hanks buffered salt solution. Flasks were then incubated in a shaking water bath at 37°C for 30 minutes. The bone chips were washed vigorously in HBS at least 3 times, then bone chips transferred in to a 1.5ml Eppendorf and snap frozen in liquid nitrogen. Under freezing condition with liquid nitrogen, the bone chips from each individual tibia was ground into a powder using a pestle and mortar system. Next the RNA was extracted with trizol as described in paragraph 2.2.2.

2.2.2. RNA extraction

Extraction of RNA was performed using the RNeasy Micro kit (Qiagen) according to the manufacturer's instructions as follows:

To each Eppendorf containing one tibia 700µl of Trizol was added to lyse the bone cells. The lysates were vortexed for 1 minute in order to homogenize the samples, then incubated at room temperature for 5 minutes. 140µl of chloroform was added to each tube then shaken vigorously. Samples were incubated at room temperature for 2-3 minutes and then centrifuged at 12,000g for 15 minutes at 4°C. The upper aqueous phase (±350µl) was transferred to a new micro centrifuge tube and 1.5 times the volume in the tube (±525µl) of 100% ethanol was added and mixed by pipetting up and down.

700µl of the sample was added to the spin columns provided by the kit, then they were centrifuged at 8,000g for 15 seconds at room temperature. Flow-through was discarded and procedure was repeated by adding the rest of the sample. Adding 500µl of RPE buffer to each sample then tubes were centrifuged at 8,000g for 15 seconds at room

temperature. Flow-through was discarded and 500µl of RPE was added again and tubes centrifuged at 8,000g for 2 minutes at room temperature.

The spin columns were transferred to a new Eppendorf and 30µl of RNase-free water was added to collect the RNA from them. Tubes were centrifuged at 8,000g for 1 minute, at room temperature. A further 30µl of RNase-free water was added and tubes were centrifuged at 8,000g for 1 minute. Finally, RNA quantities and purities were assessed using the Nano Drop 2000TM spectrophotometer. RNA samples were stored at -80°C until used.

2.2.3. Quantitative measurement of Biochemical markers concentrations in mouse serum with ELISA

2.2.3.1. Osteocalcin (OC):

Osteocalcin concentration in mouse serum was measured by using ELISA kit catalogue number: RD-OC-Mu 96 tests provided from Biotech.

Assay principle:

The mouse osteocalcin ELISA kit used was provided by RD and the microtitre plate provided in this kit has been pre-coated with an antibody specific to osteocalcin. Standards and samples were added with a biotin-conjugated antibody preparation specific to osteocalcin. Next, Avidin conjugated to Horseradish peroxidase (HRP) was added to each microplate well and incubated. After TMB substrate was added, only the wells that contain osteocalcine, Biotin-conjugated antibody and enzyme-conjugated Avidin exhibited the change in colour. The enzyme-substrate reaction was stopped by the addition of sulphuric acid solution and the colour change was measured spectrophotometrically at a wavelength of 450nm ± 10nm. The osteocalcin concentration in the samples was then determined by comparing the optical density of the samples to the standard curve. For further details, see Chapter 2 paragraph 2.3.1.

Reagents and materials provided:

Pre-coated, ready to use 96-well strip plate, plate sealer for 96 wells, standard, standard diluent 20mL, detection reagent A 120µL, assay diluent A 12mL, detection reagent B 120µL, assay diluent B 12mL, TMB substrate 9mL, stop solution 6mL, wash buffer 20mL (30 x concentrate).

All kit components and samples were brought to room temperature (18-25^{o}C) before use.

The standard was reconstituted with 2.0 mL of standard diluent, and kept for 10 minutes at room temperature then shacken gently. The concentration of the standard in the stock solution is 4000pg/ml. 7 tubes containing 0.5mL standard diluent were prepared and used for the diluted standard to produce a double dilution series: 4000pg/mL, 2000pg/mL, 1000pg/mL, 500pg/mL, 250pg/mL, 125pg/mL, 62.5pg/mL, and the last EP tube with standard diluent is the blank at 0pg/ml.

The stock detection reagents A and B were briefly centrifuged before use then diluted to the working concentrations with assay diluent A and B respectively (1:100).

To prepare 600mL of wash solution, 20mL of wash solution concentrate (30x) with 580mL of distilled water.

The needed dosage of the TMB substrate solution was aspirated with sterilized tips.

Samples was diluted in ratio 1 in 50 PBS (pH=7.0-7.2).

Assay Procedure:

Wells were assigned for diluted standards, blank and sample. 7 wells were prepared for the standards and 1 for the blank. 100µL of each dilution of standard, blank and samples was added in to the appropriate wells then covered with the plate sealer and incubated for 2 hours at 37^{o}C.

After incubation, liquid was removed from each well without wash then 100 µL of detection reagent. A working solution was added to each well and incubated for 1 hour at 37^{o}C after covering it with the plate sealer.

The solution was aspirated then wells was washed with 350µL of 1xwash solution to each well using multi-channel pipette and let for 1-2 minutes then liquid was removed from all wells completely by tapping the plate onto absorbent paper.

Wells were then washed thoroughly 3 times and any remaining wash buffer was removed after the last wash by aspirating or decanting.

100µL of detection reagent B working solution was added to each well then incubated for 1 hour at 37°C after covering it with the plate sealer. Next the plates were washed in wash buffer 5 times as described in the previous step.

90µL of substrate solution was added to each well then covered with a new plate sealer and incubated for 15-25 minutes at 37°C no more than 30 minutes with protection from light.

After the addition of the substrate solution, the liquid turned blue then it turned yellow after adding 50µL of stop solution to each well. Absorption at 450 nm was measured on a microplate reader immediately after stopping the reaction.

Calculation of Results:

Average was taken for the duplicate readings for each standard, control and sample, then the average zero standard optical density was subtracted. A standard curve was constructed by plotting the mean optical density and concentration for each standard and best fit curve was drawn through the points on the graph using plotting software (for instance, curve expert 1.30), the concentration read from the standard curve for the samples that have been diluted multiplied by the same dilution factor.

2.2.3.2. The Procollagen Type 1 N-Terminal Propeptide (P1NP):

The P1NP concentration in mouse serum was measured by using ELISA kit catalogue reference number: AC-33F1 provided by IDS.

Assay principle:

The mouse P1NP EIA kit was provided by Ids, the assay is a competitive enzyme-linked immunosorbent assay utilising a polyclonal rabbit anti-PINP antibody coated onto the inner surface of polystyrene microtitre wells. Calibrators, controls and samples are added to the wells of the microtitre plate followed by PINP labelled with biotin and the plate incubated for 1 hour at room temperature before aspiration and washing. Enzyme (horseradish peroxidase) labelled avidin is added and binds selectively to complexed biotin and, following a further wash step, colour is developed using a chromogenic substrate (TMB). The absorbance of the stopped reaction mixtures are read in a microplate plate reader, colour intensity developed being inversely proportional to the concentration of PINP.

Reagents and materials provided:

- **Calibrators (REF AC-3301A - AC-3301F):**

Lyophilised phosphate buffered saline containing rat/mouse PINP, mouse serum, goat serum, BSA and <1% sodium azide (0.025% once reconstituted), 0.5 mL per bottle.

- **MICROPLAT (REF AC-3302W):**

Microplate with polyclonal rabbit anti-PINP antibody linked to the inner surface of the polystyrene wells, 12 x 8-well strips in a foil pouch with desiccant.

- **PINP Biotin (REF AC-3303**):

Lyophilised phosphate buffered saline containing PINP labelled with biotin, and BSA. 1 mL per bottle.

- **Enzyme Conjugate (REF AC-3304):**

Phosphate buffered saline containing avidin linked to horseradish peroxidase, protein, enzyme stabilisers and preservative. 18 mL per bottle.

- **Control 1 (REF AC-3305A):**

Lyophilised rat serum diluted in PBS with BSA and <1% sodium azide (0.025% once reconstituted). 0.5 mL per bottle.

- **Control 2 (REF AC-3305B):**

Lyophilised mouse serum diluted in PBS with BSA and <1% sodium azide (0.025% once reconstituted). 0.5 mL per bottle.

- **TMB Substrate (REF AC-TMB):**

A proprietary aqueous formulation of tetramethylbenzidine (TMB) and hydrogen peroxide, 24 mL per bottle.

- **Stop Solution (REF AC-STOP):**

0.5M hydrochloric acid, 14 mL per bottle.

- **Sample Diluent (REF AC-3309):**

Phosphate buffered saline containing BSA and 0.05% sodium azide. 20 mL per bottle.

- **Wash Concentrate (REF AC-WASHL):**

Phosphate buffered saline containing Tween, 50 mL per bottle.

- **Adhesive Plate Sealers:** 8 per kit.

Other required materials:

1. Precision pipetting devices to deliver 5 µL, 45 µL and 50 µL.
2. Precision multi-channel pipettes to deliver 45 µL, 50 µL and 150 µL.
3. Microplate shaker.
4. Automatic microplate washer (optional).
5. Photometric microplate reader and data analysis equipment.

Assay Procedure

50 µL of each Calibrator, or Control were added to the appropriate wells of the Antibody Coated Plate MICROPLAT in duplicate.

Then **5 µL** of sample and **45 µL** of Sample Diluent SAMPDIL were added to the appropriate wells of the Antibody Coated Plate in duplicate.

This has been dispensed within a period of 15 minutes to minimise drift.

After that a **50 µL** of PINP Biotin was added to all wells using a multichannel pipette.

Then the plate was covered with an adhesive plate sealer and incubated on a microplate shaker (500-700 rpm) at 18-30°C for 1 hour.

After incubation all wells were washed three times with Wash Solution, then the plate was inverted and tapped firmly on absorbent tissue to remove excess Wash Solution before proceeding to the next step.

150 µL of Enzyme was added to all wells using a multichannel pipette, then the plate was covered with an adhesive plate sealer and incubated at 18-30°C for 30 minutes then washed three times.

150 µL of TMB Substrate was added to all wells using a multichannel pipette, then the plate was covered an adhesive plate sealer and incubated at 18-30°C for 30 minutes.

After incubation a **50 µL** of Stop Solution HCL was added to all wells using a multichannel pipette, then the absorbance of each well was measured at 450 nm (reference 650 nm) using a microplate reader within 30 minutes of adding the Stop Solution.

Calculation of Results

The mean absorbance for each Calibrator, Control and sample were calculated by preparing a calibration curve on semi-log graph paper and plotting the mean absorbance for each Calibrator on the ordinate against concentration of PINP on the abscissa. The values for each control and sample read from the calibration curve were in ng/mL.

To obtain the concentration of PINP in each sample, the value read from the curve was multiplied by the dilution factor used (x10).

2.2.3.3. Sclerostin:

For the quantitative determination of mouse SOST concentrations in mice serum

ELISA kit was used provided from Quantikine catalogue Number MSST00.

Assay principle:

The SOST ELISA kit was provided by R&D and the assay used is a quantitative sandwich enzyme immunoassay. A monoclonal antibody specific for mouse SOST has been pre-coated onto a microplate. Standards, control, and samples are pipetted into the wells and any SOST present is bound by the immobilized antibody. After washing away any unbound substances, an enzyme-linked polyclonal antibody specific for mouse SOST is added to the wells. Following a wash to remove any unbound antibody-enzyme reagent, a substrate solution is added to the wells. The enzyme reaction yields a blue product that turns yellow when the Stop Solution is added. The intensity of the colour measured is in proportion to the amount of SOST bound in the initial step. The sample values are then read off the standard curve.

Reagents and materials provided:

96 well polystyrene microplate coated with a monoclonal antibody specific for mouse/rat SOST, conjugate, standard, control, assay diluent RD1W, calibrator diluent RD6-12, wash buffer concentrate, colour reagent A, colour reagent B, stop solution, and plate sealers.

Reagent Preparation:

All reagents were brought to room temperature before use, the control was reconstituted with 1.0 mL of distilled water to be assayed undiluted.

To prepare 500 mL of Wash Buffer, 20 mL of Wash Buffer Concentrate was added to distilled water. Colour Reagents A and B should was mixed together in equal volumes within 15 minutes of use and Protected from light.

The standard was reconstituted with Calibrator Diluent RD6-12 to produces a stock solution of 1000 pg/mL and the stock solution was allowed to sit for a minimum of 15 minutes with gentle mixing prior to making dilutions.

Using a polypropylene tubes, 200 µL of Calibrator Diluent RD6-12 was added into each tube and the stock solution was used to produce a dilution series: 1000 pg/mL, 500 pg/mL, 250 pg/mL, 125 pg/mL 62.5 pg/mL, 31.3 pg/mL and 15.6 pg/mL. The undiluted Standard (1000 pg/mL) serves as the high standard and the Calibrator Diluent RD6-12 serves as the zero standard (0 pg/mL).

Assay Procedure:

50 µL of Assay Diluent RD1W was added to each well then 50 µL of standard, control, and sample were added, after that, the plate was covered with the adhesive strip and Incubated for 3 hours at room temperature. Each well was aspirated and washed, this process was repeated four times for a total of five washes then each well was washed by filling them with Wash Buffer (400 µL) using a squirt bottle. After the last wash, any remaining Wash Buffer was removed by aspirating or decanting and the plate was inverted and blotted against clean paper towels.

100 µL of Mouse/Rat SOST Conjugate was added to each well then covered with a new adhesive strip and incubated for 1 hour at room temperature then the aspiration and wash was repeated as in previous step.

100 µL of Substrate Solution was added to each well and incubated for 30 minutes at room temperature with Protection from light.

100 µL of Stop Solution then added to each well with thorough mixing.

The optical density of each well was determined within 30 minutes, using a microplate reader set to 450 nm, and wavelength correction active at 570 nm to correct for optical imperfections in the plate.

Calculation of Results

The duplicate readings for each standard, control and sample were averaged and blank corrected. A standard curve was created using a four parameter logistic (4-PL) curve-fit, and sample values calculated using this standard curve.

2.2.3.4. Osteopontin:

For the quantitative determination of mouse OPN concentrations in serum, ELISA kit was used provided from R&D with catalogue number: M0ST00

Assay principle:

This assay employs the quantitative sandwich enzyme immunoassay technique. A polyclonal antibody specific for mouse osteopontin has been pre-coated onto a microplate. Standards, control, and samples are pipetted into the wells and any osteopontin present is bound by the immobilized antibody. After washing away any unbound substances, an enzyme-linked polyclonal antibody specific for mouse osteopontin is added to the wells. Following a wash to remove any unbound antibody-enzyme reagent, a substrate solution is added to the wells. The intensity of the colour measured is in proportion to the amount of osteopontin bound in the initial step. The sample values are then read off the standard curve.

Reagents and materials provided:

96 well polystyrene microplate coated with a polyclonal antibody specific for mouse OPN, standard: lyophilized recombinant OPN in a buffered protein base with preventatives, control: lyophilized recombinant OPN in a buffered protein base with preservatives, conjugate: 12 ml of a polyclonal antibody specific for mouse OPN conjugated to horseradish peroxidase with preservatives, assay diluent RD1W: 12 ml of buffered protein base with preservatives, calibrator diluent RD6-12: 2 vials(21 ml/vial) of diluted animal serum with preservatives, wash buffer concentrate: 21 ml of a 25-fold concentrated solution of buffered surfactant with preservative, colour reagent A: 12 ml of stabilized hydrogen peroxide, colour reagent B: 12 ml of stabilized chromogen (tetramethylbenzidine), stop solution: 23 ml of diluted hydrochloric acid, plate sealers: 4 adhesive strips.

Other required supplies; Microplate reader capable of measuring absorbance at 450 nm, with the correction wavelength set at 450 nm or 570nm, pipettes and pipette tips, deionized or

distilled water, squirt bottle, manifold dispenser, or automated microplate washer, 500 graduated cylinder, test tubes for dilution of standards and samples.

Reagent and sample preparation:

Mouse serum samples was diluted 100-fold dilution.

All reagents were brought to room temperature before use.

The mouse OPN control was reconstituted with 1.0 ml of distilled water and mixed thoroughly.

To prepare 500 ml of wash buffer, 20 ml of wash buffer concentrate was added to distilled water.

Substrate solution- colour reagent A and B were mixed together in equal volumes within 15 minutes of use and was protected from light.

The mouse OPN slandered was reconstituted with calibrator diluent RD6-12 to produce a stock solution of 2500pg/ml and kept for 5 minutes with gentle mixing.

To produce the dilution series, the stock solution was used after pipetting 200 µL of calibrator diluent RD6-12 in to 6 tubes and were mixed gently and thoroughly before the next transfer. The undiluted mouse OPN slandered (2500 pg/ml) serves as the high standard and the calibrator diluent serves as the zero standard (0pg/ml).

Assay procedure:

All reagents were brought to room temperature before use and all samples, control, and standards were assayed in duplicate.

After preparing all reagents, standard dilutions, control, and samples, the microplate was prepared by removing the strips from the frame. Then 50 µL of assay diluent was added to each well and 50 µL of standard, control, or sample were added per well as well and mixed by tapping the frame for 1 minute. The microplate then was covered with adhesive strip and incubated for 2 hours at room temperature. Each well was aspirated and washed five times by filling each well with wash buffer (400 µL) using a dispenser.

After removing any wash buffer with the last wash by aspirating and inverting the plate against clean paper towels, 100 µL of mouse OPN conjugate was added to each well, covered with a new adhesive strip and incubated for 2 hours at room temperature. The aspiration wash was

repeated then 100 µL of substrate solution was added to each well and incubated for 30 minutes at room temperature on the benchtop protected from light.

Finally 100 µL of stop solution was added to each well with tapping the plate gently to ensure thorough mixing then the optical density was determined for each well within 30 minutes using a microplate reader set at 450 nm.

Results calculation:

The duplicate readings for each standard, control and sample were averaged the average zero standard O.D was subtracted.

Standard curve was created by reducing the data using computer software capable of generating a four parameter logistic (4-pl) curve-fit.

2.2.3.5. CTX:

The quantitative determination of bone related degradation products from C-terminal telopeptides of type I collagen in mouse serum was measured by the RatLaps (CTX-I) EIA assay.

Assay principle:

The RatLaps™ (CTX-I) EIA is an enzyme-linked immunosorbent assay which requires the pre-incubation of the streptavidinated microtitre plate MICROPLAT with a biotinylated RatLaps Antigen Ag BIOTIN. The microtitre plate wells are then washed and 20 µL of each calibrator CAL 0-5, control CTRL or unknown sample are incubated together with the Primary Antibody Ab (polyclonal antibody against the peptide sequence EKSQDGGR) at 2 - 8°C. The wells are then washed and enzyme conjugate (peroxidase conjugated anti- IgG) added to bind to the primary antibody. A further wash step is conducted, following which a chromogenic substrate SUBS TMB is added to allow colour to be developed. The colour reaction is stopped upon the addition of Stopping Solution H2SO4 and the absorbance read in a microtitre plate reader, with the colour intensity developed being inversely proportional to the concentration of RatLaps antigen in the original sample.

Reagents and materials Provided:

- Antibody coated plate (MICROPLAT): Microwell strips (12 x 8 wells) pre-coated with streptavidin, supplied in a plastic frame.
- RatLaps Calibrator(CAL 0): TRIS buffered solution containing stabilisers and 0.05% sodium azide as

Preservative; 1 vial, 5.0 mL.

- RatLaps Calibrators (CAL 1–5): TRIS buffered solution containing a synthetic peptide (EKSQDGGR) with stabilisers and 0.05% sodium azide as preservative; 1 vial each (5 in total), 0.4 mL.
- Control (CTRL): TRIS buffered solution containing a synthetic peptide (EKSQDGGR) with stabilisers and 0.05% sodium azide as preservative; 1 vial, 0.4 mLy.
- Biotinylated RatLaps Antigen (Ag BIOTIN): PBS solution containing a biotinylated peptide (EKSQDGGR) stabilisers and 0.05% sodium azide as preservative; 1 vial, 12.0 mL.
- Primary Antibody (Ab): buffered solution containing a rabbit polyclonal antibody specific for a part of the C-telopeptide α chain of rat type I collagen with stabilisers and 0.05% sodium azide as preservative; 1 vial, 12.0 mL.
- Peroxidase conjugated anti- IgG (ENZYMCONJ): buffered solution containing a peroxidise conjugated anti- rabbit IgG antibody with stabilisers and 0.05% Proclin 300 preservative; 1 vial, 12.0 mL.
- Substrate Solution (SUBS TMB): tetramethylbenzidine (TMB) substrate in an acidic buffer, 1 vial; 12.0 mL.
- Stopping Solution (H2SO4): 0.18 M sulphuric acid; 1 vial, 12.0 mL.
- Washing Solution (WASHBUF 50x): Concentrated washing solution containing detergent and preservative; 1 vial 20.0 mL.
- Adhesive Plate Sealer: 8 per kit.

Other required Martials:

Containers for preparation of the Washing Solution, Precision pipetting devices to deliver 20 µL, Distilled or deionised water, Precision 8 or 12 channel multipipette to deliver 100 µL, ELISA plate reader with 450 nm and 650 nm reference wavelength, 2 – 8°C incubator, Vortex mixer, and Automatic microplate washer.

Reagents preparation:

All reagents were brought to room temperature (18 - 22°C) for a minimum of 60 minutes before use. The appropriate number of strips were placed in the plastic frame and the unused immunostrips were stored in the tightly closed foil bag with desiccant capsules. The washing

solution was prepared by diluting 50x in distilled or deionised water adding 1 part WASHBUF 50x to 50 parts water and mixed carefully.

Assay Procedure:

After preparation of reagents, a 100 µL of Biotinylated RatLaps antigen Ag BIOTIN was pipeted into each well, covered with sealing tape and incubated for 30 ±5 minutes at room temperature (18 - 22°C). After incubation, all wells were washed 5 times with 300 µL of wash solution prepared previously. Then, 20 µL of each calibrator CAL 0 - 5, control CTRL and unknown samples were pipetted into the appropriate wells on the Antibody Coated Plate MICROPLAT followed by 100 µL of Primary Antibody Ab and the plate was covered with an adhesive plate seal and incubated overnight (18 ±3 hours) at 2 – 8°C. After incubation, the washing steps were repeated again, then 100 µL of Peroxidase conjugated anti- IgG ENZYMCONJ was pipetted into each well and the plate was covered with an adhesive plate seal and incubate for 60 ±5 minutes at room temperature (18 – 22°C).

The washing steps were repeated, then, 100 µL of Substrate Solution SUBS TMB was pipetted into each well and the plate was covered with an adhesive plate seal and incubate for 30 ±2 minutes at room temperature (18 – 22°C) in the dark.

Finally, 100 µL of Stopping Solution H2SO4 was pipetted into each well and the absorbance was measured at 450 nm with reference at 650 nm using a microplate reader within 2 hours of stopping the reaction.

To calculate the results, the mean concentrations of samples and controls were calculated using a 4 parameter logistic (4PL) curve fit, and the calibrator 0 was included.

2.2.4. µCT scanning of mouse bones

Left and right tibias of young and aged mice were scanned by µCT using a Skyscan 1272 system with a rotation step size of 0.1° over 180°, an isotropic resolution set at1.25 µm, X-ray source at 50 kV and 200 µA, 0.5 mm aluminium filter, and averaging at 3. Images were reconstructed using Skyscan “NRecon” software which provides images of the analysed bones slice-by-slice. The reconstructed set of slices was then viewed in Skyscan’s “-Data-Viewer-” for analysis. Using Skyscan “CT-Analyser” or “CTAN” software the data set is then analysed for morphometry using a macro with a fixed threshold to differentiate bone from soft tissue. Next the osteocytes were identified as small pores inside the mineralised bones using macro

set designed by Professor Rob Van T Hof. For trabecular analysis measurements were taken from 400 slices immediately distal to the growth plate of tibias.

2.2.5. Immunohistochemistry

After µCT scanning, all samples were sectioned using the film cryosectioning method described by Kawamoto (Kawamoto and Kawamoto, 2014) as follows:

First, tibias were frozen with hexane dry-ice (Fig.2.1A). A proper amount of cooled embedding medium (SCEM) was placed in a stainless steel container (Fig.2.1B) then the frozen sample was placed in the embedding medium (Fig.2.1C) and the container quickly moved into the cooled hexane to enable the embedding medium to freeze completely (Fig. 2.1D) the frozen blocks were removed from the container (Fig. 2.1E) and fixed to the cryomicrotome sample holder (Fig.2.1F) using SCEM.

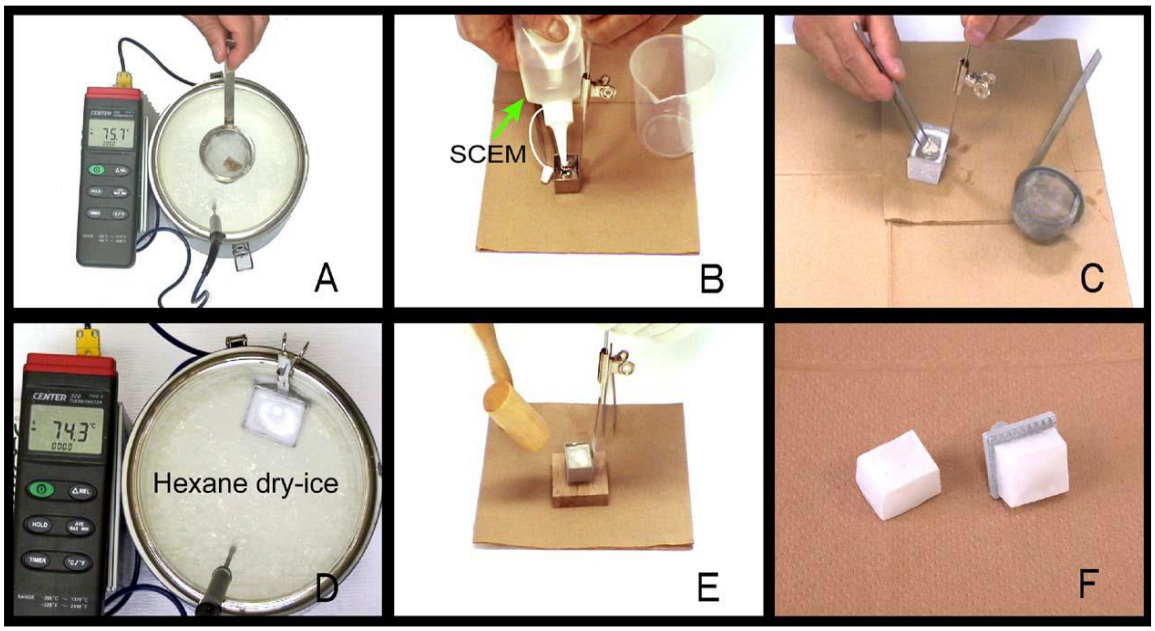

Figure 2.2. Preparing frozen sample blocks. A: freezing the sample, B: the mounting medium and stainless steel container, C and D: freeze-embedding in hexane dry-ice, E and F: fixing the frozen block to the microtome sample holder.

In order to cut hard tissues (bone), a tungsten carbide blade was used. The temperature of the cryostat chamber was usually kept at -15 to -20^{o}C. However, the temperature of

cryostat and the holder chuck adjusted to -25 and -35^{o}C respectively when cutting highly mineralized tissues. The frozen sample block was left in the cryochamber to acclimatize for approximately 10 min after fixing it to the sample holder chuck then the block was trimmed with a disposable tungsten carbide blade until the area of interest appears on the cut surface. After trimming, the blade was moved and a sharp blade edge was adjusted to the cut position. The adhesive film (Cryofilm) was mounted onto the cut surface with a fitting tool and the sample cut slowly at a constant speed. The sections were taken out of the cryochamber and left for 10-60 seconds in order to dry lightly then staining procedure was started by blocking with 10% donkey serum in PBS for 30 minutes. (The staining steps occurred by turning the specimen side down and immerse the section in the liquid).

After blocking sections were incubated with the primary antibody seclerostin diluted 1 in 100 of 10% of FCS in PBS overnight at 4^{o}C or 1-2 hours at room temperature, then washing with PBS 3 times for 10 minutes each time. Sections after that were incubated with the secondary antibody fluorescent diluted 1 in 200 of 10% FCS in PBS for 1 hour then they washed with PBS 3 times for 10 minutes each time. Finally, sections were mounted with specific mounting medium with DAPI (Vector laboratories) and covered with the cover slips and the edges were sealed completely with nail varnish to protect the sections from dryness till they have been imaged with the confocal microscope.

2.2.6. Imaging bone cryosections with confocal microscope

After immunostaining of the cryosections for SOST, the sections were imaged on a Zeiss LSM800 confocal microscope using a 40x oil immersion lens, resulting in a voxel size of 0.312 x 0.312 x 0.75 µm. The sections were imaged as stacks with sufficient layers to image the full thickness of the sections.

Sections were imaged for 3 fluorescence channels: AlexaFluor594 (red, SOST), Calcein (green, calcein labels) and DAPI (blue, nuclei). The settings for the channels are shown in Table 2.1.

Channel	AF594	Calcein	DAPI
Laser Excitation wavelength	561	488	405
Laser power	0.86%	0.08%	0.14%
Detection wavelengths	580-700	400-575	400-580
Detector Gain	737V	555V	699V
Pixel dwell time	68.94 µs	65.94 µs	65.94 µs
Averageging	2	2	2

Table 2.1: Confocal microscope settings for Imaging of SOST expression in osteocytes.

2.2.7. Histomorphometric analysis of bone formation rate

For analysis of bone formation, sections were stained in 0.1% Calcein Blue (adjusted to pH 8 using NaOH) for 3 minutes. After staining, the sections were washed three times in water and coverslipped using an aquous mountant with antifade (Vector laboratories). The sections were then imaged using a Zeiss Axio Scan.Z1 slide scanner (Carl Zeiss Ltd., UK) with a 20x lens using filter sets for DAPI and calcein, and a Zeiss Axioscan506 monochrome camera, resulting in an isotropic pixel size of 0.227 µm.

Histomorphometric analysis of bone formation was performed using a custom image analysis program (CalceinHisto), available at https://www.liverpool.ac.uk/ageing-and-chronic-disease/bone-hist/, developed by Prof. Rob van ‘t Hof (159). The software was written in Java and uses image processing modules from ImageJ.

2.3. *In vitro* loading:

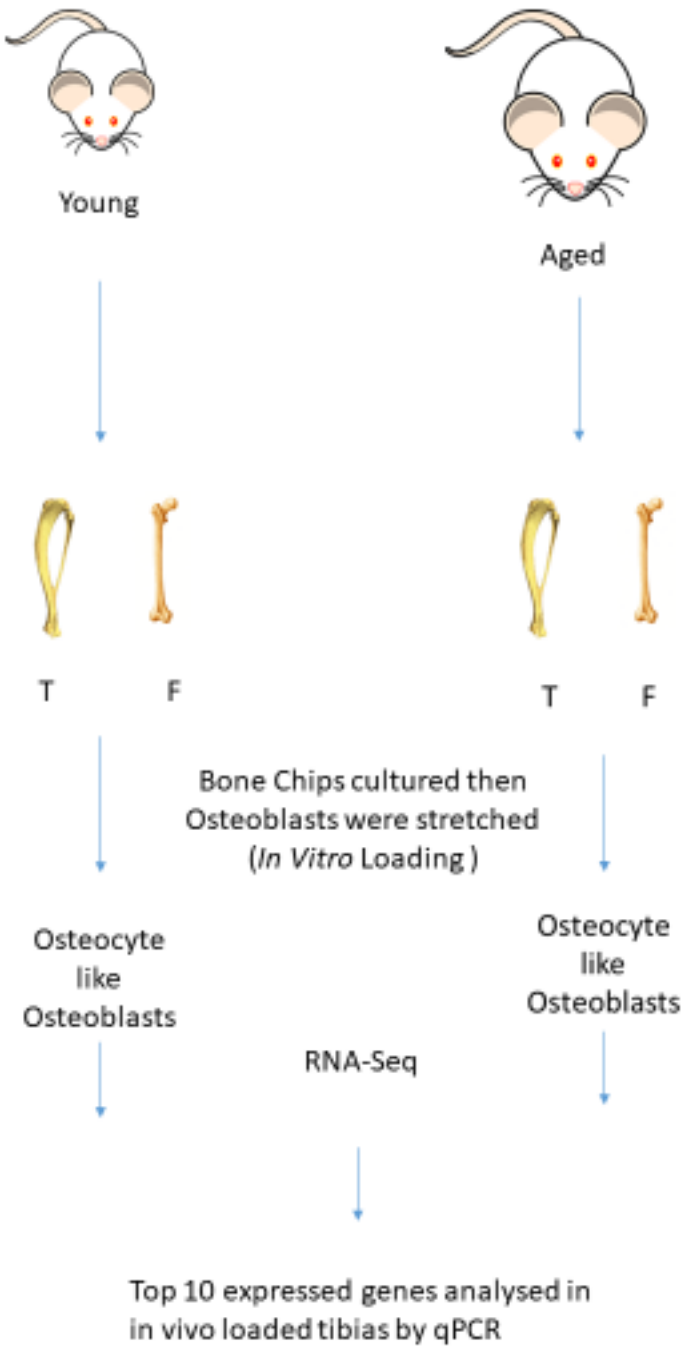

Figure 2.3. Schematic overview of the experimental design for the *in vitro* mechanical loading model for young adult and aged adult mice. T: Tibia, F: Femur.

S2.3.1. Tissue culture:

Two groups of young mice and aged mice were culled, and bone chips from the tibia and femur bone shafts were obtained as described above (paragraph 2.2.1.). After the collagenase treatment, the bone chips were washed with HBSS, and transferred to T25 flasks containing 5ml of standard αMEM each. Flasks were incubated for 3 days at 37°C in a humidified 5% CO_2 atmosphere to allow the attachment of the cells. After 3 days medium was removed then complete α MEM was added. Cells were left to grow out of the bone chips until semi-confluent with medium changes every 3-4 days.

After 3 weeks the cells were transferred to T75 to grow more cells by removing the media then washing 3 times with warm PBS then incubating the cells with trypsin for 3 minutes then adding media containing FBS 2 times of trypsin to inactivate the effect of trypsin.

Cells was centrifuged with 300g for 3 minutes after transferred to a 15ml falcon then the top supernatant removed and media added to the cells on the bottom then incubated with T75 for 2 weeks with changing media every 3 days.

2.3.2. In Vitro stretching of Osteoblasts (Flexcell Tension System):

After 2 weeks the Osteoblasts were trypsinised again, counted using a TC10 Bio-Rad Cell Counter, and plated at desired density (1×10^6 cells/well) in collagen coated stretch plates (6 well plates from flexcell). Stretching was performed in a Tension system for cell stretch (Flexcell) in a dedicated sterile humidified incubator at 37°C and at 5% CO2. The Tension system was set at 6% of strain at a frequency of 1 Hz using a continuous stretch for overnight. After completing the stretch protocol, cells were removed from the physical tension system then washed twice with sterile PBS and lysed using Trizol as described prior. The lysate was then collected in a sterile Eppendorf tube and stored at -80 °C.

The Flexcell Tension System is composed of a loading post were the coated plates are physically placed and a controlled vacuum pump. Pumps remove air from the space between the loading post and the coated surface, creates a vacuum, which allows to mechanical strain the culture as indirect movement of the loading post. Flexcell Tension System was inserted in a dedicated humidified incubator, having tubes connected to the vacuum pump outside of the incubator (figure 2.2 A and B).

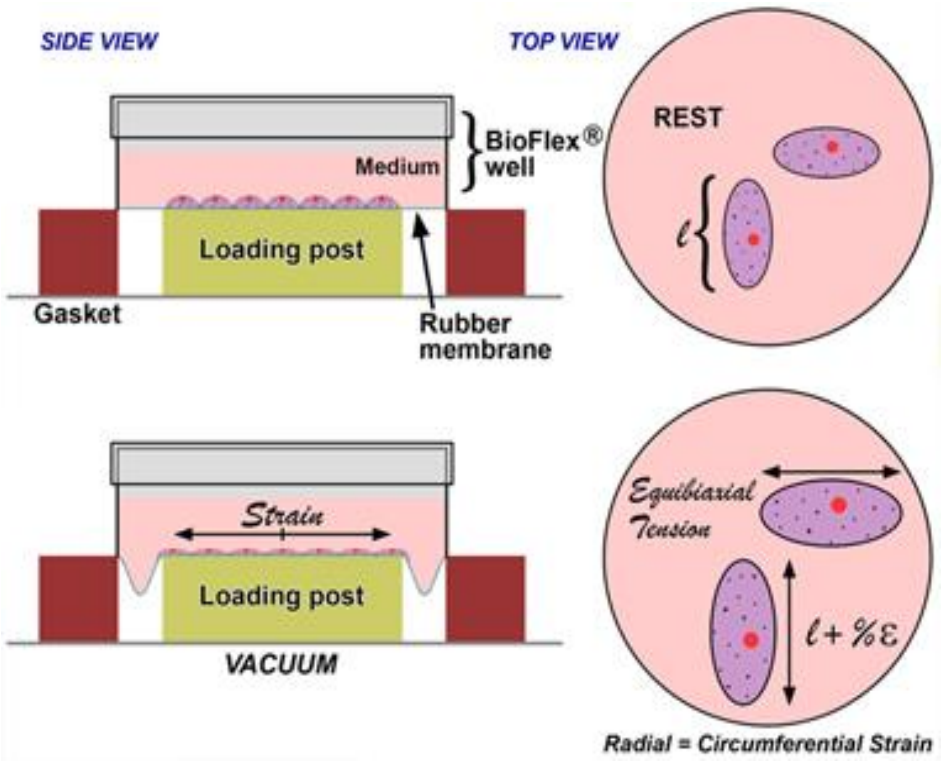

A

B

Figure 2.4. Schematic representation of Flexcell Tension System. (A) Representing strain related change on the culture from static state, (B) Photograph of the general System appearance without pump connection.

2.3.3. Complementary DNA (cDNA) synthesis

After RNA quantification using the Nano Drop, cDNA was synthesized using the EvoScript Universal cDNA Master (Roche) according to the manufacturer's instructions. All reagents were vortexed and centrifuged briefly before use. 1µg of RNA sample was used with 4µl of 5x concentrated Reaction buffer and PCR grade water to a final volume of 18µl in 0.25ml Eppendorf. Tubes were mixed well and centrifuged then incubated for 5 minutes at room temperature. After that, 2µl of 10x concentrated Enzyme mix was added and mixed well. Tubes were then incubated in a SimpliAmp Thermal Cycler using the following protocol: First, 15 minutes at 42^{o}C temperature; second, 5 minutes at 85^{o}C temperature; third, 15 minutes at 65^{o}C temperature; finally, at 4^{o}C for ∞duration. The resulting cDNA was stored at -20°. The cDNA synthesis was performed in triplicate for each RNA sample.

2.3.4. Real-time quantitative PCR

The LightCycler 480 probes master from Roche was used and the master mix was prepared as follows:

Reagent	**Volume for 1 sample**
Probes Master (2x)	5µl
Primer forward	0.4µl
Primer reverse	0.4µl
Probe	0.2µl
Water	3µl

Table 2.2: RT-qPCR master mix ingredient list for Roche primer probe sets. A different master mix was made up for each gene of interest.

Reagent	**Volume for 1 sample**
Probes Master (2x)	5µl
Primer/Probe assay	0.5µl
Water	3.5µl

Table 2.3: RT-qPCR master mix ingredient list for Fisher Scientific primer/probe assays. A different master mix was made up for each gene of interest.

After master mix was prepared, for each sample 9µl of master mix and 1µl of cDNA was added to a well in a 96-well PCR plate (Roche) making up a total reaction volume of 10µl. For all RT-qPCR, the Mono Colour Hydrolysis Probe/UPL was followed using the following settings:

Step	**Cycle(s)**	**Temperature**	**Time**
Pre-incubation	1	95°C	10min
Amplification	45	95°C	10sec
		60°C	30s
		72°C	1s
Cooling	1	40°C	30s

Table 2.4: RT-qPCR run program.

All RT-qPCR was performed using a Roche Lightcycler 480 and every sample was analysed in triplicate. CT values were obtained and expression relative to HMBS (housekeeping gene) was calculated. The housekeeping gene (HMBS) was chosen based on a study by Stephens *et al* (160). All primer/probe sets used had either been pre-validated by the lab group or validated by Roche or Taqman RealTime ready single assays.

Statistical analysis of all data was performed by one way ANOVA using Graph pad Prism, using a Sidak's multiple comparison test as post hoc test to identify differences between individual groups.

CHAPTER 3. Effect of Mechanical Loading on Bone Turnover Markers in Young Adult and Old Adult Mice.

3.1. Introduction:

Bone is remodelled throughout life. Remodelling starts with bone resorption by osteoclasts followed by bone formation by osteoblasts. Osteocytes act as mechanosensors and orchestrate the bone remodelling process. In normal bone, formation and resorption are balanced. This balance changes in ageing, leading to age-related loss of bone volume and strength (chapter1.paragraph5).

As a response to mechanical loading Osteocytes can produce molecules to regulate bone formation, or degradation in the absence of such kind of loading stimuli. Much more understanding of the molecular mechanisms that control the adaptive response of osteocytes to mechanical stimuli may lead to the development of new strategies towards fracture prevention and enhanced bone healing (161).

Biochemical markers of bone metabolism provide dynamic information about bone tissue turnover, they can be classified either as bone formation or bone resorption markers.

Bone has usually been considered as a structural organ that supports movement of the body and protects the internal organs. However, evidence has been accrued showing that bone also behaves as an endocrine organ(162), and that some of the markers of bone turnover can act as endocrine factors such as osteocalcin, FGF23 and sclerostin. Bone-derived fibroblast growth factor 23 (FGF23) for instant, is mainly secreted by osteoblasts and osteocytes but plays important roles in regulating phosphate homeostasis by inhibiting phosphate reabsorption and 1,25-dihydroxyvitamin D_3 production in the kidney and suppressing parathyroid hormone (PTH) synthesis in the parathyroid gland

which reduces the circulating phosphate levels(163). Therefore, changes in the secretion profile of bone with ageing, may affect ageing in tissues other than bone.

In this chapter I present the results of my study into the change in bone turnover markers with ageing in mice. I analysed serum markers of bone formation and bone resorption in young adult (3-4 months of age) and aged (14 months of age mice. Furthermore, I studied the effect of ageing on the bone anabolic response to mechanical loading.

3.2. Serum markers studied

3.2.1. Osteocalcin:

Osteocalcin is a 49-amino acid in human (46 in mouse) non-collagenous protein of bone matrix mineralisation produced by osteoblasts. Its synthesis is dependent on the presence of active 1, 25-dihydroxyvitamin D and requires vitamin K as a cofactor for the γ-carboxylation of its three glutamate residues to become γ-carboxyglutamate (Gla osteocalcin) by γ-glutamyl carboxylase(164). This modification leads to most secreted osteocalcin to be embedded in the bone matrix, as the γ-carboxylation increases its affinity for hydroxyapatite crystals(165). The acidic environment produced during bone resorption processes by osteoclasts stimulates decarboxylation of γ-carboxylated osteocalcin (GlaOC) trapped in the bone matrix into the Glu osteocalcin form again, reducing its affinity for hydroxyapatite and therefore promoting its release into the circulation where it can be measured by immunoassay(166). osteocalcin is degraded and excreted by the kidney. Therefore, serum concentrations of osteocalcin and its fragments are increased in patients with renal failure(167). Furthermore, osteocalcin plays different endocrine rules in many organs, it acts as a blood glucose-lowering hormone by stimulating insulin

secretion by β-cells and by favouring insulin sensitivity in muscle, liver, and white adipose tissue(168).

3.2.2. P1NP (Procollagen type 1 N-terminal propeptide):

Collagen type I is the most abundant protein of the bone and accounts for higher than 90% of the organic bone matrix which is developed from procollagen type I which in turn synthesized by osteoblasts and fibroblasts. During collagen maturation, after secretion of procollagen type I into the extracellular space, its aminoterminal and carboxyterminal propeptides (PICP and PINP) are cleaved off from both sides by specific proteases and released into the circulation(167) during its conversion to collagen type I. The mature collagen type I is then association into fibrils. P1NP is usually released in the trimeric structure (molecular weight =35,000) and then is rapidly broken down to a monomeric form by thermal degradation effects. P1NP antibodies are used to detect the trimeric structure of P1NP by ELISA or radioimmunoassay (RIA). There are two automated P1NP assays: 'total P1NP' which detects both the trimeric and monomeric forms of the peptide, and 'intact P1NP' which detects only the trimeric form. Because trimeric P1NP is cleared by the liver and monomeric P1NP is cleared by the kidney, total P1NP increases in kidney failure but intact P1NP does not(169,170).

The serum levels of P1NP have been validated as a marker for bone formation rate in osteoporosis and its measurement is being developed to be used widely in clinical applications as a specific indicator of type I collagen deposition(171).

3.2.3. Sclerostin:

Sclerostin has described briefly in the introduction chapter, paragraph 1.4

3.2.4. CTX:

The C-terminal telopeptide of fibrillar collagens (type I and II), CTX also known as carboxy-terminal collagen crosslinks. It is a specific biomarker in the serum to bone resorption(172). Carboxy-terminal crosslinked of collagen type I (CTX-1), the linear eight amino acid sequence, and the amino-terminal crosslinked (NTX-1) both are fragments of degraded collagen type I released during bone resorption via unspecific types of proteinases including, cathepsin K, as it is selectively expressed by osteoclasts(173). Recent study has shown that CTX-1 is a specific and sensitive biomarker of bone resorption that can rapidly indicate the response to bisphosphonate therapy for postmenopausal osteoporosis (174).

3.2.5. Osteopontin (OPN):

Osteopontin, also known as bone sialoprotein I (BSP-1), it is a pluripotent soluble protein found in all body fluids and expressed in many tissues and cells. It stimulates signal transduction pathways via integrin and CD44 alternatives that regulate several cellular activities including the interaction between cells and the extracellular matrix(175).

OPN is a 34 kDa non-collagenous protein that was first isolated from bone and its fragments are implicated in many signalling functions. It plays an important role in bone mineralisation and binds to extracellular calcium via its phosphorylated (serine and threonine) and acidic (aspartate and glutamate) residues (176). Recent studies have demonstrated that osteocalcin and OPN together were shown to enhance fracture strength of bone and the absence of these proteins reduces the elasticity of bone matrix and its ability to tolerate cyclical loading(177). OPN also promotes cell-mediated immune responses, and plays a role in chronic inflammatory and autoimmune diseases. Besides its

function in inflammation, OPN work as a potent inhibitor of vascular calcification(178).

3.3. Methods:

To assess the difference in response to mechanical loading in bone between young adult and old adult mice by measuring the circulation biochemical markers, female C57/bl6 mice in two different age groups, young (3 months old, N=20) and aged (15 months old, N=20) were used for this experiment.

The right tibia bones 12 mice in each age group were loaded as described in chapter 2, and 8 mice of each group used as unloaded control. Serum was obtained from all mice as described in chapter 2 and biochemical markers concentrations were measured by ELISA.

Statistical analysis of the data was performed by one way ANOVA using GraphPad Prism, using a Sidak's multiple comparison test as *post hoc* test to identify differences between individual groups.

3.5. Results:

The volume of serum obtained for each mouse varied between mice, and some mice did not produce sufficient serum to run all ELISAs. Furthermore several samples suffered from erythrolysis and were not suitable for analysis. Therefore the number of data points for the analysis was reduced with the final number of data points for each group stated in the figure legends.

3.5.1 Osteocalcin:

There was no significant effect of mechanical loading on osteocalcin levels in either the young or aged group, although there was a slight trend for an increase in the aged group (Fig. 3.1; p=0.2). When the data from loaded and non-loaded controls from each age were pooled, there was an unexpected statistically

significant 26% increase (p<0.001) in osteocalcin levels in the loaded aged mice group in comparison with the loaded young group.

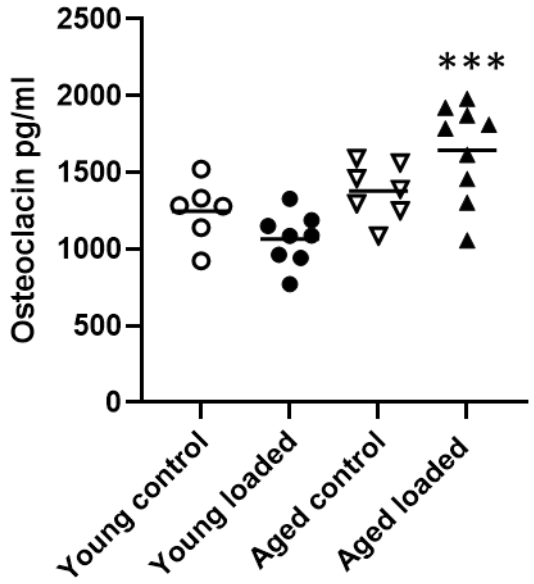

Figure 3.1. Osteocalcin serum levels in young and aged mice after loading. Young (3-months-old, N=8 loaded; N=6 control) and aged (15-month-old N=9 loaded; N=7 control) mice underwent repetitive loading of the right tibia. At the end of the experiment, serum was collected and analysed by ELISA for osteocalcin levels. Data were analysed using ANOVA. ***: p< 0.001 aged loaded versus young loaded.

3.5.2 P1NP:

As shown in Figure 3.2, mechanical loading of the tibia lead to a significant decrease in the P1NP levels in both young (p< 0.001) and aged (p<0.001) mice. Furthermore, P1NP levels were significantly lower in aged than in young mice (p=0.004), indicating reduced bone formation in aged mice.

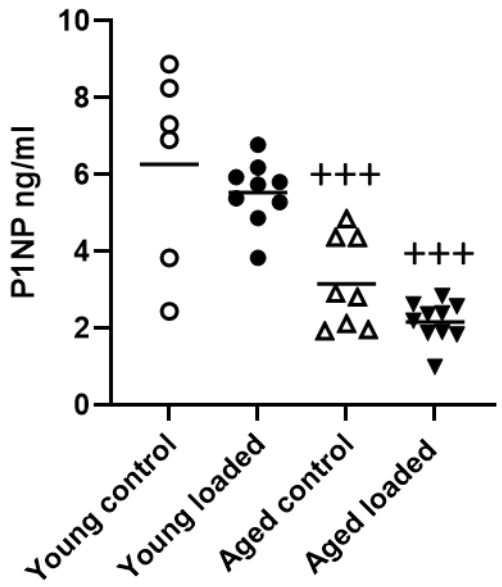

Figure 3.2. P1NP serum levels in young and aged mice after loading.
Young (3-months-old, N=9 loaded; N=6 control) and aged (15-month-old, N=10 loaded; N=8 control) mice underwent repetitive loading of the right tibia. At the end of the experiment, serum was collected and analysed by ELISA for P1NP levels. Data were analysed using ANOVA. ***: p< 0.004 Young versus Aged. +++: p<0.001 Loaded versus non-Loaded controls.

3.5.3. Sclerostin:

Overall results represent in figure 3.3. showed no differences in sclerostin levels between groups after loading and no significant decrease of sclerostin levels on old age mice group after loading compared to old un-loaded controls (p=0.08).

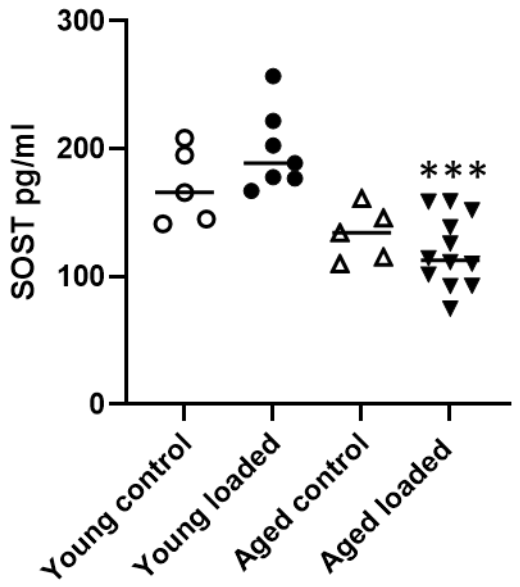

Figure 3.3. Sclerostin serum levels in young and aged mice after loading. Young (3-months-old, N=7 loaded; N=5 control) and aged (15-month-old N=12 loaded; N=5 control) mice underwent repetitive loading of the right tibia. At the end of the experiment, serum was collected and analysed by ELISA for sclerostin levels. Data were analysed using ANOVA. ***: P<0.001 aged loaded versus young loaded.

3.5.4. CTX:

Results revealed significant changes in CTX serum levels after loading in booth age groups as Figure 3.4. Showing highly significant decrease in CTX concentrations in young loaded mice group in comparison with the young un-loaded controls ($p<0.001$), and no statistically significant increase in old age loaded mice in comparison with the old un-loaded controls.

Further observation can be seen in this figure in the very highly significant decrease on CTX levels between the control old and young mice groups ($p=0.0002$).

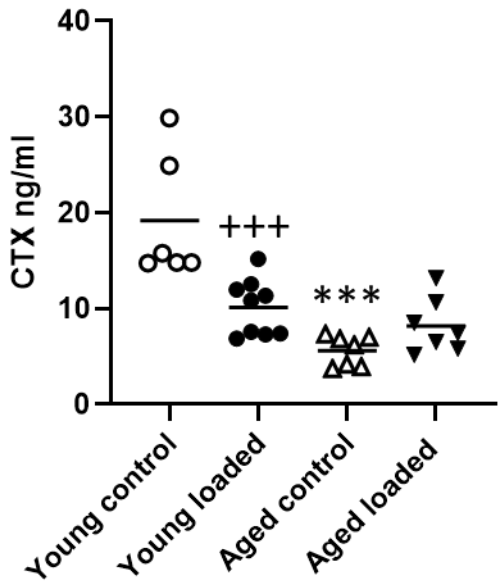

Figure 3.4. CTX serum levels in young and aged mice after loading.
Young (3-months-old, N=9 loaded; N=6 control) and aged (15-month-old N=7; N=7 control) mice underwent repetitive loading of the right tibia. At the end of the experiment, serum was collected and analysed by ELISA for CTX levels. Data were analysed using ANOVA. ***: p< 0.0002 Young control versus Aged control. +++: p<0.001 young loaded versus non-Loaded (control).

3.5.5. Osteopontin:

Overall results represent in figure 3.5. showing no differences in osteopontin levels between groups after loading, and there is a no significant increase of osteopontin levels in old age mice group after loading compared to old un-loaded controls (p=0.06).

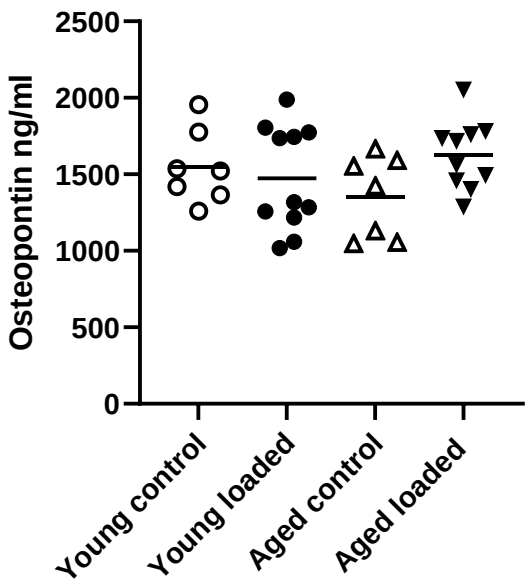

Figure 3.5. Osteopontin serum levels in young and aged mice after loading. Young (3-months-old, N=11 loaded; N=7 control) and aged (15-month-old N=10 loaded; N=7 control) mice underwent repetitive loading of the right tibia. At the end of the experiment, serum was collected and analysed by ELISA for osteopontin levels. Data were analysed using ANOVA.

As there were only few significant changes in serum markers between loaded and unloaded mice, I next pooled the values for all young mice and compared these to pooled results for the aged mice. There was no difference between young and aged mice for serum levels osteopontin. SOST levels were significantly decreased by 35% in the aged mice, whereas osteocalcin levels were increased by 25% in the aged mice (fig. 3.6). Serum levels of both P1NP and CTX showed a significant 2-fold reduction in aged mice (Fig 3.7), indicating a reduction in bone turnover in the aged mice compared to the young mice.

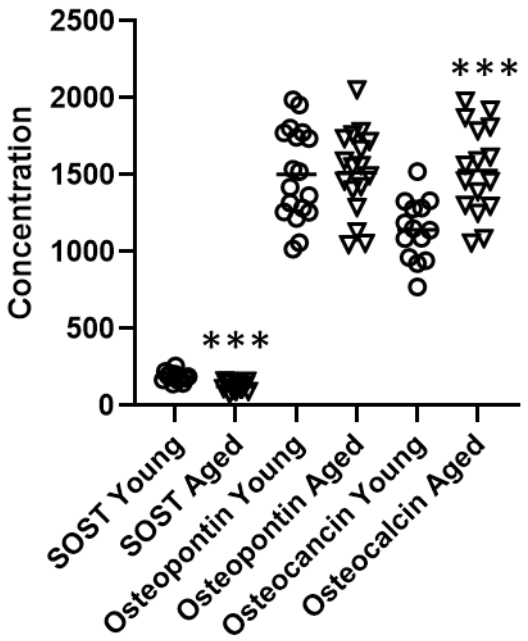

Figure 3.6. Pooled analysis of serum sclerostin, osteopontin and osteocalcin levels in young and old female mice.

Data for loaded and non-loaded mice were pooled in each age group and analysed using a t-test. Data represent average with standard deviations. Concentrations for SOST and osteocalcin are shown as pg/ml, and concentrations for osteopontin in ng/ml. ***: $p<0.001$ between young and aged. N=12 young; N=17 aged for SOST levels, N=18 young; N=17 aged for osteopontin levels, N=14 young; N=16 aged for osteocalcin levels.

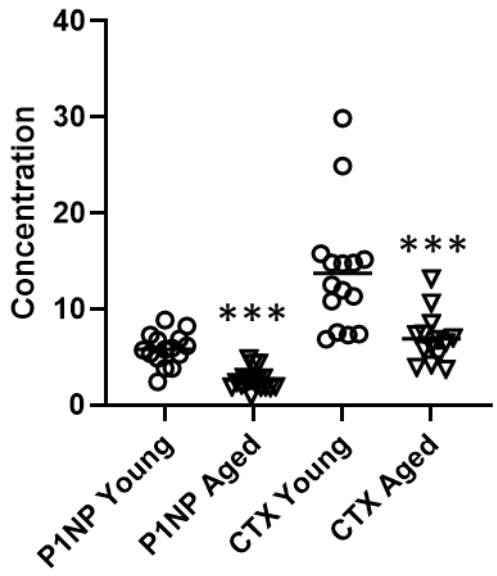

Figure 3.7. Pooled analysis of serum P1NP and CTX levels in young and old female mice.
Data for loaded and non-loaded mice were pooled in each age group and analysed using a t-test. Data represent average with standard deviations. There was a significant decrease of both bone turnover markers in aged mice. ***: $p<0.001$. P1NP and CTX concentrations are shown in ng/ml. N=17 young; N=18 aged for P1NP levels, N=15 young; N=14 aged for CTX levels.

3.6. Discussion:

Osteoporosis is a skeletal disease associated with aging, distinguished by low bone mass and associated with compromised bone microarchitecture, leading to reduced bone strength and increased risk of fractures(179). The skeleton is a dynamic organ and has the capacity to adapt itself to its mechanical environment. The control of mechanosensitive Osteocytes orchestrates the activity and enrolment of osteoblasts and/or osteoclasts by producing a variety of signalling molecules, results to the formation of a bone structure that provides an appropriate resistance to fractures and gives the bone its adaptation to mechanical loading (180).

Age-related fragility fractures indicate bone mass deficiency. In contrast mechanical loading is important for maintaining bone strength, and it has a good prospective for prevention of osteoporosis and even treatment(181).

On this view our results showed significant increase on osteocalcin, (a good serum biomarker for bone formation) levels in aged mice after loading the right tibia bone for two weeks in comparison to the old controls that did not have the mechanical loading stimuli as shown in figure 3.1. However, P1NP levels, which is a bone formation biomarker as well showed significant decrease in serum concentrations of old age mice compared with the young once even after loading as we can see a significant decrease in old loaded group compared with the young loaded mice.

Our results are in agreement with a cross-sectional study of human data (Shao et al. (182)) by analysing seven bone turnover and metabolic indicators from 1036 patients between January 2018 and October 2019. Their findings suggested that P1NP and β-CTX are highly correlated with age as they found that concentrations for these markers were significantly higher in young patients compared to aged patients. Our data are in disagreement with others(183). In contrast our results unexpectedly showed significant increase in osteocalcin levels in aged group compared to the young group (fig. 3.1.).

It is difficult to rely on osteocalcin results because of its limited sensitivity and rapid degradation, and this may have affected my results. Compared to P1NP, variance was considerably higher in the osteocalcin assay, possibly reflecting the known instability of this protein. As a hormone, osteocalcin regulates three key hormones involved in energy metabolism and it targets at least three organs: pancreas, where it promotes insulin secretion; adipocytes, where it stimulates adiponectin expression; and Leydig cells, to promote testosterone production.

In addition to its associated with HbA1c and type II diabetes. On these bases, extensive studies suggested that osteocalcin is associated to metabolic syndrome(184). As a result bone is not the only organ which is implicated to osteocalcin and the changes in term of the two parameters, ageing and mechanical loading might not give an accurate results as expected. However our results in figure 3.1. Showing decline in osteocalcin concentration in young loaded group compared to the control young group comes in agreement with a study by Mathew J. Silva and his group in Washington University as they found that mechanical loading for mice tibia bone increases cortical bone volume and there results showed significant decline of osteocalcin and CTX levels in young mice from 2-4 months old (185).

In agreement with this study, our results in figure 3.4 Showing significant decrease in CTX concentrations on the loaded young group compared to the control young group which shows that mechanical loading was effective on reducing bone resorption in young mice. However, in the aged group, results in figure 3.4. I observed the reverse as the loaded old group showed an increase in CTX levels compared to the control unloaded old group. These results indicate that aged mice do not respond with a reduction in bone resorption after mechanical loading. The CTX levels were decreased in control aged mice compared to control young mice, and this indicates an overall reduction in bone resorption. This contradicts the general idea that bone resorption is increased with ageing. However, unlike aged mice, the young adult mice still had an active growth plate, which have abundant, highly active osteoclasts, and in general have higher bone volume. Therefore, although resorption maybe increased in aged mice per bone surface, because of a much higher bone surface in young mice, total systemic bone resorption as reflected by the CTX assay could be decreased as I observed in this study.

Because the half-life of serum CTX is about 1 hour and because of the sensitivity of the assay to the food intake and it is suppressed by diurnal variation with the day hours, it preferred to be measured fasting at 08.00–09.00 am (186). Modelling techniques showed that serum CTX show considerable diurnal variation with a maximum at about 5 am, a minimum at about 2 pm, and a magnitude of about 40% around the 24-hour mean.

In consideration of the importance of sclerostin as a negative regulator of bone formation, our results showed decreased in SOST levels in aged mice compared to the young ones and a significant decrease in its levels even after loading in aged compared to young.

Osteopontin levels had a high variance in all the groups. It is very well possible that we could not detect any changes due to loading or ageing because only one bone in each mouse was loaded, while there was no change in loading in the rest of the skeleton. It is therefore possible that the contribution of the loaded bone to circulating levels of sclerostin and osteopontin was too small to be measured by the assays used. To assess the effects of loading on the local production of sclerostin in the loaded bone would need a more targeted approach such as immunohistochemistry. These studies will be described in Chapter 4.

Chapter 4. Effects of Ageing on adaptation to *in vivo* mechanical loading

4.1. Introduction

Mechanical adaptation to loading of bone appears to be compromised in both aged mice and humans (187). The exact underlying mechanisms are currently unclear. However osteocytes are the main mechanosensing cells in bone, and therefore changes in osteocyte number or activity are highly likely to play a role in the age-related reduced anabolic response to loading.

Sclerostin is secreted by the osteocyte and acts as an extracellular inhibitor of canonical Wnt signalling pathway by binding to the lipoprotein receptor-related protein-4 (LRP4), LRP5 and/or LRP6(188). Absence or decrease in sclerostin, reveal increased bone mass(188).

The question is, what is the relation between mechanical loading and seclerostin expression by osteocytes?

Robling et al. (189) have demonstrated that one of the hypothetically important mechanism by which mechanical loading controls osteocyte activity is by regulating sclerostin expression. His experimental model of loading the mouse ulna down regulates sclerostin expression, has been followed by multiple experimental loading models (190–197), that led to a suggestion simplified as follows: The local, loading-related down-regulation of osteocyte sclerostin increases bone formation by inhibiting the canonical Wnt signalling in osteoblasts whereas also, directly or indirectly by regulating the OPG that overturning the resorptive activity of osteoclasts. The validation of this model has been strongly supported by the responses of transgenic mice by sclerostin expression changes with loading. However, recent findings (198) of sclerostin-independent changes in bone formation following loading have demonstrated that this model is rather over-simplified. In addition, the mechanisms by which loading-related stimuli initiate this process by down-regulating sclerostin still unclear.

Measurement of bone mass using the Dual-Energy X-ray Absorptiometry (DEXA) scanner has been shown to be a valuable parameter in the assessment of bone fragility during ageing. However, bone mass can only partially explain the age-related decrease in bone strength (199). The other bone quality factors that affect bone strength include bone microstructure and the material properties of the bone tissue.

DXA analysis, for instance, has low sensitivity for detecting the changes in bone density that occur after ovariectomy especially in mice comparing to µCT analysis. That is because DXA scanners cannot separate cortical bone from trabecular bone, which has the most of the changes occurs on it. Van't Hof Robert and Dall'Ara Enrico(200) have found that the Piximus scanner shows bone loss at the proximal tibia of about 5–10% 3-weeks after ovariectomy in mice (which is barely statistically significant using ten animals per group), while analysis of a similar experiment using µCT analysis showed a highly significant 30–40% decrease of trabecular bone at the same site.

At the cellular level, osteocytes which are the most abundant bone cells, have several functions, including regulation of osteoid matrix maturation and mineralization(201) and the unique mechano-sensation (202) that osteocytes translate mechanical stimuli into electrical or biochemical signals and orchestrate the actions of osteoclasts and the osteoblasts formation bone homeostasis(203). Osteocytes form a connected network within the bone matrix through their dendritic processes located within the canaliculi, through which the osteocytes communicate with each other and cells on the bone surface(204). Thus, the anatomical study of osteocyte status is of high importance. To date, most imaging studies on osteocytes used microscopic techniques such as light microscopy(205), confocal microscopy (206,207), scanning electron microscopy (SEM) (208,209) and transmission electron microscopy (TEM) (210,211). These techniques provide only 2D observations or they are limited to at best a few tens micrometres in depth of the bone tissue. As a result, comprehension of three-dimensional (3D) organisation of osteocytes is difficult. To study the osteocyte environment in un decalcified sample, confocal laser scanning (CLS) microscopy, which allows the non-destructive histotomography of bone made it possible to observe osteocytes in bone by labelling the cells with fluorescence and using three-dimensionally reconstructed fluorescent images (206). On the other hand, µCT imaging and desktop high-resolution µCT scanners have been developed to visualize osteocyte lacunae and canaliculi, which were not visible with other 3D non-destructive imaging techniques, and are now of increasing interest to study perilacunar remodelling.

This chapter is analysation of the effect of ageing on the bone anabolic response to loading using the *in vivo* mouse model of loading of the tibia (158). In addition, it includes analysation of osteocyte distribution in this model by µCT and histological approaches, and changes in

sclerostin, the major regulator of osteoblast differentiation and activity (212), expression in osteocytes.

4.2 Methods

4.2.1 Animals

Procedures were performed on female C57/bl6 mice. Ages studied were 3-months of age (N=6), and 15 months of age (N=6). Mechanical loading was performed as described in Chapter 2 paragraph 2.2. Mice were labelled with calcein as described in 2.2, 7 days and 3 days before culling. After culling, the tibias were fixed overnight in buffered formalin and scanned by µCT with very high resolution imaging option that takes about 7 hours to get around 2000 slices. After µCT scanning, the tibias were processed for film cryosectioning as described in 2.2.4. Then slides were Immunohistochemistry stained with SOST primary antibody and fluorescent secondary anti body and some with calcein counter stain. Slides then imaged with confocal microscope and florescent microscope and then data analysed.

4.2.2 Development of SOST immunostaining for bone sections

4.2.2.1. Vectastain ABC method

Mouse tibias were fixed in paraformaldehyse fo0r 24h, dehydrated through graded alcohol, cleared in Xylene and embedded in wax. Blocks were sectioned at 5 µm, and dewaxed in xylene, rehydrated to water. Endogenous peroxide activity was bquenched using Blockall(Vector laboratories). I used the R&D anti-SOST primary antibody, and a biotinylated anti-goat secondary antibody. Titrtations of the antibofy showed optimal results at a: 100 dilution of the primary antibody and 1:200 for the secondary antibody. The first Immunostain method tried used the Vectastain ABC Kit with Nova red as the dye.

Immunohistochemistry on wax sections (ABC Kit) procedure:

Sections were dewaxed in xylene for 5 minutes and rehydrated for 1 minute in each 100% IMS twice, in 90%, 70% and distilled water for 5 minutes. Then the sections were incubated in the oven with the antigen retrieval (citrate buffer) for one hour at 37°C, then washed in PBS-T (PBS solution with 0.1% Tween) twice for 5 minutes. The next step was using 0.3%

hydrogen peroxide for the exogenous peroxidase activity blocking for 15 minutes at 37^{o}C or for 30 minutes at room temperature, then washed in PBS twice for 5 minutes. Sections then incubated for 20 minutes with diluted normal blocking serum and washed in PBS-T twice for 5 minutes. After that sections were incubated for 30 minutes or overnight with primary antibody diluted in buffer then washed in PBS twice for 5 minutes. Then sections were incubated for 30 minutes with diluted biotinylated secondary antibody and washed in PBS twice for 5 minutes. Then incubated for 30 minutes with VECTASTAIN ABC reagent and washed in PBS twice for 5 minutes, then incubated in peroxidase substrate solution NovaRED or DAB (after their preparation).

In some cases sections underwent antigen retrieval using sodium citrate buffer (PH=6) and boiling in a microwave for 2 minute. However, this resulted in all the cortical bone tissue falling of the slide.

To prevent tissue falling of the slides during antigen retrieval, I next used a water bath at 80^{o}C 60^{o}C for 30 minutes incubation or. However, this still resulted in loss of about 50% of the tissue. Finally, I used incubation in an oven at 37^{o}C for one hour. Although the tissue stayed on the slide, there was no difference in staining intensity with slides that did not undergo antigen retrieval. Increasing the incubation time to two hours did not improve staining intensity and led to high background stain, Figure 4.1.

The general procedure for staining with Vectastain ABC system is applying the primary antibody followed by biotinylated secondary antibody and then performed avidin and biotinylated horseradish peroxide macromolecular complex. The horseradish peroxidase is visualized by the development of a peroxidase substrate that produces the colour. However as this technique did not give a satisfactory staining levels, I used another method; ImmPRESS Reagent, which uses secondary antibodies tagged with a polymerised HRP for signal amplification.

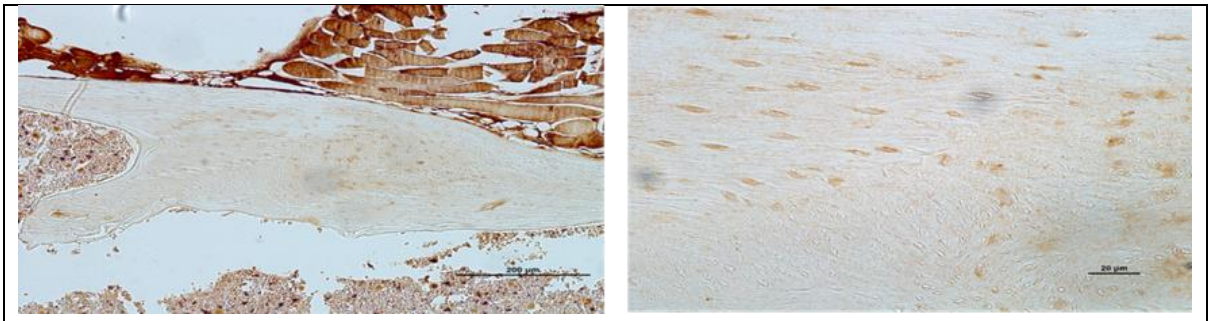

Figure 4.1. Longitudinal Wax Sections in mouse tibia bone using Vectastain ABC kit, Sodium Citrate Buffer antigen retrieval, NovaRED peroxidase substrate. SOST primary antibody 15 mg/ml diluted 1in 100 PBS and biotinylated secondary antibody.

4.2.2.2. ImmPRESS (polymerized reporter enzyme staining system)

Wax sections were stained using ImmPRESS polymerized reporter enzyme staining system which is an enzymatic, non-biotin, one-step detection kit that provides very high sensitivity with very low background staining; I used citrate buffer antigen retrieval.

ImmPRESS procedure:

Sections were dewaxed twice in xylene for 5 minutes each and rehydrated for 1 minute in each 100% IMS twice and in 90%, 70%, 50% and distilled water. Sections then incubated in the oven with UNI-TRIEVE antigen retrieval for 30-60 minutes at 70^{o}C, then washed with PBS twice for 5 minutes. Sections were blocked exogenous peroxidase activity with BLOXALL for 10 minutes and washed in PBS twice for 5 minutes. Sections were incubated with ready to use (2.5%) normal horse blocking serum for 20 minutes, then washed in PBS twice for 5 minutes. Sections then incubated with primary antibody (diluted 1 in 7 of normal serum) overnight at 4^{o}C and washed in PBS 3 times for 5 minutes. Then incubated with IMMPRESS reagent for 30 minutes and washed in PBS 3 times for 5 minutes then incubated in peroxidase substrate solution NovaRED or DAB and washed for 5 minutes with water. Then dehydrated in 100% ethanol (3 changes for 30 seconds) and xylene (3 changes for 3 minutes) and mounted in DPX.

The results showed increased target accessibility, binding specificity and signal intensity, however, the background staining level was still high (Figure 4.2.).

To avoid the background being highly stained, I used a different antigen retrieval (UNI-TRIEVE) at 70^{o}C in the oven for 30 minutes. The result was impressive (Figure 4.3.).

UNI-TRIEVE solution is quite sufficient for retrieval of all membrane and cytoplasmic antigens, nuclear antigens such as ER, PR etc. which does not require boiling or a cooling period and it is pH-independent. Due to these aspects UNI-TRIEVE is gentle towards delicate tissues and cells; in contrast with the citrate buffer which needs a low level of pH and could easily cause tissue destruction and damage to the tissue morphology. The best possible outcome does not cause background staining. This is why it is applicable to retrieving all tissues and cell preparations for the variety of applications and essays such as Immunohistochemistry (IHC) Immunofluorescence (IF) (figure 4.4).

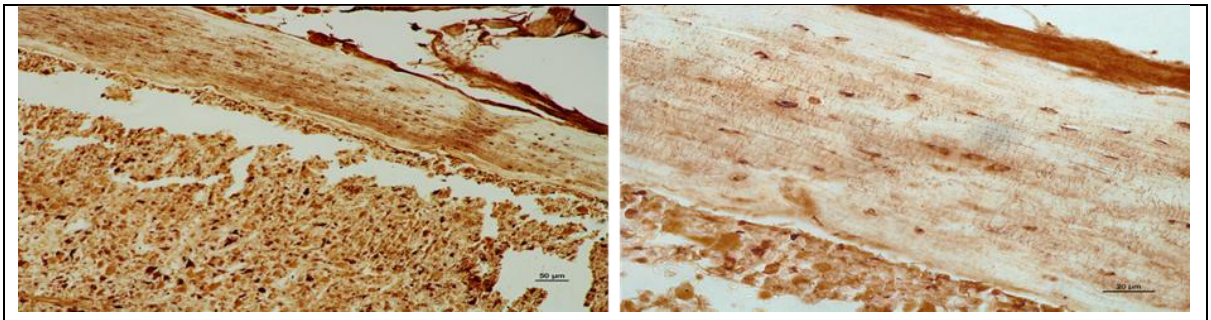

Figure 4.2. Longitudinal Wax Sections in mouse tibia using ImmPRESS (polymerized reporter enzyme staining system), Sodium Citrate Buffer antigen retrieval, NovaRED peroxidase substrate and SOST primary antibody diluted 1 in 7 of normal serum.

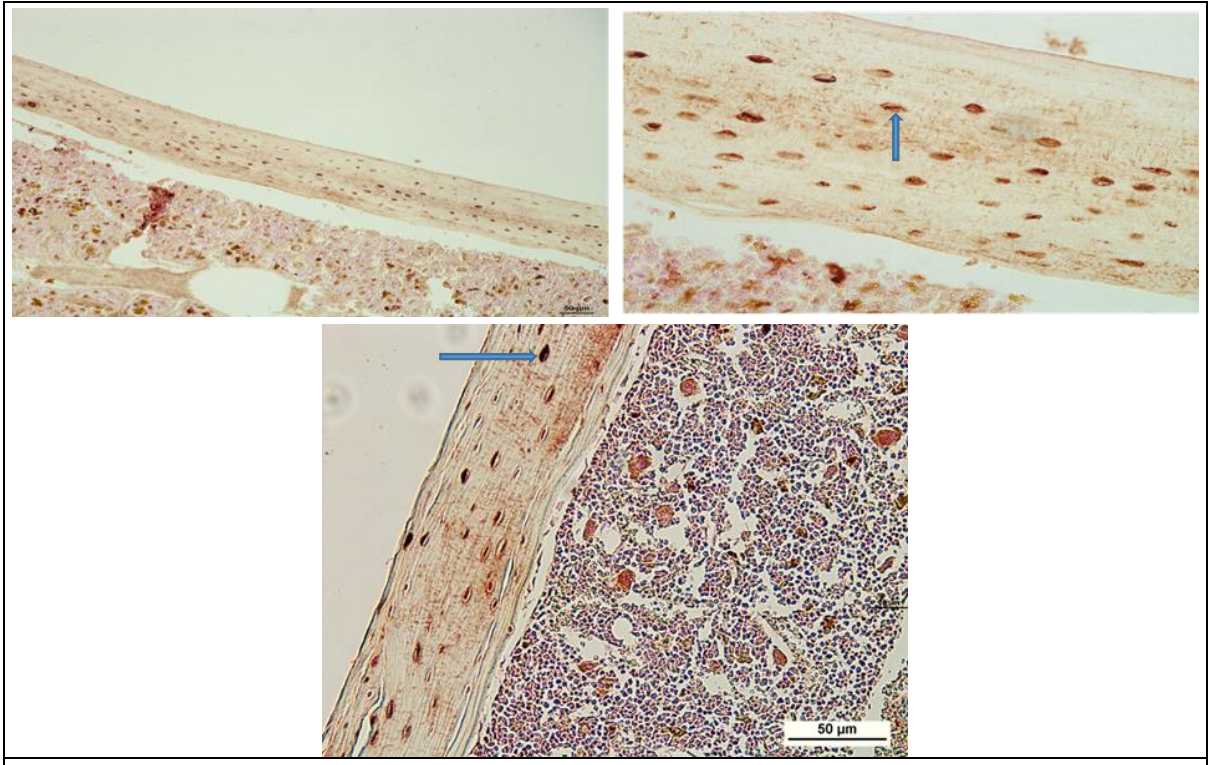

Figure 4.3. Longitudinal Wax Sections in mouse tibia using ImmPRESS (polymerized reporter enzyme staining system), UNI-TRIEVE antigen retrieval, NovaRED peroxidase substrate and SOST primary antibody diluted 1:100 with anti-goat Ig (arrows pointing to osteocytes).

4.2.2.3. *IHC in wax sections with fluorescent secondary antibody*

Sections were dewaxed in xylene twice for 5 minutes and rehydrated for 1 minute in each 100% IMS twice, in 90%, 70%, 50%, and distilled water. Sections then incubated with UNI-TRIEVE antigen retrieval in the oven for 30-60 minutes at 70^{o}C then washed in PBS twice for 5 minutes. Sections blocked with donkey serum (diluted 10% in PBS) for 30 minutes. After blocking they were incubated with the primary antibody (diluted 1 in 100 of PBS) overnight at 4^{o}C and washed in PBS 3 times for 10 minutes. Then incubated with the secondary antibody (diluted 1 in 200 PBS with FCS) for 1 hour and washed in PBS 3 times for 10 minutes then mounted with specific mounting medium.

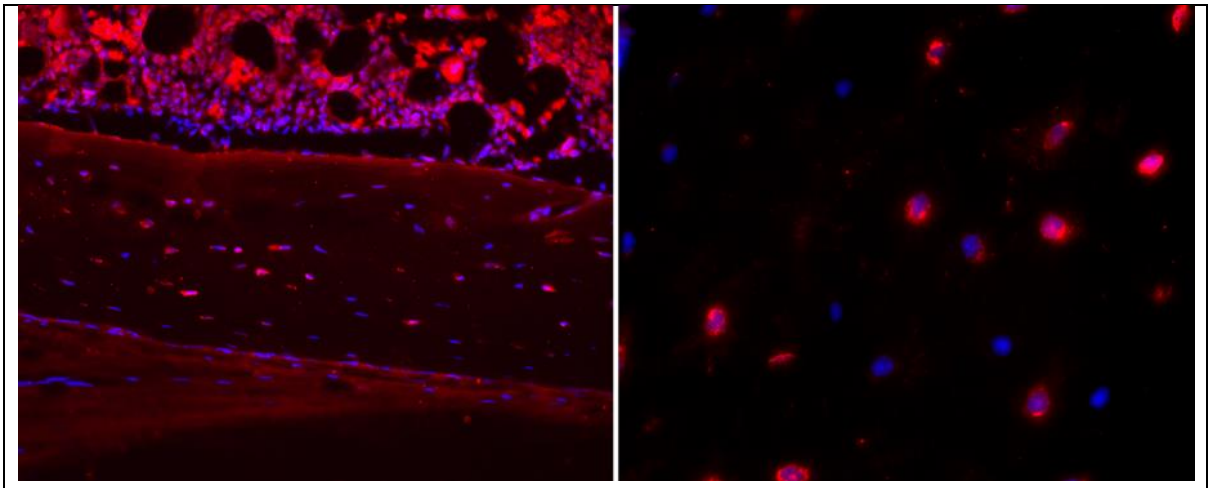

Figure 4.4. Longitudinal wax sections in mouse tibia, fluorescent IHC, Anti sclerostin primary anti body (the red colour) diluted 1:100 and Anti goat secondary anti body with DAPI that gives the blue colour.

The fluorescence method is simpler, and gives a more quantifiable stain (the HRP stains are not stoichiometric) as fluorescence levels can be easily quantified using image analysis. As a final optimisation, I performed Immunostains on tape-based cryosections as described in Chapter 2 paragraph xx. This method is faster than wax embedding, and leads to less tissue damage and better netigen preservation. Therefore the experiments in this chapter used the tape-based cryo section method combined with immunofluorescence for the determination of SOST expression in osteocytes.

4.2.3 Osteocyte lacunae visualisation by µCT

To be able to visualise osteocyte lacunae, the tibias were scanned at a resolution of 1.25 µm with Skyscan (as described in chapter 2). The reconstructed 3d image stacks were analysed using a custom macro in CT Analysis. Example of the visualisation of osteocyte lacunae is shown in figure 4.5. The main parameters measured were percentage osteocyte volume per bone volume, osteocyte number per bone volume, osteocyte diameter, and osteocyte separation.

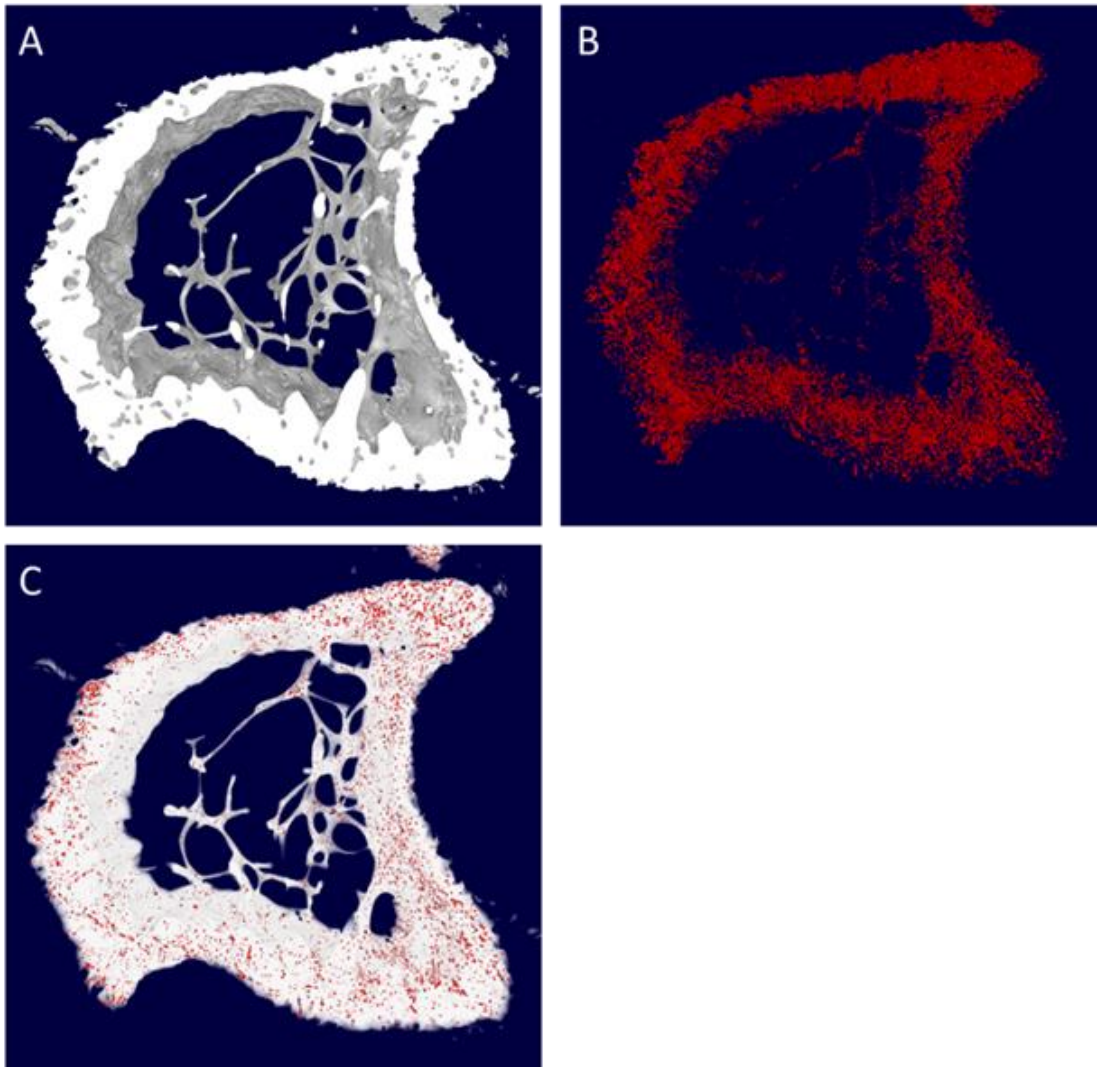

Figure 4.5. 3D images of mouse tibia scanned with µCT, represent Osteocyte lacunae visualisation (A) cortical and trabecular bone, (B) osteocyte lacunae, (C) osteocyte lacunae distribution in the bone.

4.3 Results

4.3.1 Effects of ageing and mechanical loading on trabecular structure of the proximal tibia

Ageing lead to a 6-fold decrease in trabecular bone volume (Fig. 4.6 and 4.7 A). This was due to a decrease in trabecular number (Fig. 4.7 D), leading to an increase in trabecular separation (fig. 4.7 C). Trabecular thickness was not affected by ageing (Fig. 4.7 B). Ageing had no effect on the architectural parameters trabecular pattern factor and structure model index (Fig. 4.7 E and F). The mechanical loading of the tibia did not lead to any significant changes in the trabecular bone at the proximal tibia.

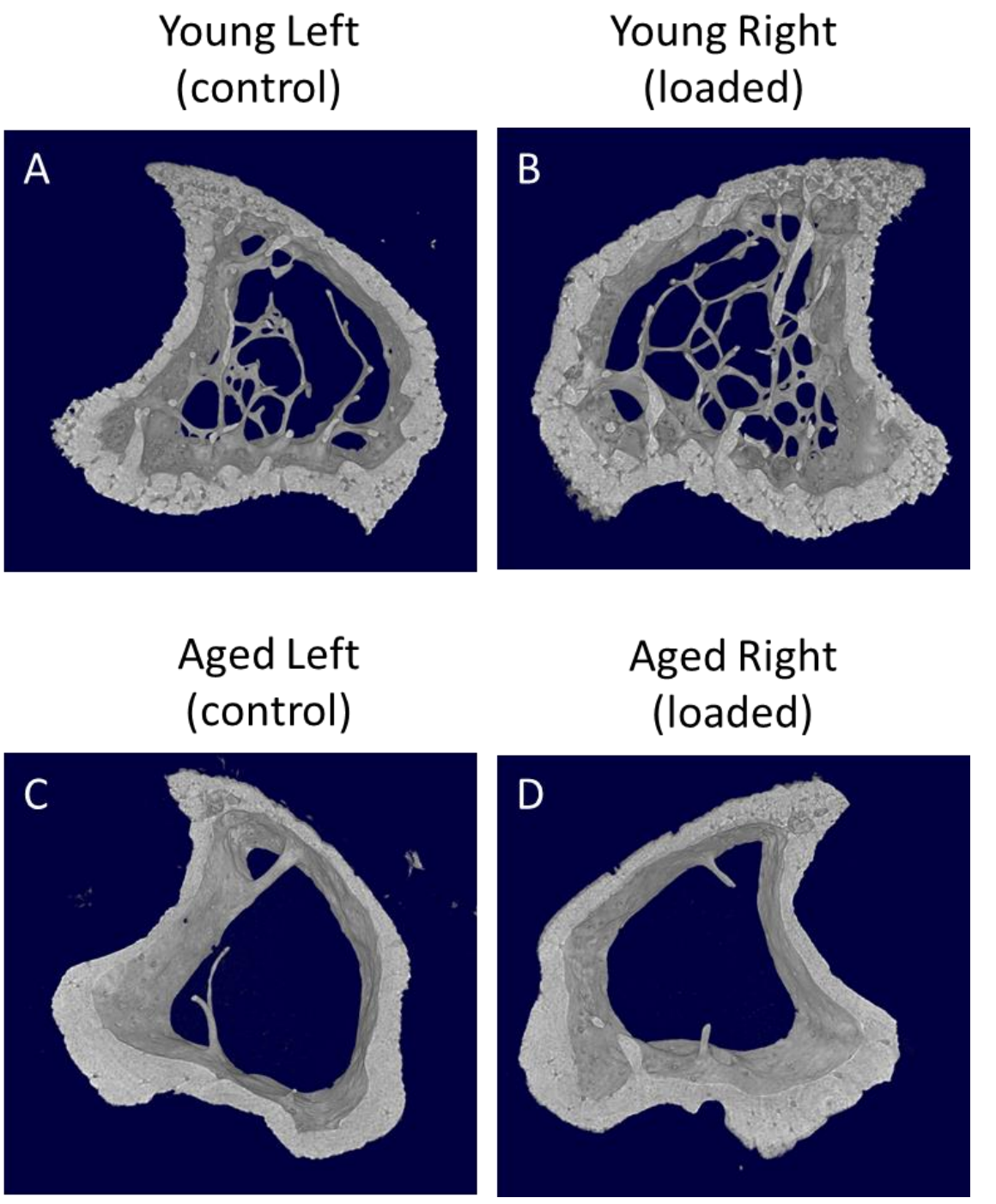

Figure 4.6. µCT images of young and aged mouse tibias (right loaded, left non-loaded). Note the substantial loss of trabecular bone in the aged samples.

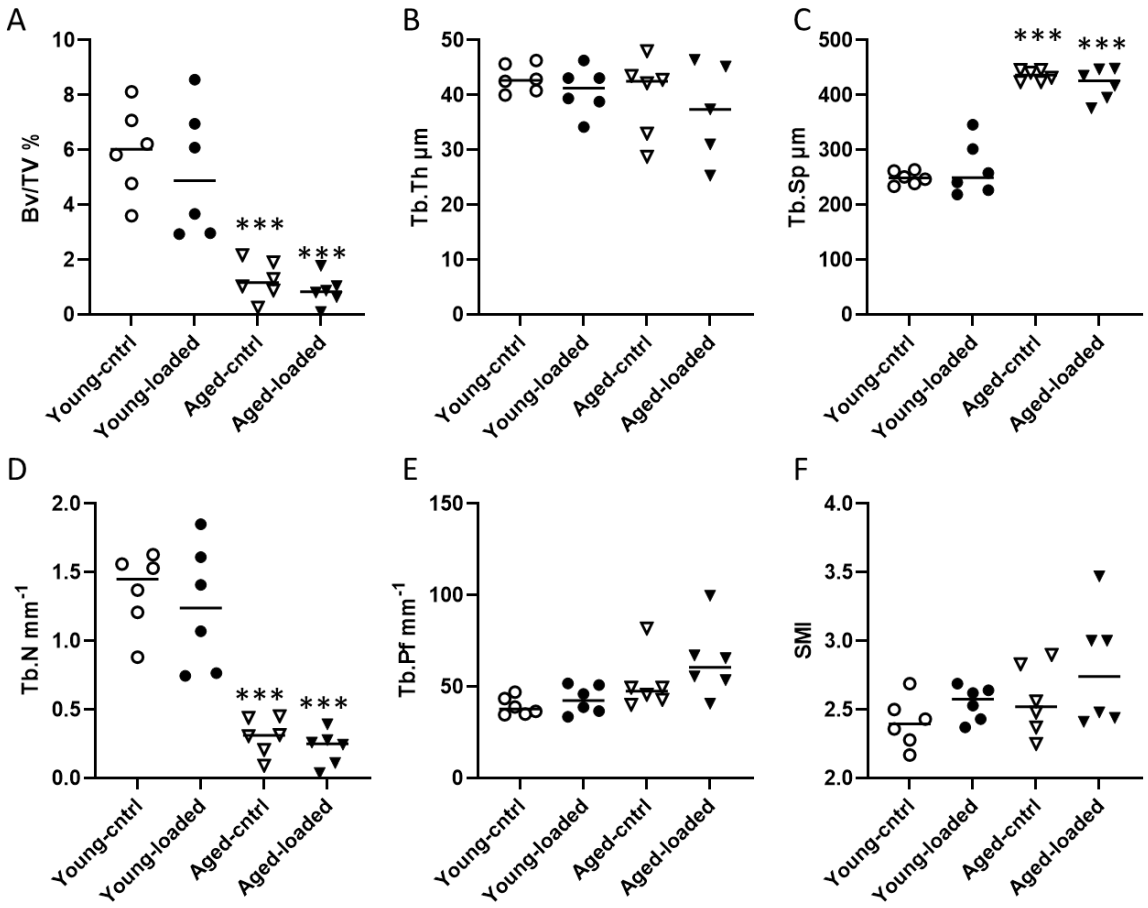

Figure 4.7. Analysis of trabecular bone of young and aged tibias after loading. Trabecular bone of the proximal tibia was analysed by µCT. Circles represent data from young animals (N=6), triangles from aged (N=6). Open symbol represent data from control tibias, closed symbols from loaded tibias. Data were analysed using ANOVA, ***: $p < 0.001$ between young and aged. BV/TV: bone volum per tissue volume; Tb.Th: trabecular thickness; Tb.Sp: trabecular separation; Tb.N: trabecular number; Tb.Pf: trabecular pattern factor. SMI: structure model index.

4.3.2 Effect of ageing and mechanical loading on bone formation

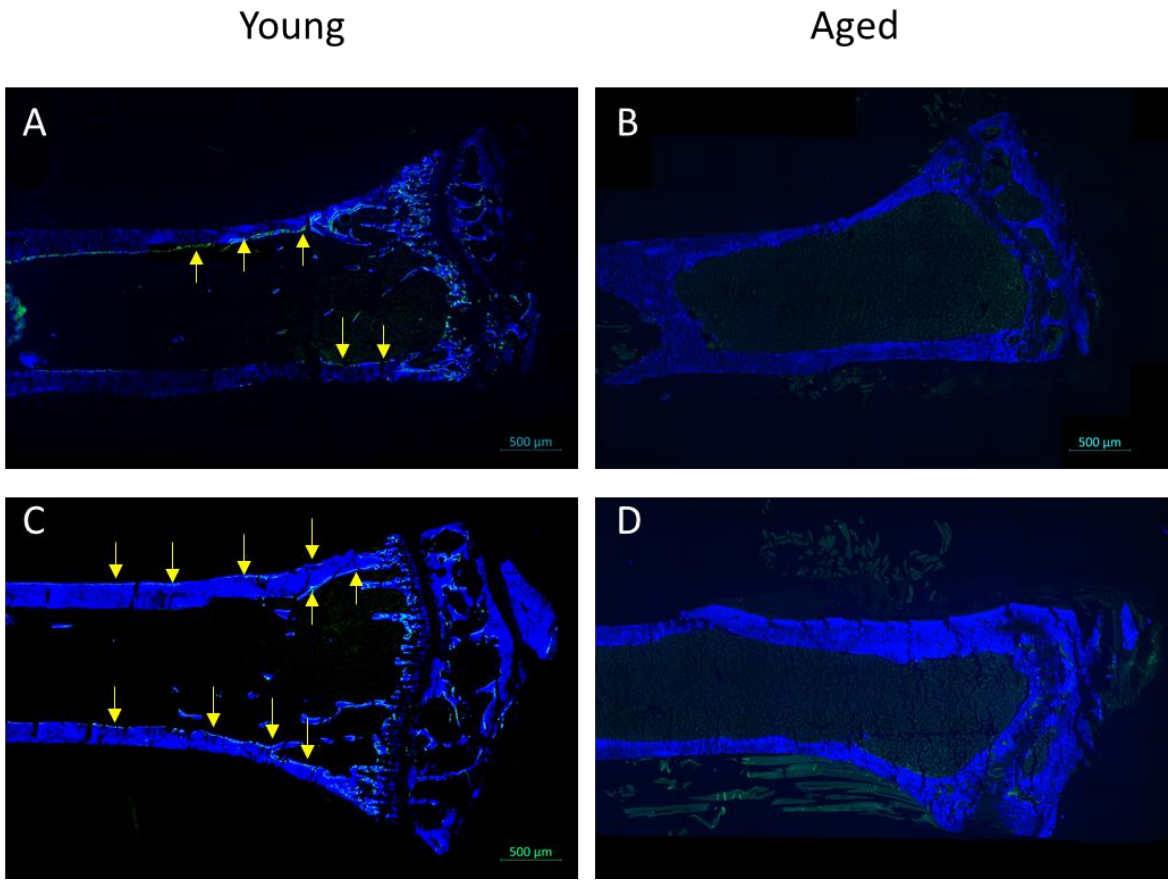

Figure 4.8. Images of florescent microscopy for calceine labelled young and aged mice. Mineralised tissue was counterstained with calceine blue (blue fluorescent) and calceine labels are green. **A:** Left (control) tibia in young mouse, showing calceine double label representing bone formation in the endosteal side of the cortex (yellow arrows) and the trabecular bone. **B:** Left (control) tibia bone for aged mouse virtually no calceine double label can be seen due to very low levels of bone formation. **C:** Right (loaded) tibia for young mouse, showing calceine double label representing bone formation in both endosteal and periosteal side of the cortical bone (yellow arrows) as well as increased calceine labelling of the trabecular bone. **D:** Right (loaded) tibia in aged mouse, showing no increase in calceine labelling after loading.

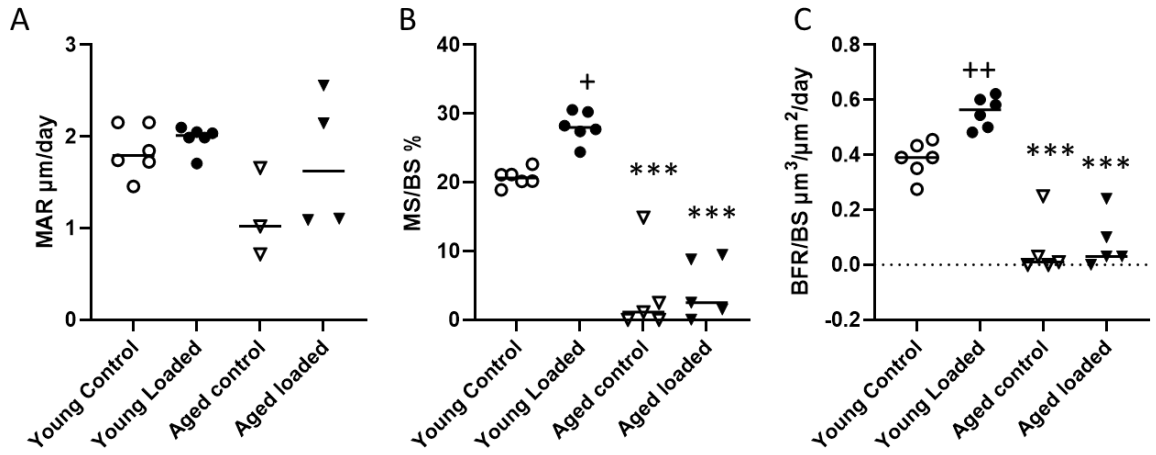

Figure 4.9. Effect of ageing on loading induced bone formation in trabecular bone of young and aged mice tibias analysed by µCT. Circles represent data from young animals (N=6), triangles represent data from aged animals (N=6). Open symbol represent data from control (left) tibias, closed symbols from loaded (right) tibias. Data were analysed using one way ANOVA, ***: p< 0.001 between young and aged mice. +: p<0.5 between loaded and control; ++: p<0.01 between loaded and control. MAR: mineral apposition rate; MS/BS: mineralising surface per bone surface; BFR/BS: bone formation rate per bone surface.

Analysis of the calcein double labels in the trabecular bone of the aged animals showed very little double label (Figure 4.8), in contrast to the young animals, which showed a mineralising surface of approximately 40% (Fig. 4.9). Mechanical loading of the tibia did not affect the bone formation in the trabecular bone of the aged animals. In contrast, in the young animals the bone formation rate was increased by 38%, due to an increase in the mineralising surface per bone surface, while the mineral apposition rate was not changed.

A similar effect of loading was seen in the cortical bone, with again a lack of effect in aged animals, and a 78% increase in bone formation rate in the young mice (Fig. 5.10), again due to an increase in the mineralising surface with no effect on the mineral apposition rate (MAR). This increase in mineralising surface was almost exclusively due to activation of bone formation in the periosteal surface of the cortex after loading (compare figure 5.8 A and C). The unloaded control legs showed virtually no double label on the periosteal surface.

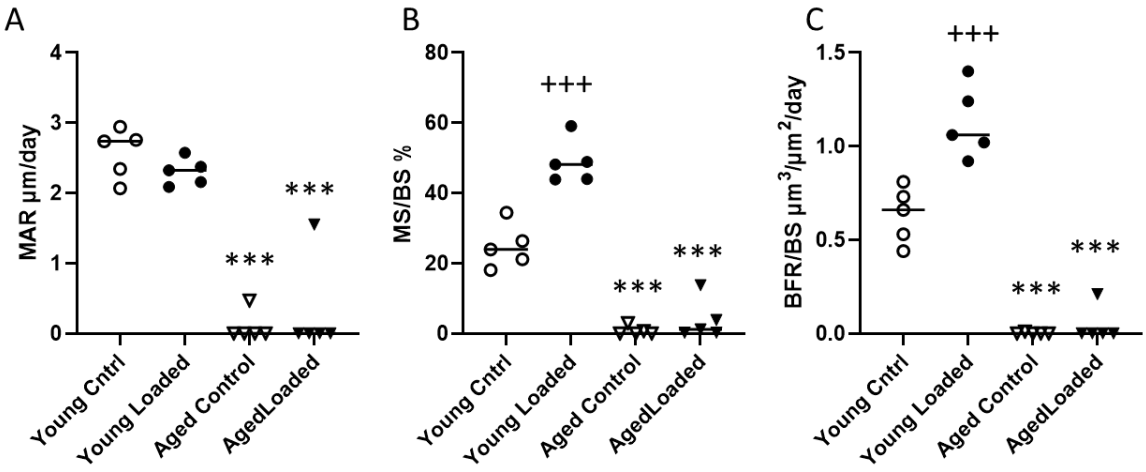

Figure 4.10. Effect of ageing on loading induced bone formation in cortical bone of young and aged mice tibias analysed by µCT. Circles represent data from young animals (N=6), triangles represent data from aged animals (N=6). Open symbol represent data from control (left) tibias, closed symbols from loaded (right) tibias. Data were analysed using one way ANOVA, ***: p< 0.001 between young and aged mice, +++: p< 0.001 between loaded and control tibias.

4.3.3 Analysis of sclerostin expression after loading (confocal)

One of the main regulators of bone formation that is known to respond to mechanical loading, is sclerostin (SOST), a negative regulator of bone formation. The effect of ageing and loading on expression of SOST in osteocytes was analysed using immunofluorescence. Although there was a lower fluorescence intensity in the aged mice compared to the young mice, but this was not statistically significant (Fig. 5.7). Mechanical loading had no effect on immunofluorescence levels in the osteocytes.

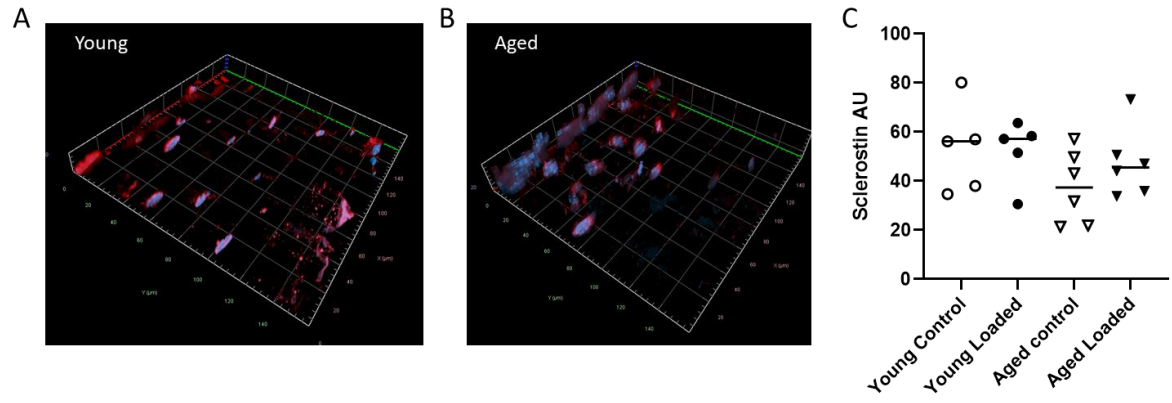

Figure 4.11. Effect of ageing and loading on sclerostin expression in osteocytes. A and B: representative 3D confocal images of a young and aged mouse respectively. Nuclei are counterstained with DAPI (blue), sclerostin immunostain is visible as red. C: Analysis of average Immunostain intensity per cell. Between 20 and 40 cells were analysed for each bone. Circles represent data from young animals (N=6), triangles represent data from aged animals (N=6). Open symbols represent data from control (left) tibias, closed symbols from loaded (right) tibias. Data were analysed using one way ANOVA. There was no significant difference between the groups.

4.3.4 Effect of ageing on osteocyte number

Osteocytes are the main cells regulating the response of bone to mechanical loading. Therefore, the lack of response to loading ion the aged mice could be due to insufficient numbers of osteocytes in the aged mice. Osteocytes are long lived cells and the number of osteocytes was unlikely to change in the relatively short period of the loading experiment (2 weeks). I analysed the presence of osteocyte lacunae in the bones of the young and aged mice using very high resolution µCT (Fig. 4.8). The osteocyte lacuna volume per bone volume was significantly decreased by approximately 50% in aged compared to young mice. This was not due to a decrease in osteocyte lacuna diameter (Fig. 4.8 B), but to a decrease in osteocyte lacuna number (Fig. 4.8 C) leading to an increase in osteocyte lacuna separation (Fig 4.8 D).

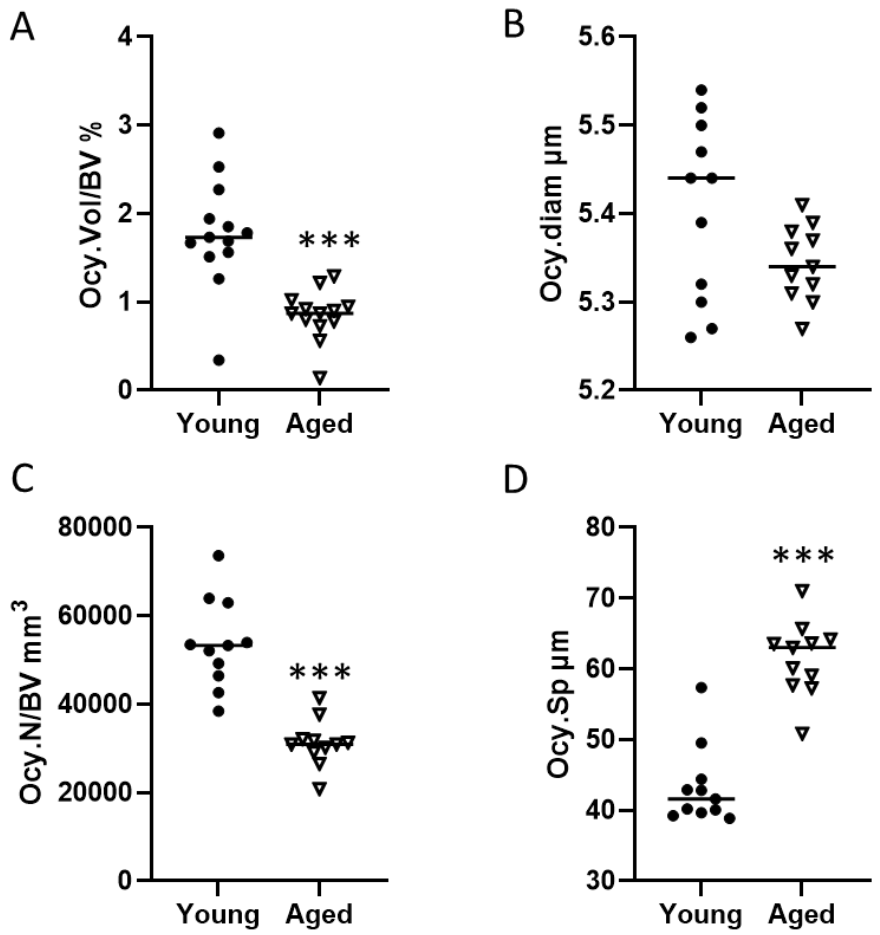

Figure 4.12. Osteocyte density in young and aged mice tibias. Osteocyte lacunae were visualised using high resolution (1.25 µm) µCT scans, and volume, diameter and distribution measured. A: Osteocyte lacunar volume per bone volume as a percentage, showing decreased lacunar volume. B: Osteocyte lacuna diameter. C: Osteocyte lacuna number per bone volume, showing a decrease in number. D: osteocyte lacuna separation showing an increase in separation with age. Circles in dictate data from young mice (N=12), and triangles from aged mice (N=12). Data were analysed using a t-test, ***: $p < 0.001$ between young and aged mice. Ocy.Vol/BV: Osteocyte lacuna volume per bone volume; Ocy.diam: Osteocyte lacuna diameter.

4.4 Discussion

The main aim of the work in this chapter was to analyse the effect of ageing on the bone anabolic response to loading. In addition, as osteocytes are the main sensors of mechanical loading in bone, we analysed the effect of ageing on osteocyte number and distribution and osteocyte expression of the loading-sensitive bone formation regulator sclerostion.

Surprisingly, when we compared bone volume and architecture of loaded and control tibias using µCT, we did not observe any effect of loading, either in young or aged mice. However, µCT can only analyse changes in mineralised tissue, and mineralisation is a slow process (213)Taken together with the fact that the loading procedure was only performed over a short period of time (2 weeks), it is likely that the µCTanalysis could not reliably measure the new, low mineralised bone formed in response to loading.

In contrast, analysis of bone formation using dynamic bone histomorphometry, showed a clear increase in bone formation rates in the young mice in response to mechanical loading. The reason why this methodology can detect the effect of loading is because the calcein double labels are incorporated during the bone formation, and the calcein blue counterstain is very sensitive to calcium and will label up tissues with very low hydroxyapatite levels such as newly formed bone (159). In agreement with existing literature, the response to mechanical loading was almost completely absent in the aged mice (214). In addition, the basic bone formation levels in the aged mice were extremely low, with double labels completely absent in a number of tibias analysed.

In the young mice, the increase in bone formation was significant in both the trabecular and cortical bone, and was due to an increase in mineralising surface rather than mineral apposition rate. This indicates that loading leads an increase in numbers of active osteoblasts, rather than an increase in the activity of individual osteoblasts. The increase in osteoblast number could be due to activation of bone lining cells, and /or increased differentiation of osteoblast precursors into active osteoblasts.

As sclerostin is believed to be a major osteocyte produced factor that regulates osteoblast activity, especially in response to loading and unloading of bone(197), I analysed the effect of ageing and loading on sclerostin expression by osteocytes. Sclerostin is an inhibitor of bone formation, and levels are therefore expected to decrease after mechanical loading of bone, to allow for increased bone formation. However, I observed no difference in sclerostin expression after loading(197), either in the young or the aged mice. This in in agreement with the results on serum levels of sclerostin described in chapter 3. However, Robling et all(189) did observe a decrease in young mice after mechanical loading, however, in their experiments mice only underwent one cycle of mechanical loading and were culled 24h later. Therefore, one explanation for the lack of effect of loading on sclerostin expression here could be one of timing. The animals were culled and serum and bone collected three days after the last loading episode. It is possible that the effect of loading on sclerostin expression is very transient, and by this time sclerostin levels had returned to normal levels again. It may also be that only a small subset of osteocytes respond to the loading, and this number is insufficient to significantly affect serum levels (which reflect total body sclerostin synthesis), and that analysis of individual osteocyte expression levels need to be specifically targeted to areas within the bone that are most responsive to the mechanical loading. One of the areas that shows a very distinct increase in bone formation after loading is the periosteal cortical bone, especially on the lateral side. Future experiments could therefore specifically analyse osteocytes in this bone area. However, due to time constraints I was not able to perform this analysis, and in addition, due to the fact that the cortex is thick and very rigid, the cortical bone suffers from considerable cracking damage during cryosectioning, making consistent analysis difficult.

Finally, I analysed the effect of ageing on osteocyte number. I developed a method to analyse osteocyte lacunae in 3D using very high resolution µCT image analysis. The number of osteocyte lacunae was significantly decreased in aged mice, leading to an increase in osteocyte separation distance. This may partially explain the decreased response to loading in the aged mice, as a reduction in the cells sensing the loading and controlling the activity of the osteoblasts and osteoclasts may lead to a decrease in the signals send by the osteocytes. The increased spacing between the osteocytes could also lead to a reduction of the connections between the osteocytes, leading to a less efficient network. In addition, previous

studies have found: Aging is accompanied by a decline in osteocyte connectivity and viability in the bone of osteoporotic patients and aged mice (215). This is most likely due to osteocyte cell death, apoptosis, and autophagy. A recent study by Tiede-Lewis et al. (216) showed that the dendrite number was greatly reduced in aged mice, where reduced connectivity preceded osteocyte death.

Osteocyte death leaves behind empty lacunae that can fill in with mineral, a process called micropetrosis. Micropetrosis may act as a neutralization mechanism in aged bone by removing the empty lacunae that can cause stress congregator if left open. The programed cell death that osteocytes undergo, especially in the presence of bone micro-damage, stimulates the release of chemical signals for osteoclasts to remodel the damaged bone (57). Osteocytes can also undergo the process of autophagy (217). Autophagy is a cellular state that promotes survival especially under stressful conditions, and autophagic cells remove unnecessary organelles until they can return to the healthy state. However, if the stress causing the autophagy has not stopped, then the cells can undergo apoptosis, leaving dead or osteonecrotic bone that does not heal or respond to mechanical loading.

Aging is accompanied by a decline in osteocyte connectivity and viability in the bone of osteoporotic patients and aged mice(215). Furthermore, Tiede-Lewis et al. (216) study showed that the dendrite number was greatly reduced in aged mice, where reduced connectivity preceded osteocyte death. Deletion of superoxide dismutase 2 in osteocytes resulted in an osteoporosis-like bone phenotype due to increased generation of reactive oxygen species (ROS) (218). Osteocytes in aged mice also have increased expression of markers of senescence that may contribute to increased osteoclast activity and bone resorption (219). Although, a possible confounder would be the load distribution in different age group young and old, as the same applied load may give different discrete loads within the bone, as animal's skeletal morphology changes different age levels.

The results described in this chapter clearly show an impaired response to mechanical loading in aged mice. This may be partially due to the decrease in osteocyte number. My results do not show a clear role for sclerostin in the age-related responsiveness to loading. The molecular mechanisms underlying the reduced response remain therefore unknown. To investigate the molecular mechanisms affected by ageing, is studied the effects of loading and ageing on gene expression in chapter 5

Chapter 5. Effect of mechanical loading on osteoblast and osteocyte gene expression.

5.1. Introduction:

Many studies have shown that the process of bone formation and resorption are sensitive to local mechanical loads especially regeneration of bone tissue.

At the cellular level, Osteocytes orchestrate the bone adaptation to its mechanical environment. Osteocytes are embedded into the mineralized matrix and they are capable of sensing mechanical signals applied to the bone and then react to these loads by controlling osteoblast and osteoclast activities through cell-to-cell communication and via secreted factors. Mechanical stimuli regulate several cellular functions, including gene expression, protein synthesis, cell proliferation and differentiation (203,220,221).

Previous research has shown that the anabolic effect of mechanical loading is decreased with ageing (222). A study carried out by Nilsson Holguin et al. hypothesized that aging limits the response of the tibia to axial compression over a range of adult ages on C57BL/6 mice (5 , 12 and 22 Months old) (223). Indeed my results as shown in chapter 3 showed that bone formation is stimulated by in vivo mechanical loading especially on young mice, but the effect is reduced in aged mice.

However, the underlying mechanism for reduced response to mechanical loading in aged mice is currently unknown. To my knowledge there are not any current one try to understand the molecular mechanisms, in this chapter I analysed the effect of ageing on changes in gene expression patterns after mechanical loading. Osteocytes are post mitotic cells, impossible to isolate in high numbers and cannot be cultured at high purity. I therefore used osteocyte-like osteoblasts, grown out of bone chips in culture as a model. I used RNA sequencing to identify changes between young and aged primary bone cells grown out of bone chips, using stretch as the mechanical load, as described in chapter 2.3. To my knowledge there are currently no studies that have analysed this. After analysis of the RNA Sequencing data, I selected the 10 most significantly differentially expressed genes and analysed the effect of in vivo using the tibial loading model. The RNA obtained from the cleaned tibial bones is predominantly

derived from osteocytes, and therefore this technique allowed me to analyse the response to loading by osteocytes.

RNA sequencing (RNA-Seq.) uses high-throughput techniques to provide a good understanding into the transcriptome of the cell. In addition to quantifying gene expression, the data produced by RNA-Seq can facilitate the discovery of novel transcripts, identification of alternatively spliced genes, and detection of allele specific expression (224).

A typical RNA-Seq. experiment consists of RNA extraction first from the biological material (cells or tissues) which should be of sufficient quality that measured using an Agilent Bio analyser, which produces an RNA Integrity Number (RIN) between 1 and 10 with 10 being the highest quality samples showing the least degradation. Second isolating RNA molecules using specific protocols, then converting it to cDNA by reverse transcription and sequencing adaptors are ligated to the ends of the cDNA fragments Following amplification by PCR then the RNA-Seq. library is ready for sequencing (225).

How is gene expression data analysed?

The data flow for analysing RNA-Seq. data includes, creating FASTQ-format files sequenced reads from the NGS platform then aligning these reads to an interpreted reference genome and calculating expression of genes. Although basic sequencing analysis tools are easy to access, RNA-Seq. analysis presents considerable computational challenges and requires a specific thoughts to the essential biases in expression data. Figure 5.1. Explains RNA sequencing and data analysis (225).

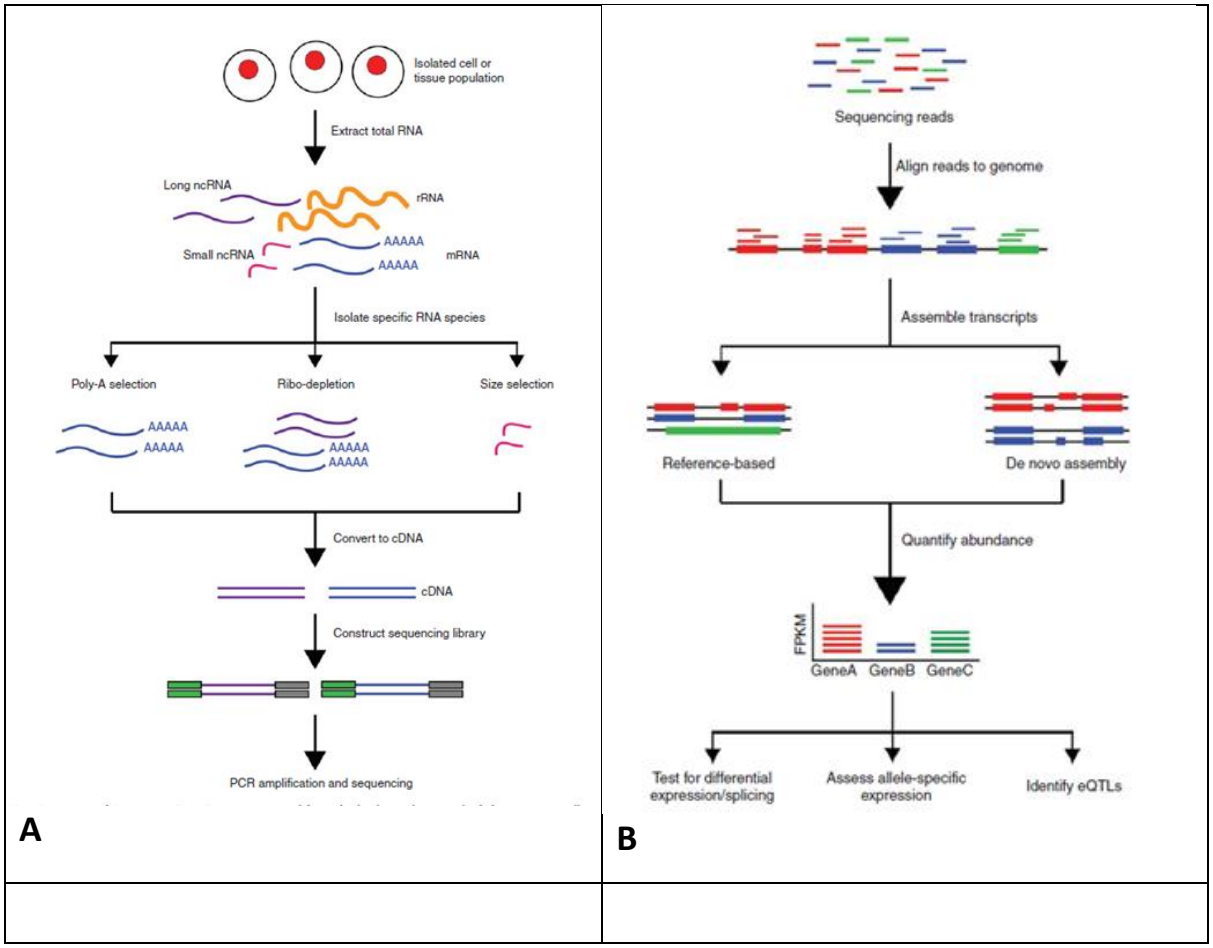

Figure 5.1. (A) Overview of RNA-Seq. Experiment: First, RNA extraction. Second, subsets of RNA molecules are isolated. Next, the RNA conversion to cDNA by reverse transcription and sequencing adaptors are ligated to the ends of the cDNA fragments. Following amplification by PCR, then the library is ready for sequencing.

(B) Overview of RNA-Seq. data analysis. Expression reads are first aligned to a reference genome. Second, the reads may be assembled into transcripts using reference transcript annotations or assembly styles. Next, the expression level of each gene is estimated by counting the number of reads that align to each exon or full-length transcript. Downstream analyses with RNA-Seq data include testing for differential expression between samples.

5.2. Methods:

Two groups of young mice (3 months old N=6) and aged mice (15 months old, N=5) were culled, and bone chips from the tibia and femur bone shafts were obtained as described in

2.2.1. Bone tissue was cultured as described in 2.3.1. Then after 5 weeks Osteocytes- like osteoblasts were harvested. For mechanical testing, cells were stretched by exposing to a tension system as described in 2.3.2. Next, that RNA was extracted from the cells as described in 2.2.2. Then RNA Next Generation Sequencing was carried out by LEXOGEN. The STAR aligner (Spliced Transcripts Alignment to a Reference) was used for aligning reads directly to a reference genome via the utilization of a pre-generated index of the reference. The reads are provided in a text file in the FASTQ format, which is then aligned by the tool. The results of this alignment are the aligned reads in SAM or binary SAM (BAM) format.

Differential expression analysed was performed with DESeq2 which is a Bioconductor package implemented in R, by LEXICOM. *DESeq2* uses a Wald test to provide statistical significance of each gene's potential differential expression. Multiple comparison errors were controlled for using the default Benjamini and Hochberg method, (aka "FDR"). (226)).

Possible interactions between genes products was analysed using String (https://string-db.org).

In addition, I performed a literature search on the known functions and possible role in bone metabolism of the most significantly differentially expressed genes, and studied their expression by qPCR after mechanical loading of the tibia in mice as described in Chapter 2.3.4. RNA extracted from tibias of each age group was tested by qPCR using specific validated primer-probe sets for each gene provided by Thermo Scientific. Figures 5.9. – 5.17. Represent the relative expression results, and delta CT was normalized against HMBS and sclerostin as housekeeping genes.

Statistical analysis of the data was performed by one way ANOVA using Graphpad Prism, using a Sidak's multiple comparison test as post hoc test to identify differences between individual groups.

5.3. Results:

5.3.1. Highly differentiated osteoblast with some futures of osteocytes

Osteoblasts grown of bone chips are highly differentiated and showed some futures of osteocytes, microscopically they have similar shape as they start to extend their dendritic

processes. Functionally they expressed some similar genes such as osteocalcin, sclerostin and podoplanin.

Figure 5.2. Showing qPCR for some genes in RNA extracted from osteoblasts grown of bone chips and osteocytes obtained from purified compact bone homogenate. The high expression levels of osteocalcin indicate a highly differentiated osteoblast with high podoplanin and sclerostin expression indicating an osteocyte-like differentiation stage.

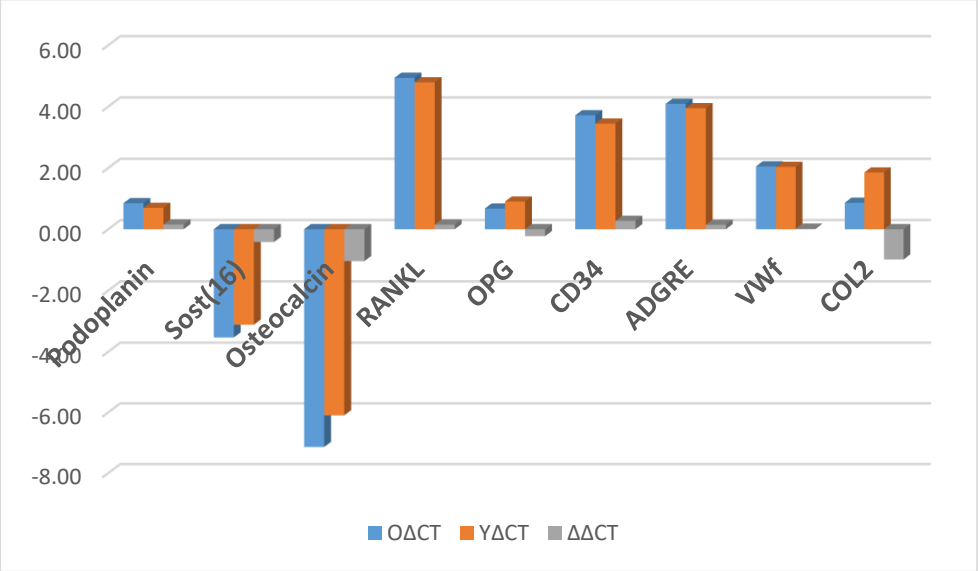

Figure 5.2. Relative expression for Podoplanin, sclerostin, osteocalcin, RANKL and OPG (genes of interest) and other contamination genes, normalised using HMBS as housekeeping gene. Blue; Delta CT for old mice samples, orange; Delta CT for young mice samples and grey; the Delta delta CT.

5.3.1. Effect of stretch on gene expression in young and aged osteoblasts.

Figure 4.3 shows a graphical representation of the effect of mechanical stretch for each gene for young (A) and aged (B) osteoblasts. Differential expression analysis for a total of 24116 genes showed 67 genes upregulated significantly and 10 genes downregulated in young stretched osteoblast compared to control young osteoblasts. Surprisingly, we found no significantly differentially expressed genes in aged osteoblasts. Regarding the Log 2 fold

change, Table 5.1. (A) is showing the top 20 upregulated genes in loaded young osteoblasts and Table 5.1. (B) is showing the 10 down regulated genes. Not all of these genes are statistically significant, therefore, table 5.2. Is showing the top significantly changed genes depending on the adjusted p value.

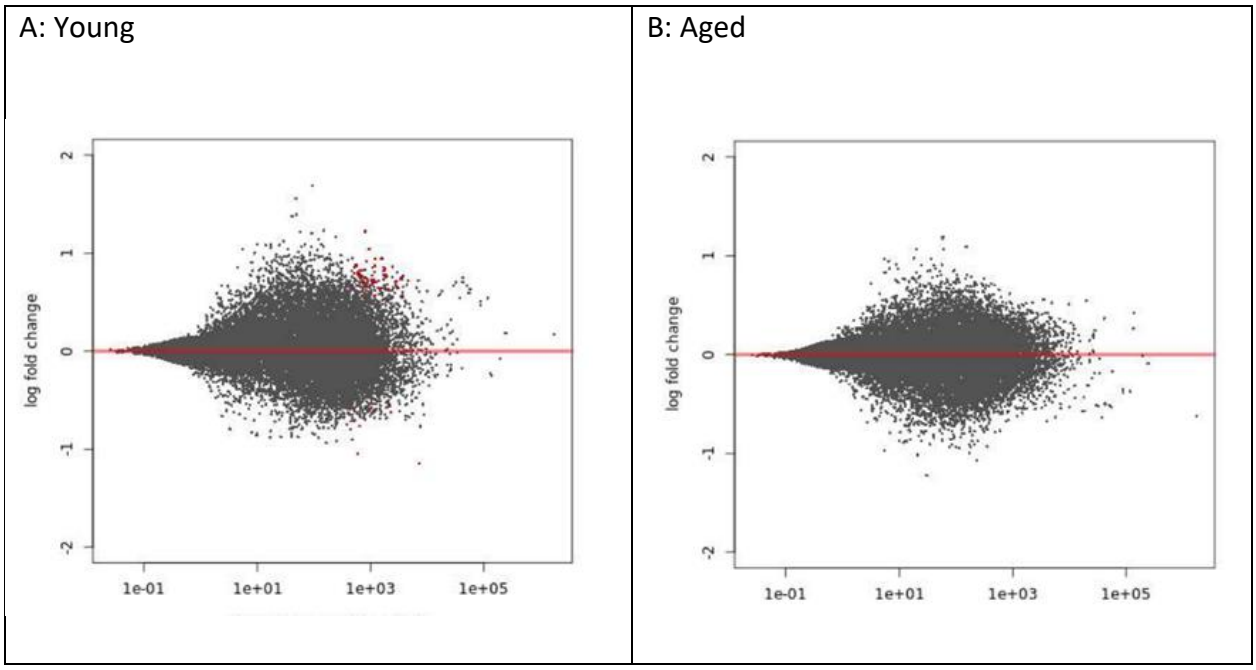

Figure 5.3. Plot of normalized counts of RNASeq. Data of stretched versus non-stretched osteoblasts (A) young, (B) aged. X axis: normalised count, Y-axis: 2-log fold differences between stretched and non-stretched. Expression that is significantly different between stretched and non-stretched cells is indicated by red dots. Note that red dots are only present in A, not in B.

A

Gene Name	log2FoldChange	padj
Mir99ahg	1.22	2.29E-02
Ankrd12	1.04	6.60E-03
Dek	0.95	5.43E-02
Kcnq1ot1	0.95	7.66E-02
Ppig	0.94	3.24E-02
Baz2b	0.92	4.24E-03
Zfc3h1	0.88	6.06E-02
Pnisr	0.87	5.95E-02
Bdp1	0.87	6.82E-02
Atrx	0.86	5.43E-02
Upf3b	0.85	4.19E-02
Usp34	0.84	5.98E-02
Nemf	0.83	5.43E-02
Esf1	0.82	9.00E-02
Ccdc88a	0.82	9.74E-02
4932438A13Rik	0.81	7.59E-02
Akap9	0.81	4.19E-02
Mdm4	0.8	9.00E-02
Ythdc1	0.79	9.00E-02
Thoc2	0.78	1.91E-02

B

Gene Name	log2FoldChange	padj
Serpine1	1.15	1.76E-02
Flnc	1.05	1.76E-02
Trim47	0.71	9.08E-02
Trpc4ap	0.68	6.60E-03
Itgb5	0.68	9.77E-02
Mknk2	0.61	7.89E-02
Csnk1g2	0.6	8.70E-02
Mgat4b	0.57	9.74E-02
Lasp1	0.54	8.26E-02
5031439G07Rik	0.5	9.08E-02

Table 5.1. (A) Top 20 up regulated genes, (B) Top down regulated genes in young osteoblast after stretching in contrast with the control young un-stretched osteoblast sorted by the Log 2 fold change. Padj= adjusted p value.

Gene Name	**Log 2 FC**	**P Value**	**Padj**
Baz2b	0.919192842	1.38E-06	0.004243344
Ankrd12	1.042359996	6.45E-06	0.006603317
Thoc2	0.783940615	3.73E-05	0.019100478
RABEP1	0.73774337	4.85E-05	0.021295695
Mir99ahg	1.22190828	5.96E-05	0.022862838
Ppig	0.939394384	9.51E-05	0.032443115
Tpr	0.752288228	0.000191077	0.041914101
Upf3b	0.853111303	0.000187291	0.041914101
Akap9	0.808574221	0.000180619	0.041914101
Rbm6	0.783211178	0.000161294	0.041914101
Tnfaip8	0.704004285	0.000188857	0.041914101

A

Gene Name	Log 2 FC	P Value	Padj
Trpc4ap	-0.682412944	6.20E-06	0.006603317
Serpine1	-1.149219758	2.33E-05	0.017611375
Flnc	-1.049316399	2.87E-05	0.017611375

B

Table 5.2. The highest significant (A) Upregulated, (B) Downregulated genes in young osteoblast after stretching in contrast with the control young un-stretched osteoblast sorted by p value.

5.3.2. Analysis of gene expression between Young and aged osteoblasts

Surprisingly, ageing had very little effect on gene expression in the non-stretched control osteoblasts, with only one significantly up regulated gene, Hoxc4 (Figure 5.4 B).

Figure 5.4 A Shows a graphical representation of the effect of ageing in stretched osteoblasts as obtained using RNASeq. In contrast to the non-stretched osteoblasts, after stretching there were 32 genes up regulated significantly and 34 genes down regulated in young stretched

osteoblasts compared to the old stretched osteoblasts. Table 2 shows the top 20 up regulated genes and the top 20 down regulated genes.

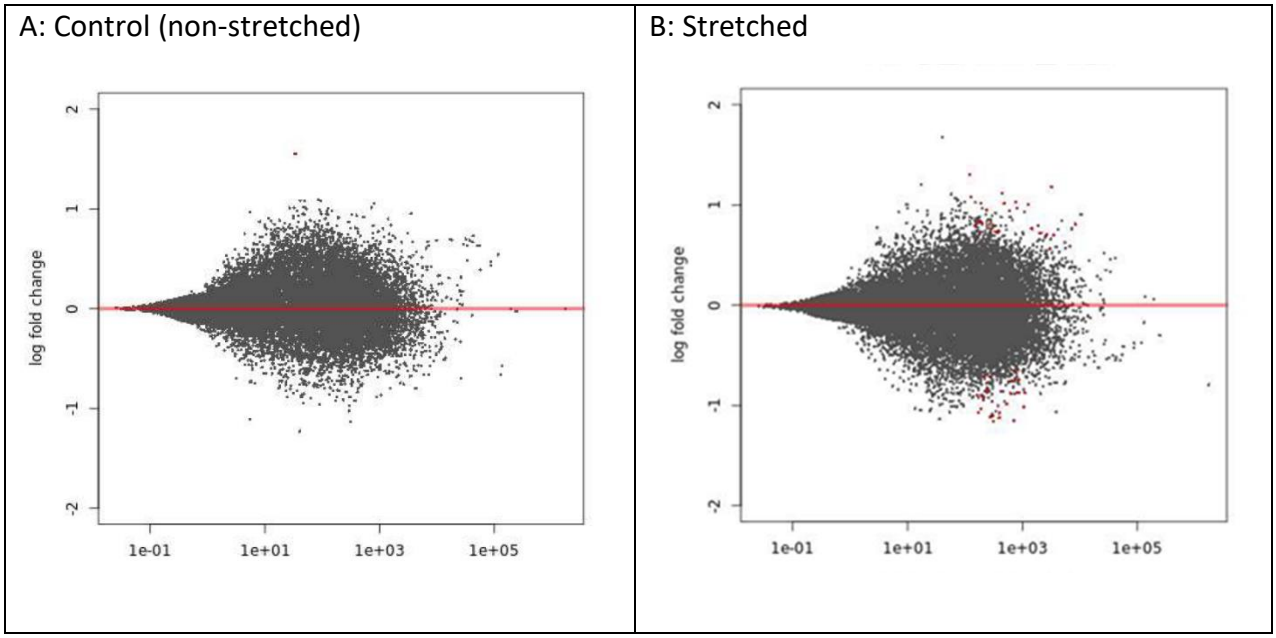

Figure 5.4. Plot of normalized counts of RNASeq. data of young versus aged osteoblasts. A: without stretch, B: After stretch. X axis: normalised count, Y-axis:2-log fold differences between Young and Aged. Expression that is significantly different between young and aged osteoblasts is indicated by red dots. Note that red dots are only present in B, not in A.

Gene Name	log2FoldChange	padj
Ephb3	1.31	3.79E-02
Tuba1a	1.18	8.41E-04
Tubb2b	1.11	7.59E-02
Dhcr7	1.08	7.59E-02
Cryab	1.03	8.66E-02
Rcc1	1.02	7.59E-02
Hspb1	1.01	6.55E-02
Plpp1	1.01	5.45E-02
Tubb2a	0.97	6.27E-02
Shisa4	0.95	7.46E-02
Flnc	0.94	7.46E-02
Erf	0.82	7.98E-02
Rce1	0.82	9.32E-02
Kctd11	0.81	7.59E-02
Tubb5	0.8	6.56E-02
Gnl3l	0.8	1.79E-02
Pcbp4	0.79	7.66E-02
Ccdc102a	0.79	7.46E-02
Pdia6	0.79	7.46E-02
Inppl1	0.76	5.77E-02

Gene Name	log2FoldChange	padj
Fam13b	1.16	5.81E-03
Btg1	1.15	5.38E-02
Flywch1	1.12	7.59E-02
Dcaf6	1.11	4.00E-03
Cpne8	1.1	2.70E-03
Slc25a37	1.08	7.07E-02
Rel	1.07	7.08E-02
Sdccag8	1.04	7.59E-02
Hmgb1	1.02	7.59E-02
Gatsl2	1	7.46E-02
Wdr3	0.99	5.45E-02
Ginm1	0.96	2.15E-02
Mctp1	0.94	6.56E-02
Phospho2	0.91	3.82E-02
Armcx3	0.9	5.38E-02
Cebpz	0.88	3.09E-02
Supt16	0.88	1.00E-01
Nemf	0.87	7.46E-02
Rictor	0.87	9.94E-02
Epc2	0.86	9.54E-02

Table 5.3. Top 20 upregulated genes (A) and down regulated (B) in young stretched osteoblasts in contrast to old stretched osteoblasts sorted by the Log 2 Fold Change.

Gene Name	Log 2 FC	Pvalue	Padj
Tuba1a	1.181064376	1.01E-07	0.000841208
Gnl3l	0.799007731	1.07E-05	0.017862877
Ephb3	1.307141119	3.63E-05	0.037860222

A

Gene Name	Log 2 FC	Pvalue	Padj
Cpne8	-1.101863778	6.47E-07	0.002697808
Dcaf6	-1.113385063	1.44E-06	0.004001731
Fam13b	-1.155441029	2.79E-06	0.005809351
Ginm1	-0.955593874	1.55E-05	0.021517395
Cebpz	-0.879580981	2.60E-05	0.03093295
Phospho2	-0.910897747	4.12E-05	0.038182361

B

Table 5.4. The highest significant (A) Upregulated, (B) Downregulated genes in young stretched osteoblast in contrast with old stretched osteoblast sorted by p value.

5.3.3. Protein-protein interaction (PPI) network analysis

To find out the potential interactions between the proteins encoded by the differentially expressed genes, the STRING tool was employed (https://string-db.org). Results are shown in figures 5.5, 5.6, 5.7 and 5.8. These figures show the networks, with the nodes corresponding to the proteins and the edges representing the interactions.

Figure 4.6 shows an extensive network of interactions between the genes upregulated after mechanical loading in young osteoblasts. The network seems to be centred on the Thoc2 and Atrx genes.

A cluster of genes connected to the Transcriptional regulator ATRX gene which encodes one of the chromatin remodelling proteins is upregulated after loading. Part of this network is the Ubiquitin carboxyl-terminal hydrolase 34 (Usp34) that removes conjugated ubiquitin from AXIN1 and AXIN2, thereby acting as a regulator and activator of the Wnt signaling pathway.

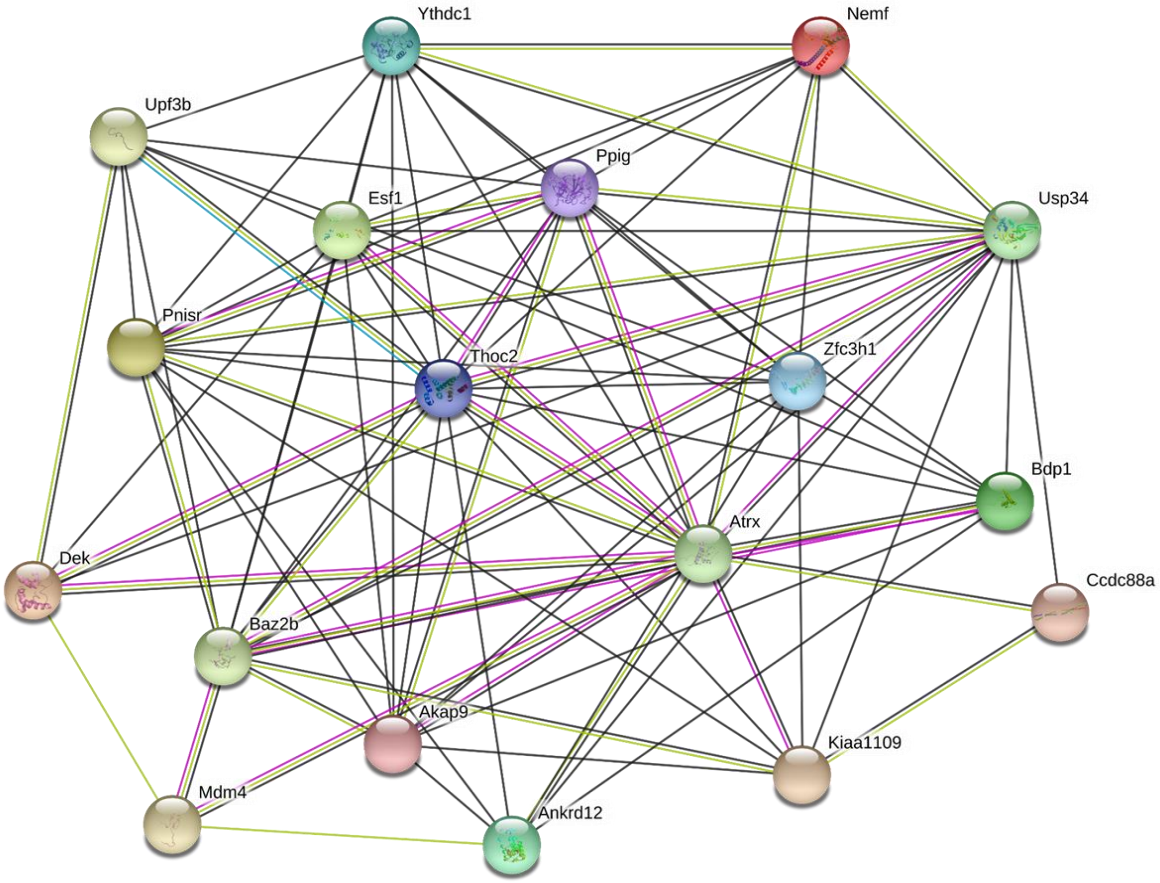

Figure 5.5. Protein-protein interaction network pathway analysis between up regulated genes in young stretched osteoblasts versus control young un-stretched osteoblasts using STRING. Marbles represent genes, lines represent the connection between genes, and more lines means more relationship.

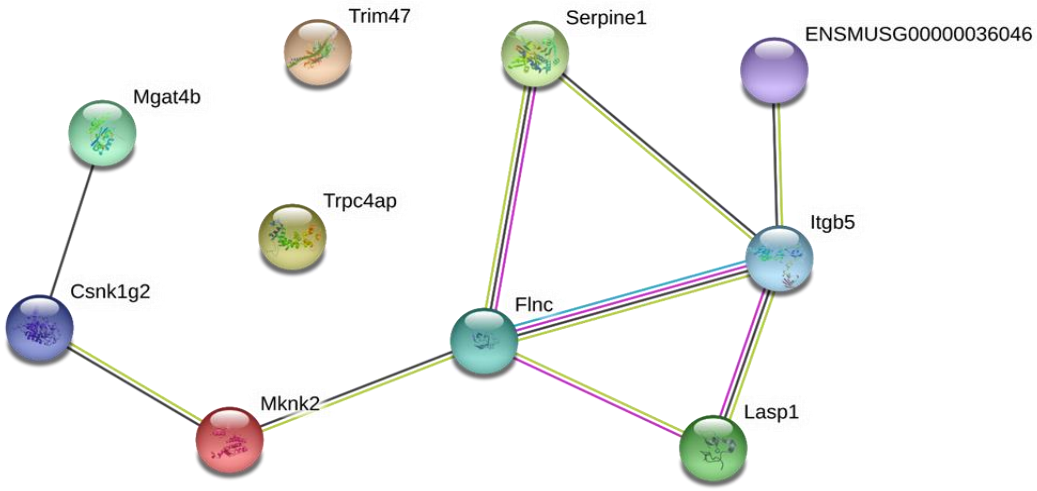

Figure 5.6. Protein-protein interaction network pathway analysis between differential expressions of down regulated genes in young stretched osteoblasts versus control young non-stretched osteoblasts using STRING. Marbles represent genes, lines represent the connection between genes, and more lines means more relationship.

Figure 5.6 shows a less extensive network of genes downregulated after stretch in young osteoblasts. The network centres on Flnc, which encodes filamin C, an actin cross-linking protein, widely expressed in cardiac and skeletal muscles (227).

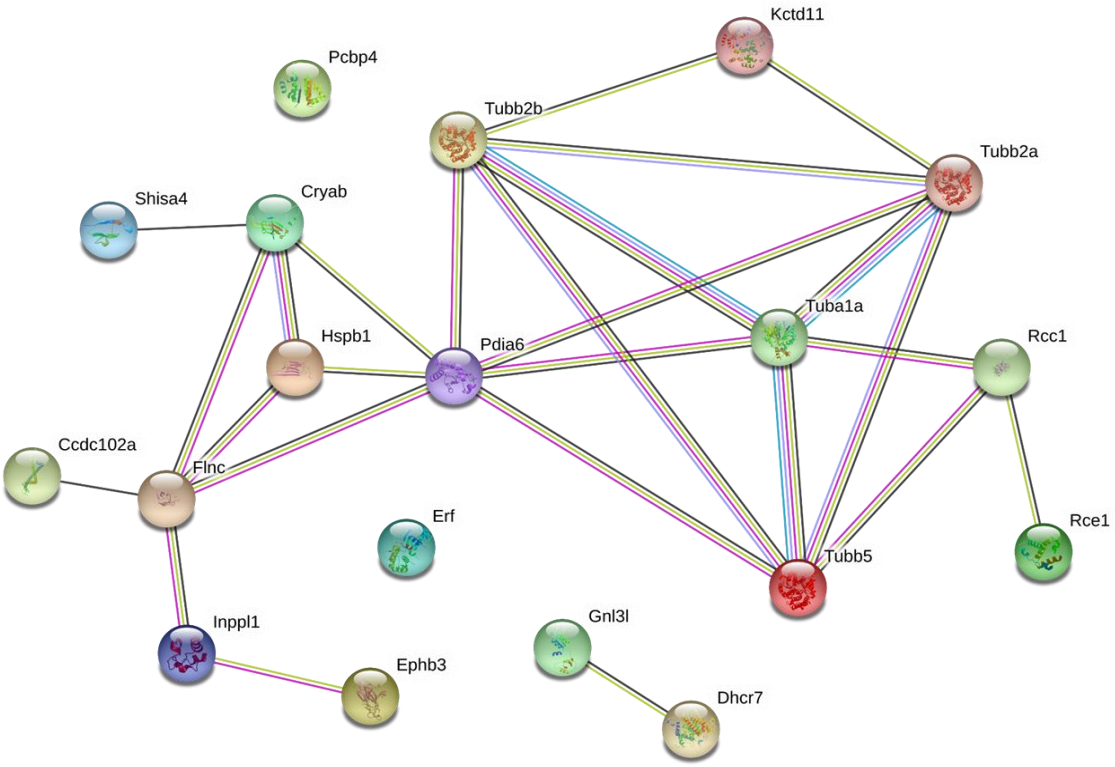

Figure 5.7. Protein-protein interaction network pathway analysis between differential expressions of up regulated genes in young stretched osteoblasts versus old stretched osteoblasts using STRING. Marbles represent genes, lines represent the connection between genes, and more lines means more relationship.

The network in figure 5.7 shows the network of genes differentially upregulated in young stretched osteoblasts compared to aged stretched osteoblasts. A cluster of genes centred on tubulin which is the major constituent of microtubules related to cytoskeleton is up regulated in young osteoblasts.

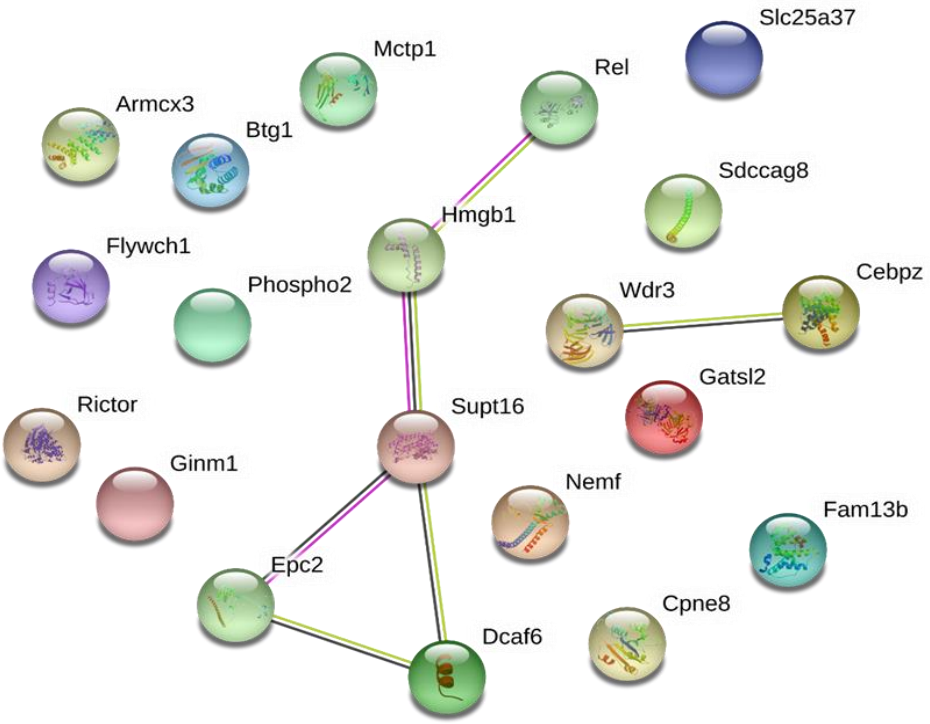

Figure 5.8. Protein-protein interaction network pathway analysis between differential expressions of down regulated genes in young stretched osteoblasts versus old stretched osteoblasts using STRING. Marbles represent genes, lines represent the connection between genes, and more lines means more relationship.

The downregulated genes in young stretched osteoblasts versus aged stretched osteoblasts is shown in figure 5.8. A cluster of genes centred on tubulin which is the major constituent of microtubules related to cytoskeleton is up regulated in young osteoblasts.

5.3.4. Analysis of Top 10 differentially expressed genes in in vivo loading model

We selected the top differentially expressed genes (based on relatively high expression and significance of the adjusted p-value), and analysed the effect of *in vivo* loading of the tibia on the expression of these genes as described in chapter 2 paragraph 2. The right tibias for each young and old mouse received mechanical loading, while the left tibias was considered as

control. The RNA quality and yield for the aged samples was good, however, the samples from the young mice showed evidence of RNA degradation such as poor 260/280 ratios, low yield and high CT values for the HMBS and SOST housekeeping genes (higher in the young by 3-4 cycles). As a consequence of this, a number of genes (especially those with relatively low expression) could not be detected in the qPCR reaction in the samples from young mice.

5.3.4.1. Tuba1a:

Tubulin Alpha 1a, Tubb2b (Tubulin Beta 2B), Tubb2a and Tubb5, these 4 genes represent upregulation in our differential expression gene analysis. They are structural genes that encode for Tubulin, their products participate in the formation of microtubules the structural proteins that participate in cytoskeletal structure(228). Specifically, microtubules are composed of a heterodimer of alpha and beta-tubulin molecules. Both of these 55,000-MW monomers are found in all eukaryotes, and their sequences are highly conserved. Tubulin is the major constituent of microtubules. Each tubulin subunit binds two molecules of GTP, one at an exchangeable site on the beta chain and one at a non-exchangeable site on the alpha chain (5).

As shown in figure 5.9. Relative expression for Tuba1a was significantly increased two folds in loaded tibias compared to the un-loaded tibias in young mice with p value 0.03. There is a significant 4-fold reduction of the gene expression in old unloaded tibias compared to the young ones (p=0.02). There was no significant effect of loading on Tuba1a expression in aged tibias, and after loading there is still a highly significant decrease in the right loaded old tibias in comparison to the right loaded young tibias with p value = 0.001. These results are similar to those in the RNA Seq analysis of the stretched osteoblasts, however, the effect of stretching was not significant in the young osteoblast in that experiment.

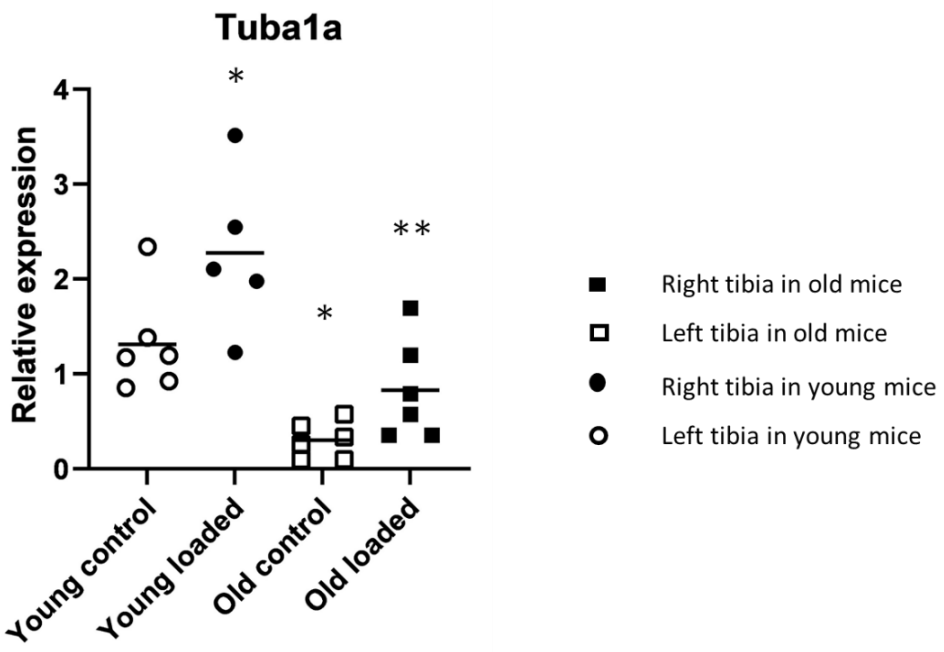

Figure 5.9. Relative expression for Tuba1a gene in young and aged mice tibias after loading. Young (3-months-old, N=5 loaded; N=6 control) and aged (15-month-old N=6 loaded; N=6 control) mice underwent repetitive loading of the right tibia. At the end of the experiment, RNA extracted from the left and right tibias then qPCR. Data were analysed using ANOVA. *: $p < 0.05$, **: $p < 0.005$ between young and aged groups.

5.3.4.2. Ankrd12: Ankyrin repeat domain 12

This gene encodes a member of the ankyrin repeats-containing cofactor family. These proteins may inhibit the transcriptional activity of nuclear receptors through the recruitment of histone deacetylases. The encoded protein interacts with p160 coactivators and also represses transcription mediated by the coactivator alteration/deficiency in activation 3 (ADA3). Alternatively spliced transcript variants encoding multiple isoforms have been observed for this gene(229).

Ankrd12 relative expression showed a significant 2-fold increase in loaded tibias of young mice compared to the control non-loaded with p value 0.01. There is significant (p=0.01) >10-fold reduction in the Ankrd12 gene expression in the old mice compared to the young mice. This reduction is even more significant (p=0.0001) in the old mice after loading in comparison

to the young mice after loading. There was no significant effect of loading on Ankrd12 expression in aged mice (Fig 5.10). These results closely mirror the results from the RNA Seq data, with a similar 2 fold increase after loading in young cells only.

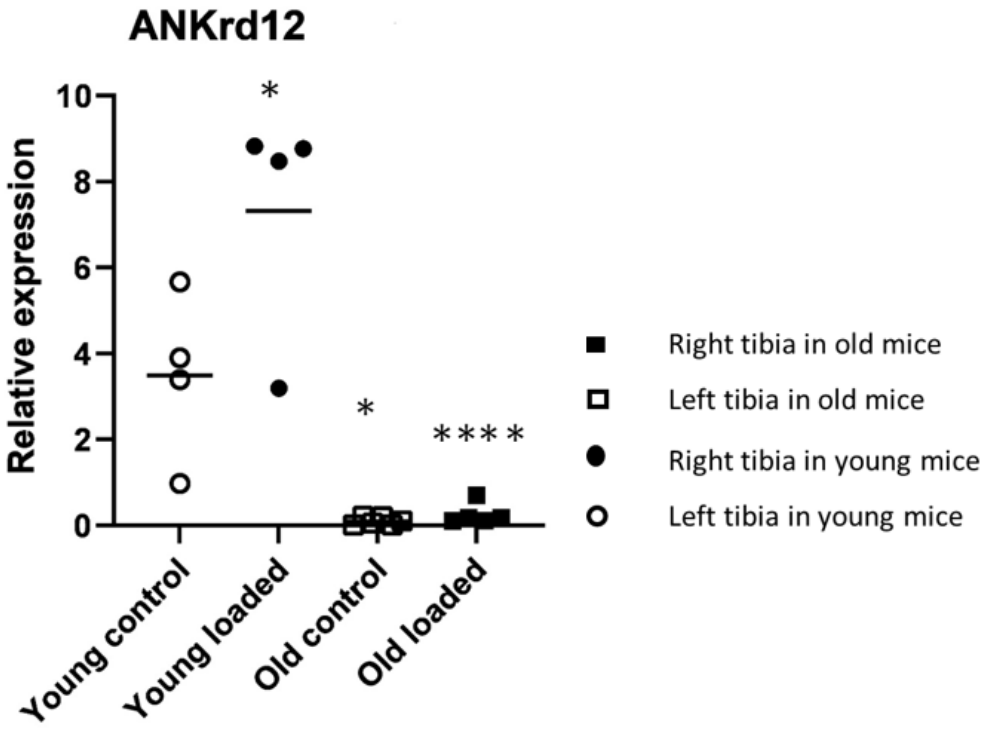

Figure 5.10. Relative expression for Ankkrd12 gene in young and aged mice tibias after loading. Young (3-months-old, N=4 loaded; N=4 control) and aged (15-month-old N=5 loaded; N=6 control) mice underwent repetitive loading of the right tibia. At the end of the experiment, RNA extracted from the left and right tibias then qPCR. Data were analysed using ANOVA. *: $p < 0.05$ between loaded and non-loaded, ****: $p < 0.005$ between young and aged (loaded) groups.

5.3.4.3. BAZ2B:

Bromodomain Adjacent To Zinc Finger Domain 2B. This gene belongs to the bromodomain gene family. Members of this gene family encode proteins that are integral components of chromatin remodelling complexes. The encoded protein showed strong preference for the activating H3K14Ac mark in a histone peptide screen, suggesting a potential role in transcriptional activation. Its expression is positively associated with heel bone mineral density, suggesting a role in bone metabolism (230).

Although expression of BAZ2B was increased after loading in both young and aged mice, this difference was not statistically significant. Likewise expression appeared to be increased in aged mice, but again this was not statistically significant (Fig 5.11). Although the trend and magnitude of the change after loading was the same as that seen in the stretched osteoblasts, the qPCR result showed no statistical significance, possibly due to the poor quality of RNA for the young samples, with a qPCR result for only 3 control and 4 loaded tibias.

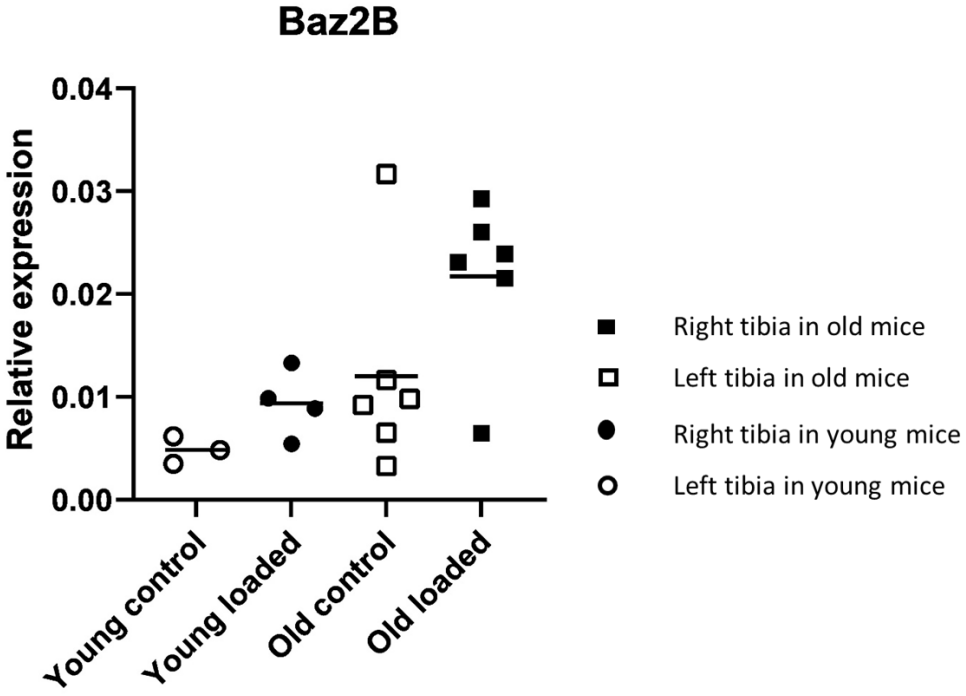

Figure 5.11. Relative expression for Baz2B gene in young and aged mice tibias after loading. Young (3-months-old, N=4 loaded; N=3 control) and aged (15-month-old N=6 loaded; N=6 control) mice underwent repetitive loading of the right tibia. At the end of the experiment, RNA extracted from the left and right tibias then qPCR. Data were analysed using ANOVA.

5.3.4.4. Serpine1:

Serpin Family E Member 1 or Endothelial Plasminogen Activator Inhibitor. This gene encodes a member of the serine proteinase inhibitor (serpin) superfamily. This member is the principal inhibitor of tissue plasminogen activator (tPA) and urokinase (uPA), and hence is an inhibitor of fibrinolysis. Defects in this gene are the cause of plasminogen activator inhibitor-1 deficiency (PAI-1 deficiency), and high concentrations of the gene product are associated with thrombophilia. Alternatively spliced transcript variants encoding different isoforms have been found for this gene.

Mechanical loading led to a 50% increase in serpine 1 mRNA in young mice, however, this was not statistically significant (Fig. 5.12). Similarly there was no significant increase was observed after loading in aged mice. However, serpine 1 expression showed a significant (p=0.03) 3-fold increase in aged loaded tibias compared to young loaded tibias. These results are very different from those obtained in the RNA Seq experiment, where there was only a significant effect in young cells, and we observed a decrease in expression after stretch instead of an increase.

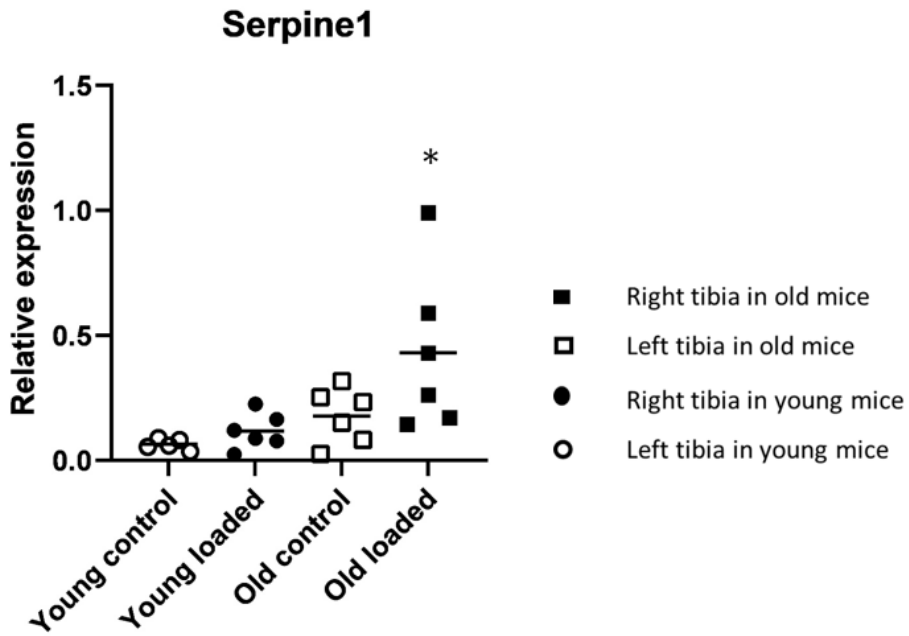

Figure 5.12. Relative expression for Serpine1 gene in young and aged mice tibias after loading. Young (3-months-old, N=6 loaded; N=5 control) and aged (15-month-old N=6 loaded; N=6 control) mice underwent repetitive loading of the right tibia. At the end of the experiment,

RNA extracted from the left and right tibias then qPCR. Data were analysed using ANOVA. *: $p < 0.05$ between aged loaded and young loaded groups.

5.3.4.5. Ephb3:

Ephrin ligands and their receptors are expressed in embryonic tissues that form the skeleton. Specifically, efnB1 is expressed in the prechondrogenic mesenchymal condensations and efnB2 is expressed in the embryonic calvarial sutures. EfnB1, EphB2 and EphB3 are expressed at the tips of the ribs where they would be expected to regulate rib development. With respect to Eph receptors, EphB1 and EphB2 are also expressed in the embryonic calvarial sutures, and EphA3 and EphA7 are expressed in the limb mesenchyme. EphB4 is expressed in the chondrocytes, osteoblasts and osteoclasts of the growth plate. EphA4 is expressed in the prechondrogenic limb mesenchyme of the chicken. These associations suggest that these ligands and receptors might be binding partners that regulate the development and homeostasis of both intramembranous and endochondral bone.

Studies at the cellular level have identified multiple efn ligands and Eph receptors expressed by cells of osteoblast and osteoclast lineage, as well as their precursors. EfnB1, efnB2 and EphB receptors are expressed throughout osteoblast development, but more restricted in osteoclast precursors.

Studies involving conditional disruption of efnB1 in osteoblasts and osteoclasts have revealed that efnB1expressed in both osteoblasts and osteoclasts regulates skeletal development by influencing bone formation and bone resorption processes, respectively.

Ephb3 could not be detected in the young samples and showed no significant effect of loading in the aged mice.

5.3.4.6. Atrx:

Alpha Thalassemia/Mental Retardation Syndrome X-Linked or ATRX Chromatin Remodeller. ATRX encodes a chromatin remodelling protein, the protein encoded by this gene contains an

ATPase/helicase domain, and thus it belongs to the SWI/SNF family of chromatin remodeling proteins. This protein is found to undergo cell cycle-dependent phosphorylation, which regulates its nuclear matrix and chromatin association, and suggests its involvement in the gene regulation at interphase and chromosomal segregation in mitosis. Mutations in this gene are associated with X-linked syndromes exhibiting cognitive disabilities as well as alpha-thalassemia (ATRX) syndrome. These mutations have been shown to cause diverse changes in the pattern of DNA methylation, which may provide a link between chromatin remodelling, DNA methylation, and gene expression in developmental processes. Multiple alternatively spliced transcript variants encoding distinct isoforms have been reported.

Mutations in the human ATRX gene cause developmental defects, including skeletal deformities and dwarfism. However, loss of ATRX in cartilage led to a delay in the ossification of the hips in some mice. (Loss of ATRX in chondrocytes has minimal effects on skeletal development.

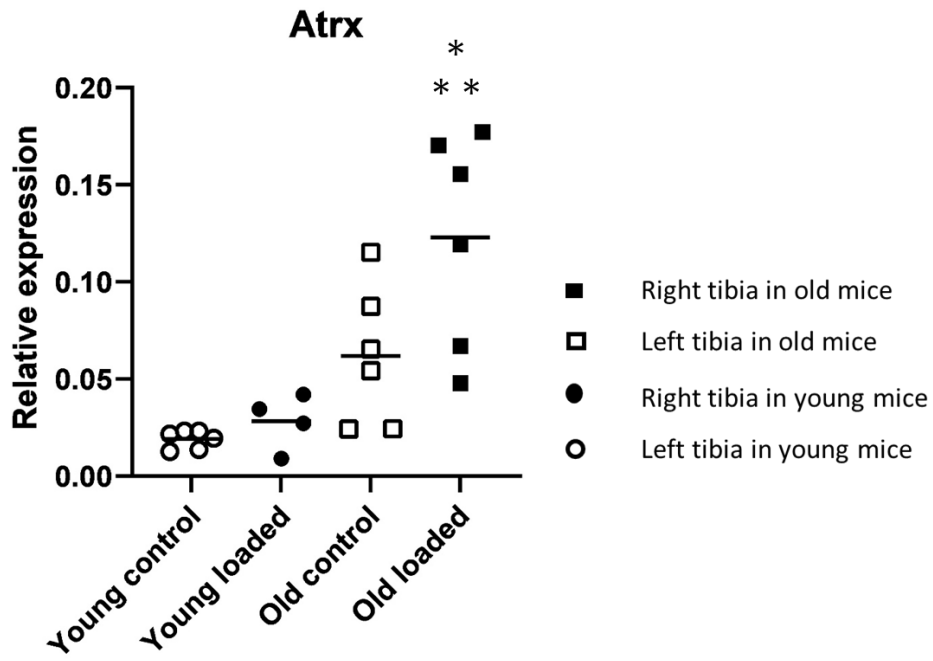

Figure 5.13. Relative expression for Atrx gene in young and aged mice tibias after loading. Young (3-months-old, N=4 loaded; N=6 control) and aged (15-month-old N=6 loaded; N=6 control) mice underwent repetitive loading of the right tibia. At the end of the experiment, RNA extracted from the left and right tibias then qPCR. Data were analysed using ANOVA. ***: $p < 0.005$ between aged and young groups after loading.

Atrx expression was 3-fold higher in tibias of aged mice compared to young mice, however, this was not statistically significant (Fig. 5.13). In contrast to the RNA Seq data, mechanical loading did not significantly change Atrx expression in young mice, however, it resulted in a 2-fold increase in Atrx expression in aged mice (p=0.03), and expression was four times higher in aged loaded tibias than in young loaded tibias (p=0.002).

5.3.4.7. Usp34:

Ubiquitin Specific Peptidase 34, here, we identify USP34 as a previously unknown regulator of osteogenesis. The expression of USP34 in human MSCs increases after osteogenic induction while depletion of USP34 inhibits osteogenic differentiation. Conditional knockout of Usp34 from MSCs or pre-osteoblasts leads to low bone mass in mice. Deletion of Usp34 also blunts BMP2-induced responses and impairs bone regeneration. Mechanically, a study demonstrated that USP34 stabilizes both Smad1 and RUNX2 and that depletion of Smurf1 restores the osteogenic potential of Usp34-deficient MSCs in vitro Taken together, our data indicate that USP34 is required for osteogenic differentiation and bone formation(10).

Similar to the RNA Seq experiment, there was a 2-fold increase in Usp34 expression in young tibias, however, the result was non-significant. There was also significant increase in the aged tibias. There was no significant effect of age on its expression. However, there is a wide distribution on the data this may affect the statistical significance.

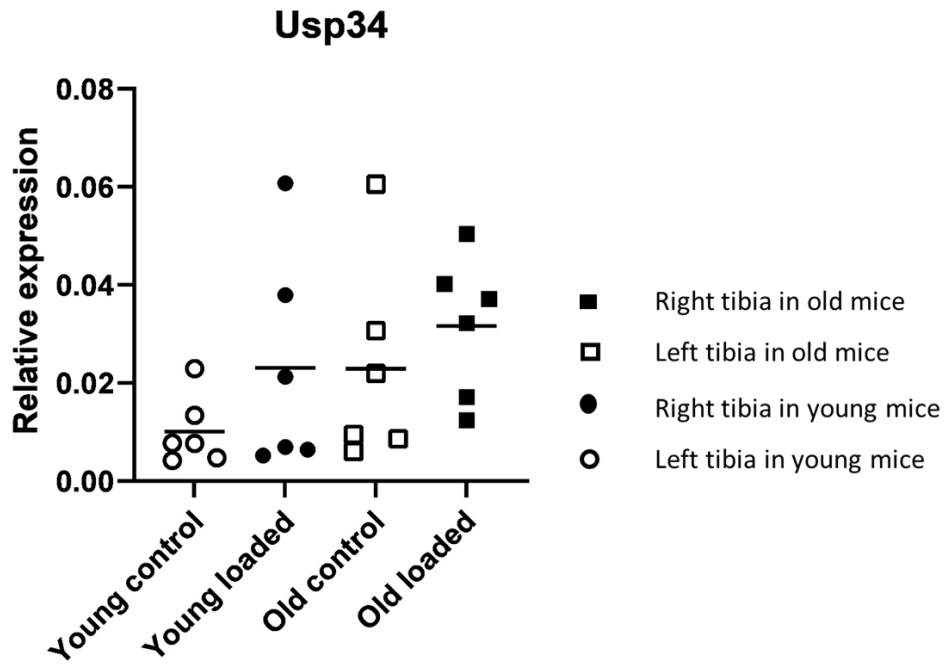

Figure 5.14. Relative expression for Usp34 gene in young and aged mice tibias after loading. Young (3-months-old, N=6 loaded; N=6 control) and aged (15-month-old N=6 loaded; N=6 control) mice underwent repetitive loading of the right tibia. At the end of the experiment, RNA extracted from the left and right tibias then qPCR. Data were analysed using ANOVA.

5.3.4.8. Inppl1:

Inositol Polyphosphate Phosphatase like 1, the protein encoded by this gene is an SH2-containing 5'-inositol phosphatase that is involved in the regulation of insulin function. The encoded protein also plays a role in the regulation of epidermal growth factor receptor turnover and actin remodelling. Additionally, this gene supports metastatic growth in breast cancer and is a valuable biomarker for breast cancer. Diseases associated with INPPL1 include Opsismodysplasia and Schneckenbecken Dysplasia. (Opsismodysplasia is a rare skeletal dysplasia involving delayed bone maturation. Clinical signs observed at birth include short limbs, small hands and feet, relative macrocephaly with a large anterior fontanel, and characteristic craniofacial abnormalities including a prominent brow, depressed nasal bridge, a small anteverted nose, and a relatively long philtrum. Death in utero or secondary to respiratory failure during the first few years of life has been reported, but there can be long-

term survival. Typical radiographic findings include shortened long bones with delayed epiphyseal ossification, severe platyspondyly, metaphyseal cupping, and characteristic abnormalities of the metacarpals and phalanges (11), (definition Schneckenbecken dysplasia (or chondrodysplasia with snail-like pelvis) is a prenatally lethal spondylodysplastic dysplasia. Epidemiology Less than 20 cases have been reported in the literature so far. Clinical description. The typical radiographic finding is the snail-like configuration of the hypoplastic iliac bone. Additional features include flattened hypoplastic vertebral bodies, short ribs, short and wide fibulae, short and broad long bones with a dumbbell-like appearance, and precocious ossification of the tarsus. Etiology This syndrome is caused by loss-of-function mutations of the SLC35D1 gene (1p32-p31) Genetic counselling Schneckenbecken dysplasia is transmitted in an autosomal recessive manner). Among its related pathways are RET signaling and Innate Immune System. Gene Ontology (GO) annotations related to this gene include actin binding and SH3 domain binding.

Phosphatidylinositol (PtdIns) phosphatase that specifically hydrolyzes the 5-phosphate of phosphatidylinositol-3, 4, 5-trisphosphate (PtdIns (3,4,5)P3) to produce PtdIns(3,4)P2, thereby negatively regulating the PI3K (phosphoinositide 3-kinase) pathways. Plays a central role in regulation of PI3K-dependent insulin signaling, although the precise molecular mechanisms and signaling pathways remain unclear. While overexpression reduces both insulin-stimulated MAP kinase and Akt activation, its absence does not affect insulin signaling or GLUT4 trafficking. Confers resistance to dietary obesity. May act by regulating AKT2, but not AKT1, phosphorylation at the plasma membrane. Part of a signaling pathway that regulates actin cytoskeleton remodeling. Required for the maintenance and dynamic remodeling of actin structures as well as in endocytosis, having a major impact on ligand-induced EGFR internalization and degradation. Participates in regulation of cortical and submembraneous actin by hydrolyzing PtdIns(3,4,5)P3 thereby regulating membrane ruffling (PubMed:21624956). Regulates cell adhesion and cell spreading. Required for HGF-mediated lamellipodium formation, cell scattering and spreading. Acts as a negative regulator of EPHA2 receptor endocytosis by inhibiting via PI3K-dependent Rac1 activation. Acts as a regulator of neuritogenesis by regulating PtdIns(3,4,5)P3 level and is required to form an initial protrusive pattern, and later, maintain proper neurite outgrowth. Acts as a negative regulator of the FC-gamma-RIIA receptor (FCGR2A). Mediates signaling from the FC-gamma-RIIB receptor

(FCGR2B), playing a central role in terminating signal transduction from activating immune/hematopoietic cell receptor systems. Involved in EGF signaling pathway. Upon stimulation by EGF, it is recruited by EGFR and dephosphorylates PtdIns(3,4,5)P3. Plays a negative role in regulating the PI3K-PKB pathway, possibly by inhibiting PKB activity. Down-regulates Fc-gamma-R-mediated phagocytosis in macrophages independently of INPP5D/SHIP1. In macrophages, down-regulates NF-kappa-B-dependent gene transcription by regulating M-CSF - induced signaling. May also hydrolyze PtdIns(1,3,4,5)P4, and could thus affect the levels of the higher inositol polyphosphates like InsP6. Involved in endochondral ossification.

Inppl1 expression was significantly higher in aged than in young tibias, both in control and loaded tibias (Fig 4.15). However, in contrast to the RNA Seq data, only aged tibias showed a significant effect of loading, with a 2-fold increase of expression in loaded aged tibias ($p<0.001$).

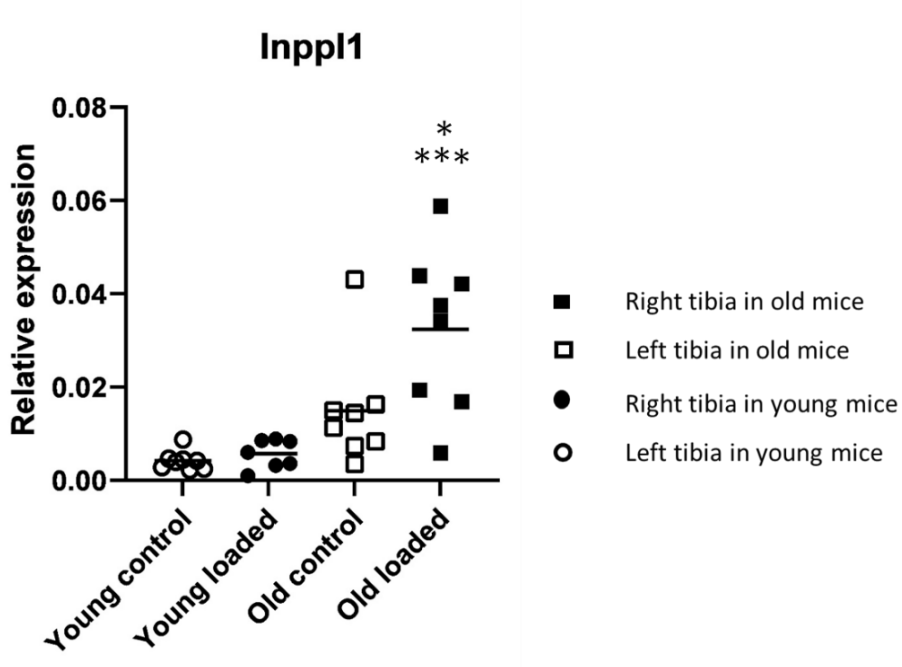

Figure 5.15. Relative expression for InppI1 gene in young and aged mice tibias after loading. Young (3-months-old, N=7 loaded; N=7 control) and aged (15-month-old N=8 loaded; N=8 control) mice underwent repetitive loading of the right tibia. At the end of the experiment, RNA extracted from the left and right tibias then qPCR. Data were analysed using ANOVA. ****: $p < 0.0001$ between aged and young groups.

5.3.4.9. Trpc4ap:

Short Transient Receptor Potential Channel 4-Associated Protein, is a Protein coding gene. Among its related pathways are ion channel transport and TRP channels. Gene Ontology (GO) annotations related to this gene include phosphatase binding.

Substrate-specific adapter of a DCX (DDB1-CUL4-X-box) E3 ubiquitin-protein ligase complex required for cell cycle control. The DCX (TRUSS) complex specifically mediates the polyubiquitination and subsequent degradation of MYC. Also participates in the activation of NFKB1 in response to ligation of TNFRSF1A, possibly by linking TNFRSF1A to the IKK signalosome. Involved in JNK activation via its interaction with TRAF2. Also involved in elevation of endoplasmic reticulum Ca (2+) storage reduction in response to CHRM1.

Trpc4ap expression was higher in aged than in young tibias, although this difference was only significant after loading (4-fold increase, $p<0.01$, Fig 4.16). There was no significant effect of loading on Trpc4ap expression in young tibias, whereas Trpc4ap expression showed a 2-fold increase after loading in aged tibias. This is in contrast to the RNA Seq analysis, where we observed an effect of loading in young osteoblasts only, and we observed a decrease in expression rather than an increase.

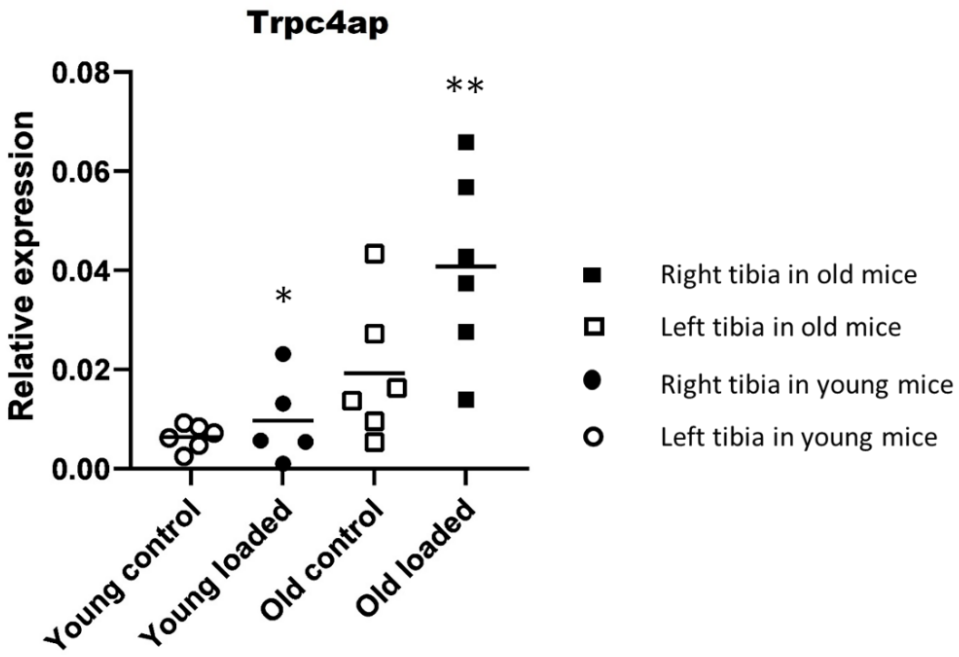

Figure 5.16. Relative expression for Trpc4ap gene in young and aged mice tibias after loading. Young (3-months-old, N=5 loaded; N=6 control) and aged (15-month-old N=6 loaded; N=6 control) mice underwent repetitive loading of the right tibia. At the end of the experiment, RNA extracted from the left and right tibias then qPCR. Data were analysed using ANOVA. **: $p < 0.01$ between aged and young groups after loading.

5.3.4.10. Shisa4:

Shisa Family Member 4, mShisa, which is homologous to xShisa1 that we previously reported as a head inducer in Xenopus. mShisa encodes an antagonist against both Wnt and Fgf signalings; it inhibits these signalings cell-autonomously as xShisa1 does. The mShisa expression is lost or greatly reduced in Otx2 mutant visceral endoderm, anterior mesedoderm and anterior neuroectoderm. (Mouse homologues of Shisa antagonistic to Wnt and Fgf signalings (12).

SHISA3 blocks the maturation and transportation of Frizzled receptors to the cell surface, thereby inhibiting the Wnt/β-catenin signaling pathway in lung cancer. However, the function of Shisa3 in bone biology remains uninvestigated. This study found that Shisa3 was strongly

expressed in the calvarial bones of mice, especially in osteoblasts. In addition, adenovirus-mediated gene transfer of murine Shisa3 significantly inhibited Wnt3a-induced nuclear translocation of β-catenin and mRNA expression of the Wnt target gene Axin2. (The Shisa3 knockout mouse exhibits normal bone phenotype (13).

Expression of Shisa4 showed a similar pattern as that observed in the RNA Seq experiment, with higher expression in loaded young tibias than loaded aged tibias (3-fold increase, p=0.04, Fig. 5.17). However, the effect of loading was non-significant, possibly because only three samples from the young mice were analysable for this gene in the qPCR analysis.

Figure 5.17. Relative expression for Shisa4 gene in young and aged mice tibias after loading. Young (3-months-old, N=3 loaded; N=3 control) and aged (15-month-old N=6 loaded; N=6 control) mice underwent repetitive loading of the right tibia. At the end of the experiment, RNA extracted from the left and right tibias then qPCR. Data were analysed using ANOVA. *: $p < 0.05$ between aged and young groups after loading.

5.4. Discussion

In this chapter I analysed the effect of ageing on gene expression of bone cells in response to mechanical loading. I used 2 different model systems. The first used osteocyte-like osteoblast grown out of bone chips that were subjected to stretching of the substrate as the mechanical load, with analysis of gene expression by RNA Sequencing. The second model used the same *in vivo* loading of the tibia as used in Chapter three, and analysed gene expression in the osteocyte-rich cell population from the bone shaft of the tibias by qPCR.

Generally, both model systems showed a greater response to mechanical loading in young cells than in aged cells.

Our results showed the most upregulated genes in response to mechanical loading in young osteoblasts are connected to the transcriptional regulator ATRX gene which encodes the chromatin remodelling protein, this protein contains an ATPase/helicase domain, and thus it belongs to the SWI/SNF family of chromatin remodeling proteins. This protein is found to undergo cell cycle-dependent phosphorylation, which regulates its nuclear matrix and chromatin association, and suggests its involvement in the gene regulation at interphase and chromosomal segregation in mitosis.

Mutations in the human ATRX gene cause developmental defects, including skeletal deformities and dwarfism. However, loss of ATRX in cartilage led to a delay in the ossification of the hips in some mice (231).

Interestingly, the main finding in this chapter is that in response to mechanical loading, the Transcriptional regulator ATRX gene which encodes the chromatin remodelling proteins linked to the Ubiquitin carboxyl-terminal hydrolase 34(Usp34) that removes conjugated ubiquitin from AXIN1 and AXIN2 and acting as a regulator and activator to the Wnt signalling pathway which is also upregulated in young osteoblasts.

USP34 identified as a regulator of osteogenesis. The expression of USP34 in human MSCs increases after osteogenic induction while depletion of USP34 inhibits osteogenic differentiation. Conditional knockout of Usp34 from MSCs or pre-osteoblasts leads to low bone mass in mice. Deletion of Usp34 also blunts BMP2-induced responses and impairs bone regeneration. Mechanically, Guo et al (232) demonstrated that USP34 stabilizes both Smad1

and RUNX2 and that depletion of Smurf1 restores the osteogenic potential of Usp34-deficient MSCs *in vitro* Taken together, their data indicate that USP34 is required for osteogenic differentiation and bone formation. In addition it Inhibits Osteoclast Differentiation by Regulating NF-κB Signaling (233).

Our gene expression results showed upregulation for the group of Tuba1a, Tubb2a, Tubb2b and Tubb5 in young osteoblasts comparing to the aged once, this genes are structural genes that encodes for Tubulin and there products participate in the formation of microtubules the structural proteins that participate in cytoskeletal structure. Specifically, microtubules are composed of a heterodimer of alpha and beta-tubulin molecules. Tubulin is the major constituent of microtubules.

On the other hand we found that the Shisa4 gene is upregulated in young osteoblast after stretching compared to the aged osteoblasts. Shisa Family Member 4, is homologous to *xShisa1*.*Shisa family* encodes an antagonist against both Wnt and Fgf signalings; it inhibits these signalings cell-autonomously as *xShisa1* does. If the *mShisa* expression is lost or greatly reduced in *Otx2* mutant visceral endoderm, anterior mesendoderm and anterior neuroectoderm (234).

SHISA3 blocks the maturation and transportation of Frizzled receptors to the cell surface, thereby inhibiting the Wnt/*β*-catenin signaling pathway in lung cancer. However, the function of Shisa3 in bone biology remains uninvestigated. Unless, a study found that Shisa3 was strongly expressed in the calvarial bones of mice, especially in osteoblasts. In addition, adenovirus-mediated gene transfer of murine Shisa3 significantly inhibited Wnt3a-induced nuclear translocation of *β*-catenin and mRNA expression of the Wnt target gene *Axin2* (235).

Our finding from string interaction is that Shisa4 linked to Cryab gene which is upregulated as well. Crystallin Alpha B is encoding for the small heat shock protein, it is a transcriptional target of the BMP signaling pathway. Ciumas et al demonstrated that CRYAB expression is upregulated strongly by BMPs in an EC line and in human lung microvascular ECs and human umbilical vein ECs and they showed that BMP signals through the BMPR2-ALK1 pathway to upregulate CRYAB expression through a transcriptional indirect mechanism involving Id1. The study observed that the known anti apoptotic effect of the BMPs is, in part, because of the

upregulation of CRYAB expression in EC (236)**.** CRYaB upregulation in hBMSCs during osteogenesis, is a novel marker of this process (236).

Chapter 6. Discussion

Osteoporosis is a metabolic bone disease that affects the bone remodelling process, and causes bone mass loss and consequently a bone strength reduction, resulting in an increase in fragility and susceptibility to fracture (72) affecting people over the age of 50, and most commonly occurs in elderly women (237).

Despite advances in the understanding and treatment of osteoporosis, osteoporosis is still prevalent and with the increase in life expectancy, the incidence of osteoporotic fractures is still expected to increase (238). Osteoporotic fractures often result in hospitalisation, pain, reduced quality of life, and a reduced life expectancy. There is therefore still a need to improve our understanding of the mechanisms underlying osteoporosis, so that better treatments can be devised.

The major factor increasing the risk of osteoporotic fractures is ageing. With age bone properties change, bone modifications may include the mechanical function, shape of bones, bone cells, the matrix they produce, and the mineral that is deposited on this matrix (239). The mechanisms by which ageing increases this risk are probably multifactorial and currently not fully understood. However, one important factor appears to be that ageing results in a reduced bone anabolic effect of mechanical loading. Understanding the mechanisms that underlay this decrease in response to loading could lead to new avenues for treating age-related osteoporosis. The cells that act as mechanosensors in bone are the osteocytes, whereas the osteoblasts are the cells that produce the new bone in response to loading.

The purpose of this PhD research is to study age related changes in osteoblasts and osteocytes and compare their response to mechanical loading between two different age groups, young and aged adults.

The model systems used in this study were the *in vitro* model of primary mouse osteoblast cultures undergoing mechanical loading by stretching of the culture substrate, and the *in vivo* model of cyclic loading of the mouse knee by compressing the tibia bone. I compared the responses in cells and knees from young (3-month-old) and aged (14-15-month-old) mice.

The main finding of this study is that there was no increase in bone formation after loading in aged mice, no change in gene expression after loading in aged osteocytes and osteoblasts compared to the young mice and their osteocytes and osteoblasts.

Biochemically, the same effect was observed in studying the circulating factors produced by bone cells. The bone formation biomarker P1NP showed a significant decrease in aged mice serum compared to the young once and it did not respond to mechanical loading as young mice responded.

Using bone histomorphometry and μCT analysis, this study found that there was a substantial decrease in trabecular and cortical bone volume in aged mouse tibias compared to young mice, combined with a major decrease in bone formation in response to mechanical loading. In addition, the number of osteocyte lacunae was significantly decreased in aged mice tibias, leading to an increase in osteocyte separation distance. This reduction in osteocytes, which are the mechanosensing cells in bone that direct the actions of osteoblasts and osteoclasts functions, may partially explain the decreased response to loading in the aged mice.

A major growth factor that regulates bone formation, is the wnt-inhibitor sclerostin. Loading is reported to result in decreased sclerostin levels, leading to increased bone formation (193). However, this study observed no difference in Sclerostin expression after loading in osteocytes either in the young or the aged mice. One reason why I did not observe any changes in sclerostin levels could be that I only loaded 1 knee. This could lead to local changes in sclerostin levels that could not be measured in the serum of the mice due to the fact that the rest of the animals' skeleton (a much larger quantity of bone tissue) was not loaded.

Loading of the knee leads to a distinct change in gene expression pattern in the osteocytes and osteoblasts of young mice. Most of the genes that responded to the stretching of young osteoblasts (*In vitro* loading) were the genes related to the chromatin remodelling, mitosis, and the Wnt signalling pathway which is critical to the bone formation through binding to the Frizzled proteins. In contrast, I did not observe changes in gene expression in the aged osteoblasts. Some of the changes observed in the cultured osteoblasts, could also be observed in the osteocytes from loaded knees. Further analysis of the differentially expressed genes identified could indicate which pathways are essential for the bone anabolic response to mechanical loading of bone. Targeting of these pathways could possibly restore

responsiveness in aged individuals. The gene expression studies suffered from some issues which may have affected the results.

First of all, sample numbers were relatively low and only one time point after loading was studied. The low sample number limited the statistical power of the study, and the single follow up time point means that it was not possible to identify changes in gene expression at different time points. The main reasons for the single time point and limited sample numbers were the cost and time requirements for ageing mice to 15 months. This is very expensive and the funding levels for my studies did not allow for more animals. The yield of osteoblasts from aged mice was low, and not sufficient for multiple time points. Furthermore, PhD projects need to be completed within 3 years. Therefore, there was not enough time to generate aged mice for additional experiments or to increase sample numbers.

A second issue was cell purity. The osteoblast cultures take a long time (more than 4 weeks), and some cells may have dedifferentiated during the culture period. Contaminating fibroblasts and macrophages may have proliferated faster than the osteoblasts, leading to a mixed cell population, with the relative contributions of the cell types possible different between different cultures. The cleaned knee bone tissue was used as a source of osteocyte RNA. However, osteocyte purity was most likely not 100%. Especially endothelial cells from the many capillaries within the bone, and some remaining lining cells on the bone surface as likely contaminants of these samples. Furthermore, like with the osteoblast cultures, the level of contaminating cells may have been different between individual samples. This could mean that difference between samples was due to a difference in cellular composition, rather than the effects of loading or ageing. Finally, the bone tissue was treated with collagenase to remove non-osteocytic cells. It is unclear whether this collagenase treatment may have affected the gene expression patterns of the osteocytes.

Therefore, to improve the quality of this studies, I propose to increase the sample numbers and study more time points after loading, both earlier and later.

The issue of sample purity may be more difficult to address. However, recent advances in gene expression analysis now allow the analysis of the gene expression patterns in a single cell, or small numbers of cells. This opens up the possibility for analysis of gene expression studies in pure populations of osteocytes and osteoblasts by combining RNASeq with micro-

dissection. Microdissection is the isolation of small sections of pure tissue from microscope slides. This means that after section the bones, areas only containing osteocytes or only containing osteoblasts could be harvested and subsequently analysed by RNASeq. When loading the knee, certain parts of the bone experience compression, whereas other regions undergo a decrease in loading. It would seem logical that regions undergoing such very different loading patterns would respond with different changes in gene expression patterns. Microdissection could be used to compare cells from different parts of the loaded bone, thereby substantially improving the detail of bone cell responses.

In summary, my studies have shown a substantial decrease in responsiveness to mechanical loading by aged bone cells, and identified genes that are differentially expressed after mechanical loading. Although further studies of the pathways involved in mechanosensing are required, some of these genes may be pharmaceutical targets to restore the bone anabolic response to mechanical loading in the elderly, and thereby prevent or treat osteoporosis.

References

1. Reiner B, Bertha F. Osteoporosis : Diagnosis,Prevention,Therapy. second edi. Springer-Verlag Berlin Heidelberg; 2009. 313 p.

2. Kollet O, Dar A, Lapidot T. The Multiple Roles of Osteoclasts in Host Defense : Bone Remodeling and Hematopoietic Stem Cell Mobilization. 2007;

3. Burr DB. Chapter 1 - Bone Morphology and Organization [Internet]. Second Edi. Basic and Applied Bone Biology. Elsevier Inc.; 2019. 1–26 p. Available from: https://doi.org/10.1016/B978-0-12-813259-3.00001-4

4. Buckwalter JA, Glimcher MJ, Cooper RR, Recker R. Bone Biology. 2010;1256–75.

5. Cundy T, Reid IR, Grey A, Biology B. M etabolic bone disease [Internet]. Third Edit. Clinical Biochemistry. Elsevier Ltd.; 2014. 604–635 p. Available from: http://dx.doi.org/10.1016/B978-0-7020-5140-1.00031-6

6. Bianchi S, Martinoli C. Ultrasound of the Musculoskeletal System. Sartor ALB· LWB· H-PH· MK· MM· CN· K, editor. Germany: Springer; 2007. 974 p.

7. Kini U, Nandeesh BN. Physiology of Bone Formation, Remodeling, and Metabolism. 2012. 29–57 p.

8. Capulli M, Paone R, Rucci N. Osteoblast and osteocyte: Games without frontiers. Arch Biochem Biophys [Internet]. 2014;561:3–12. Available from: http://dx.doi.org/10.1016/j.abb.2014.05.003

9. Wennberg C, Hessle L, Lundberg P, Mauro S, Milla L. Functional Characterization of Osteoblasts and Osteoclasts from Alkaline Phosphatase Knockout Mice. J BONE Miner Res. 2000;15(10):1879–88.

10. Shapiro F. Bone development and its relation to fracture repair. The role of mesenchymal osteoblasts and surface osteoblasts. Eur Cell Mater. 2008;15:53–76.

11. Birmingham E, Niebur GL, Mchugh PE, Shaw G, Barry FP, Mcnamara LM, et al. OSTEOGENIC DIFFERENTIATION OF MESENCHYMAL STEM CELLS IS REGULATED BY

OSTEOCYTE AND OSTEOBLAST CELLS IN A SIMPLIFIED BONE NICHE. Eur Cells Mater. 2012;23(353):13–27.

12. Nakashima K, Zhou X, Kunkel G, Zhang Z, Deng JM, Behringer RR, et al. The Novel Zinc Finger-Containing Transcription Factor Osterix Is Required for Osteoblast Differentiation and Bone Formation. Cell. 2002;108:17–29.

13. Anderson HC. Matrix Vesicles and Calcification. Curr Rheumatol Rep. 2003;5(3):222–6.

14. Yoshiko Y, Candeliere GA, Maeda N, Aubin JE. Osteoblast autonomous Pi regulation via Pit1 plays a role in bone mineralization. Mol Cell Biol [Internet]. 2007;27(12):4465–74. Available from: http://mcb.asm.org/content/27/12/4465.short

15. Kremer EA, Chen YAN, Suzuki KO, Nagase H, Gorski JP. Hydroxyapatite induces autolytic degradation and inactivation of matrix metalloproteinase-1 and -3. J Bone Min Res. 1998;13(12):1890–902.

16. Boivin G, Meunier PJ. The Degree of Mineralization of Bone Tissue Measured by Computerized Quantitative Contact Microradiography. Calcif Tissue Int. 2002;70(6):503–11.

17. Franz-Odendaal TA, Hall BK, Witten PE. Buried alive: How osteoblasts become osteocytes. Dev Dyn. 2006;235(1):176–90.

18. Histology: A Text and Atlas: With Correlated Cell and Molecular Biology, 8e | Medical Education | Health Library [Internet]. [cited 2021 Feb 24]. Available from: https://meded-lwwhealthlibrary-com.liverpool.idm.oclc.org/book.aspx?bookid=2583#?

19. Xing L, Boyce BF. Regulation of apoptosis in osteoclasts and osteoblastic cells. Biochem Biophys Res Commun. 2005;328(3):709–20.

20. Crockett JC, Mellis DJ, Scott DI, Helfrich MH. New knowledge on critical osteoclast formation and activation pathways from study of rare genetic diseases of osteoclasts : focus on the RANK / RANKL axis RB. 2011;1–20.

21. Knowles HJ, Athanasou NA. Canonical and non-canonical pathways of osteoclast

formation. Histol Histopathol. 2009;24(3):337–46.

22. McKee JS and MD. Molecular and cellular biology of alveolar bone. 2000;24:99–126.

23. Boyce BF, Xing L. Functions of RANKL/RANK/OPG in bone modeling and remodeling. Arch Biochem Biophys. 2008;473(2):139–46.

24. Matsumoto M, Kogawa M, Wada S, Takayanagi H, Tsujimoto M, Katayama S, et al. Essential role of p38 mitogen-activated protein kinase in cathepsin K gene expression during osteoclastogenesis through association of NFATc1 and PU.1. J Biol Chem. 2004;279(44):45969–79.

25. Miyamoto T. The dendritic cell-specific transmembrane protein DC-STAMP is essential for osteoclast fusion and osteoclast bone-resorbing activity. Mod Rheumatol. 2006;16(6):341–2.

26. Mulari MTK, Zhao H, Lakkakorpi PT, Väänänen HK. Osteoclast ruffled border has distinct subdomains for secretion and degraded matrix uptake. Traffic. 2003;4(2):113–25.

27. Arana-Chavez VE, Bradaschia-Correa V. Clastic cells: Mineralized tissue resorption in health and disease. Int J Biochem Cell Biol. 2009;41(3):446–50.

28. Lakkakorpi PT, Horton MA, Helfrich MH, Karhukorpi EK, Vaananen HK. Vitronectin receptor has a role in bone resorption but does not mediate tight sealing zone attachment of osteoclasts to the bone surface. J Cell Biol. 1991;115(4):1179–86.

29. Luxenburg C, Geblinger D, Klein E, Anderson K, Hanein D, Geiger B, et al. The architecture of the adhesive apparatus of cultured osteoclasts: From podosome formation to sealing zone assembly. PLoS One. 2007;2(1).

30. Feng X, McDonald JM. Disorders of bone remodeling. Annu Rev Pathol. 2011;6:121–45.

31. Rochefort GY, Pallu S, Benhamou CL. Osteocyte: The unrecognized side of bone tissue. Osteoporos Int. 2010;21(9):1457–69.

32. Currey JD. The many adaptations of bone. J Biomech. 2003;36(10):1487–95.

33. Florencio-Silva R, Sasso GRDS, Sasso-Cerri E, Simões MJ, Cerri PS. Biology of Bone Tissue: Structure, Function, and Factors That Influence Bone Cells. Biomed Res Int [Internet]. 2015;2015:1–17. Available from: http://www.hindawi.com/journals/bmri/2015/421746/

34. Kuo SP, Bradley LA, Trussell LO. Osteocytes: Master Orchestrators of Bone. Hear Res. 2010;29(30):9625–34.

35. Robling AG, Bonewald LF. The Osteocyte : New Insights. 2020;

36. Zhang K, Barragan-Adjemian C, Ye L, Kotha S, Dallas M, Lu Y, et al. E11/gp38 Selective Expression in Osteocytes: Regulation by Mechanical Strain and Role in Dendrite Elongation. Mol Cell Biol. 2006;26(12):4539–52.

37. Wetterwald A, Hofstetter W, Cecchini MG, Lanske B, Wagner C, Fleisch H, et al. Characterization and cloning of the E11 antigen, a marker expressed by rat osteoblasts and osteocytes. Bone. 1996;18(2):125–32.

38. Schulze E, Witt M, Kasper M, Löwik CWGM, Funk RHW. Immunohistochemical investigations on the differentiation marker protein E11 in rat calvaria, calvaria cell culture and the osteoblastic cell line ROS 17/2.8. Histochem Cell Biol. 1999;111(1):61–9.

39. Poole KES. Sclerostin is a delayed secreted product of osteocytes that inhibits bone formation. FASEB J. 2005;1842–5.

40. Ubaidus S, Li M, Sultana S, De Freitas PHL, Oda K, Maeda T, et al. FGF23 is mainly synthesized by osteocytes in the regularly distributed osteocytic lacunar canalicular system established after physiological bone remodeling. J Electron Microsc (Tokyo). 2009;58(6):381–92.

41. Manolagas SC. Choreography from the Tomb: An Emerging Role of Dying Osteocytes in the Purposeful, and Perhaps Not So Purposeful, Targeting of Bone Remodeling. Int Bone Miner Soc Knowl Environ. 2006;3(1):5–14.

42. Dallas SL, Prideaux M, Bonewald LF. The osteocyte: An endocrine cell . . . and more. Endocr Rev. 2013;34(5):658–90.

43. Mullender MG, Van Der Meer DD, Huiskes R, Lips P. Osteocyte density changes in aging and osteoporosis. Bone. 1996;18(2):109–13.

44. Bonewald LF. Osteocytes as dynamic multifunctional cells. Ann N Y Acad Sci. 2007;1116:281–90.

45. Noble BS, Stevens H, Loveridge N, Reeve J. Identification of apoptotic changes in osteocytes in normal and pathological human bone. Bone. 1997;20(3):273–82.

46. Aguirre JI, Plotkin LI, Stewart SA, Weinstein RS, Parfitt AM, Manolagas SC, et al. Osteocyte Apoptosis Is Induced by Weightlessness in Mice and Precedes Osteoclast Recruitment and Bone Loss. J Bone Miner Res. 2006;21(4):605–15.

47. Plotkin LI. Apoptotic osteocytes and the control of targeted bone resorption. Curr Osteoporos Rep. 2014;12(1):121–6.

48. Bellido T. Osteocyte-driven bone remodeling. Calcif Tissue Int. 2014;94(1):25–34.

49. Boabaid F, Cerri PS, Katchburian E. Apoptotic bone cells may be engulfed by osteoclasts during alveolar bone resorption in young rats. Tissue Cell. 2001;33(4):318–25.

50. Cerri PS, Boabaid F, Katchburian E. Combined TUNEL and TRAP methods suggest that apoptotic bone cells are inside vacuoles of alveolar bone osteoclasts in young rats. J Periodontal Res. 2003;38(2):223–6.

51. Faloni APS, Sasso-Cerri E, Katchburian E, Cerri PS. Decrease in the number and apoptosis of alveolar bone osteoclasts in estrogen-treated rats. J Periodontal Res. 2007;42(3):193–201.

52. Knothe Tate ML. “Whither flows the fluid in bone?” An osteocyte’s perspective. J Biomech. 2003;36(10):1409–24.

53. Xiao Z, Zhang S, Mahlios J, Zhou G, Magenheimer BS, Guo D, et al. Cilia-like structures and polycystin-1 in osteoblasts/osteocytes and associated abnormalities in skeletogenesis and Runx2 expression. J Biol Chem. 2006;281(41):30884–95.

54. Santos A, Bakker AD, Zandieh-Doulabi B, de Blieck-Hogervorst JMA, Klein-Nulend J. Early activation of the β-catenin pathway in osteocytes is mediated by nitric oxide,

phosphatidyl inositol-3 kinase/Akt, and focal adhesion kinase. Biochem Biophys Res Commun. 2010;391(1):364–9.

55. Bonewald LF. The amazing osteocyte. J Bone Miner Res. 2011;26(2):229–38.

56. Burger EH, Klein-Nulend J. Mechanotransduction in bone - role of the lacuno-canalicular network. FASEB J. 1999;13(9001):S101–12.

57. OLIVIER VERBORGT, GARY J. GIBSON and MBS. Loss of Osteocyte Integrity in Association with Microdamage and Bone Remodeling After Fatigue In Vivo. J BONE Miner Res. 2009;15(1):60–7.

58. Miller SC, de Saint-Georges L, Bowman BM, Jee WS. Bone lining cells: structure and function. Scanning Microsc. 1989;3(3):953–60.

59. Aarden EM, Nijweide PJ, Burger EH. Function of osteocytes in bone. J Cell Biochem. 1994;55(3):287–99.

60. Andersen TL, Sondergaard TE, Skorzynska KE, Dagnaes-Hansen F, Plesner TL, Hauge EM, et al. A Physical Mechanism for Coupling Bone Resorption and Formation in Adult Human Bone. Am J Pathol. 2009;174(1):239–47.

61. Mosley JR. ewOsteoporosis and bone functional adaptation: mechanobiological regulation of bone architecture in growing and adult bone, a revi. J Rehabil Res Dev. 2000;37(2):189–99.

62. Everts V, Delaissé JM, Korper W, Jansen DC, Tigchelaar-Gutter W, Saftig P, et al. The Bone Lining Cell: Its Role in Cleaning Howship's Lacunae and Initiating Bone Formation. J Bone Miner Res. 2002;17(1):77–90.

63. Pawlina W, Ross MH. Histology: A Text and Atlas: With Correlated Cell and Molecular Biology, 8e. 2020.

64. Gelse K, Po E, Aigner T. Collagens — structure , function , and biosynthesis. 2003;55:1531–46.

65. Creecy A, Brown KL, Rose KL, Voziyan P, Nyman JS. Post-translational modifications in collagen type I of bone in a mouse model of aging. Bone [Internet]. 2021;143(November 2020):115763. Available from:

https://doi.org/10.1016/j.bone.2020.115763

66. Sommarin Y, Wendel M, Shen Z, Hellman U, Heinegård D. Osteoadherin , a Cell-binding Keratan Sulfate Proteoglycan in Bone , Belongs to the Family of Leucine-rich Repeat Proteins of the Extracellular Matrix. J Biol Chem. 1998;273(27):16723–9.

67. Wen L, Chen J, Duan L, Li S. Vitamin K - dependent proteins involved in bone and cardiovascular health (Review). 2018;3–15.

68. Baron R, Hesse E. Update on bone anabolics in osteoporosis treatment: Rationale, current status, and perspectives [Internet]. Vol. 97, Journal of Clinical Endocrinology and Metabolism. The Endocrine Society; 2012 [cited 2021 Mar 2]. p. 311–25. Available from: /pmc/articles/PMC3275361/

69. Bartl R, Bartl C, Bartl R, Bartl C. Modelling and Remodelling of Bone. In: The Osteoporosis Manual [Internet]. Springer International Publishing; 2019 [cited 2021 Mar 4]. p. 21–30. Available from: https://doi.org/10.1007/978-3-030-00731-7_3

70. Crockett JC, Michael J, Coxon FP, Lynne J, Helfrich MH, Crockett JC, et al. Bone remodelling at a glance Bone Remodelling at a Glance. 2011;2011:991–8.

71. Zuo C, Huang Y, Bajis R, Sahih M, Li Y. Osteoblastogenesis regulation signals in bone remodeling. 2012;1653–63.

72. Owen R, Reilly GC. In vitro models of bone remodelling and associated disorders. Vol. 6, Frontiers in Bioengineering and Biotechnology. 2018.

73. Funck-brentano T. Anti-Sclerostin Antibodies in Osteoporosis and Other Bone Diseases. J Clin Med. 2020;9(3439):1–16.

74. Moester MJC, Papapoulos SE, Löwik CWGM, Van Bezooijen RL. Sclerostin: Current knowledge and future perspectives. Calcif Tissue Int. 2010;87(2):99–107.

75. Kusu N, Laurikkala J, Imanishi M, Usui H, Konishi M, Miyake A, et al. Sclerostin Is a Novel Secreted Osteoclast-derived Bone Morphogenetic Protein Antagonist with Unique Ligand Specificity. JBC. 2003;278(26):24113–7.

76. Balemans W, Ebeling M, Patel N, Hul E Van, Olson P, Dioszegi M, et al. Increased bone density in sclerosteosis is due to the deficiency of a novel secreted protein (SOST).

Hum Mol Genet. 2001;10(5):537–44.

77. Seme M. SOST Is a Ligand for LRP5 / LRP6 and a Wnt Signaling Inhibitor. J Biol Chem. 2005;280(29):26770–5.

78. Bovijn J, Krebs K, Chen C, Boxall R, Censin JC. Lifelong genetically lowered sclerostin and risk of cardiovascular disease. 2019;

79. Brunetti G, Amato GD, Chiarito M, Tullo A, Colaianni G. An update on the role of RANKL – RANK / osteoprotegerin and WNT - ß - catenin signaling pathways in pediatric diseases. World J Pediatr [Internet]. 2019;15(1):4–11. Available from: https://doi.org/10.1007/s12519-018-0198-7

80. Grugni GBG, Delvecchio LPM, Giordano AVP, Amato MGGD. Analysis of Circulating Mediators of Bone Remodeling in Prader – Willi Syndrome. 2018;102:635–43.

81. Sobacchi C, Schulz A, Coxon F P VA and HMH. Osteopetrosis: genetics, treatment and new insights into osteoclast function. Nat Publ Gr [Internet]. 2013;(July). Available from: http://dx.doi.org/10.1038/nrendo.2013.137

82. Tolar J, Teitelbaum SL, Orchard PJ. Osteopetrosis. N Engl J Med. 2004;2839–49.

83. Stark Z, Savarirayan R. Osteopetrosis. Orphanet J Rare Dis. 2009;12:1–13.

84. PECK, WA. Consensus Development Conference : Diagnosis, Prophylaxis, and Treatment of Osteoporosis. Am J Med [Internet]. 1993 [cited 2021 Mar 19];94(6):646–50. Available from: https://ci.nii.ac.jp/naid/10029758389

85. SAIKA M, INOUE D, KIDO S AMT. 17b-Estradiol Stimulates Expression of Osteoprotegerin by a Mouse Stromal Cell Line, ST-2, via Estrogen Receptor-a. Endocrinology. 2001;142(6):2205–12.

86. Eghbali-fatourechi G, Khosla S, Sanyal A, Boyle WJ, Lacey DL, Riggs BL. Role of RANK ligand in mediating increased bone resorption in early postmenopausal women. J Clin Invest. 2003;111(8):1221–30.

87. Nakamura T, Imai Y, Matsumoto T, Sato S, Takeuchi K, Igarashi K, et al. Estrogen Prevents Bone Loss via Estrogen Receptor a and Induction of Fas Ligand in Osteoclasts. Cell. 2007;130(5):811–23.

88. Feng, Xu and McDonald JM. Disorders of Bone Remodeling. 2013;121–45.

89. Schett G, David J. The multiple faces of autoimmune - mediated. Nat Publ Gr [Internet]. 2010;6(12):698–706. Available from: http://dx.doi.org/10.1038/nrendo.2010.190

90. Redlich K, Smolen JS. Inflammatory bone loss : pathogenesis and therapeutic intervention. Nat Publ Gr. 2012;11(March).

91. Odén A, Mccloskey E, Kanis JA, Harvey NC, Johansson H. Burden of high fracture probability worldwide: secular increases 2010–2040. Osteoporos Int. 2015 May 28;26.

92. Christos Th. Vottis, MD, Evanthia Mitsiokapa, MD, Vasilios G. Igoumenou, MD, Panayiotis D. Megaloikonomos, MD, Ioannis P. Galanopoulos, MD, George Georgoudis, PT, Panayiotis Koulouvaris, MD, Panayiotis J. Papagelopoulos, MD, and Andreas F. Mavrogenis M. Fall Risk Assessment Metrics for Elderly Patients With Hip Fractures _ Orthopedics. 2018;41(3):142–56.

93. Healthcare Quality Improvement Partnership. Annual report National hip fracture debate. 2019;

94. Park H. The impact of osteoporosis on health-related quality of life in elderly women . Biomed Res. 2018;29(16):3223–7.

95. Franklin D. Shuler, MD, PhD; Jacob Conjeski M, David Kendall, MA; Jonathon Salava M. Understanding the Burden of Osteoporosis and Use of the World Health Organization FRAX. Orthop. 2012;35(9):798–806.

96. Pouresmaeili F, Kamalidehghan B, Kamarehei M, Goh YM. A comprehensive overview on osteoporosis and its risk factors. Ther Clin Risk Manag. 2018;2029–49.

97. Turner CH, Robling AG. Designing Exercise Regimens to Increase Bone Strength. Exerc Sport Sci Rev. 2003;31(1):45–50.

98. Migliaccio S, Brama M, Spera G. The differential effects of bisphosphonates, SERMS (selective estrogen receptor modulators), and parathyroid hormone on bone remodeling in osteoporosis. Clin Interv Aging. 2007;2(1):55–64.

99. Serrano AJ, Begoña L, Anitua E, Cobos R, Orive G. Systematic review and meta-analysis of the efficacy and safety of alendronate and zoledronate for the treatment of postmenopausal osteoporosis. Gynecol Endocrinol. 2013;29(12):1005–14.

100. Seeman E. Reduced bone formation and increased bone resorption : rational targets for the treatment of osteoporosis. Osteoporos Int. 2003;14(3):2–9.

101. Coxon FP, Thompson K, Roelofs AJ, Ebetino FH, Rogers MJ. Visualizing mineral binding and uptake of bisphosphonate by osteoclasts and non-resorbing cells. Bone. 2008;42(5):848–60.

102. Rogers MJ. New Insights Into the Molecular Mechanisms of Action of Bisphosphonates. 2003;9(32):2643–58.

103. Riggs BL, Hartmann LC. Selective Estrogen-Receptor Modulators — Mechanisms of Action. N Engl J Med. 2003;348(12):618–29.

104. Taranta A, Brama M, Teti A, Luca VDE, Scandurra R, Spera G, et al. The Selective Estrogen Receptor Modulator Raloxifene Regulates Osteoclast and Osteoblast Activity In Vitro. Bone. 2002;30(2):368–76.

105. Gianni W, Ricci A, Gazzaniga P, Brama M, Pietropaolo M, Agliano AM, et al. Raloxifene Modulates Interleukin-6 and Tumor Necrosis Factor- ⎵ Synthesis in Vivo : Results from a Pilot Clinical Study. J Clin Endocrinol Metab. 2004;89(12):6097–9.

106. DAVID W. DEMPSTER, FELICIA COSMAN, ETAH S. KURLAND, HUA ZHOU, JERI NIEVES, LILLIAN WOELFERT, ELIZABETH SHANE, KATARINA PLAVETIC´, RALPH MU¨LLER, JOHN BILEZIKIAN and RL. Effects of Daily Treatment with Parathyroid Hormone on Bone Microarchitecture and Turnover in Patients with Osteoporosis_ A Paired Biopsy Study_. J BONE Miner Res. 2001;16(10):1846–53.

107. Massachusetts F, Hospital G, Aires B, Gairdner SC, Lilly E, Brull PUL, et al. EFFECT OF PARATHYROID HORMONE (1-34) ON FRACTURES AND BONE MINERAL DENSITY IN POSTMENOPAUSAL WOMEN WITH OSTEOPOROSIS. N Engl J Med. 2001;344(19):1434–41.

108. Brixen KT, Christensen PM, Ejersted C, Langdahl BL. Teriparatide (Biosynthetic

Human Parathyroid Hormone 1 – 34): A New Paradigm in the Treatment of Osteoporosis. Basic Clin Pharmacol Toxicol. 2004;94:260–70.

109. Cosman F, Lindsay R. Therapeutic Potential of Parathyroid Hormone. Curr Osteoporos Rep. 2004;2:5–11.

110. Ettinger B, Martin JS, Crans G, Pavo I. Differential Effects of Teriparatide on BMD After Treatment With Raloxifene or Alendronate. J BONE Miner Res. 2004;19(5):745–51.

111. COSMAN, F.; NIEVES, J.; WOELFERT, L. ; FORMICA, C.; GORDON, S.; SHEN, V. and LINDSAY R. Parathyroid Hormone Added to Established Hormone Therapy_ Effects on Vertebral Fracture and Maintenance of Bone Mass After Parathyroid Hormone Withdrawal. J BONE Miner Res. 2001;16(5):925–31.

112. Stuart M, Waite R, Li X, Zhu H. Effects of sclerostin antibodies in animal models of osteoporosis. Bone [Internet]. 2017;96:63–75. Available from: http://dx.doi.org/10.1016/j.bone.2016.10.019

113. Mcclung MR. Romosozumab for the treatment of osteoporosis. Osteoporos Sarcopenia [Internet]. 2018;4(1):11–5. Available from: https://doi.org/10.1016/j.afos.2018.03.002

114. Joshua N Farr, Daniel G Fraser, Haitao Wang, Katharina Jaehn, Mikolaj B Ogrodnik, Megan M Weivoda, Matthew T Drake, Tamara Tchkonia, Nathan K LeBrasseur, James L Kirkland, Lynda F Bonewald, Robert J Pignolo, David G Monroe and SK. Identification of Senescent Cells in the BoneMicroenvironment. JBMR [Internet]. 2016 [cited 2021 Apr 30];6:1920–9. Available from: https://www.nice.org.uk/guidance/indevelopment/gid-ta10072/documents

115. Chaplin S. Romosozumab for the treatment of severe osteoporosis. Prescriber. 2020;31(6):27–9.

116. Imel EA, White KE. Pharmacological management of X-linked hypophosphataemia. Br J Clin Pharmacol. 2019;85(6):1188–98.

117. Brauer CA, Coca-perraillon M, Cutler DM, Rosen AB. Incidence and Mortality of Hip Fractures in the United States. JAMA. 2009;302(14):1573–9.

118. Kanis JA, Mccloskey E, Branco J, Brandi M. Goal-directed treatment of osteoporosis in Europe. Osteoporos Int. 2014;25:2533–43.

119. Tu KN, Lie JD, King C, Wan V, Candidate P, Cameron M, et al. Osteoporosis : A Review of Treatment Options Osteoporosis : A Review of Treatment Options. P&T. 2018;43(2):92–104.

120. Reginster J, Ferrari S, Hadji P, Ferrari S. Current challenges in the treatment of osteoporosis : an opportunity for bazedoxifene Review Current challenges in the treatment of osteoporosis : an opportunity for bazedoxifene. CMRO. 2014;30(6):1165–1176.

121. Shoback D, Rosen CJ, Black DM, Cheung AM, Murad H, Eastell R. Pharmacological Management of Osteoporosis in Postmenopausal Women: An Endocrine Society Guideline Update. J Clin Endocrinol Metab. 2020;105(3):587–94.

122. Baker PN, Salar O, Ollivere BJ, Forward DP, Weerasuriya N, Moppett IK, et al. Evolution of the hip fracture population : time to consider the future ? A retrospective observational analysis. BMJ Open. 2014;4(e004405):1–8.

123. Matthijnssens J, Ciarlet M, Rahman M, Attoui H, Estes MK, Gentsch JR, et al. Redox-based regulation of signal transduction: principles, pitfalls, and promises. Free Radic Biol Med. 2009;153(8):1621–9.

124. Burkle A. Mechanisms of ageing. Eye. 2001;15:371–5.

125. Przybilla J, Rohlf T, Loeffler M, Galle J. Understanding epigenetic changes in aging stem cells - a computational model approach. Aging Cell. 2014;13(2):320–8.

126. Hayflick, L and Moorhead P. THE SERIAL CULTIVATION OF HUMAN DIPLOID CELL STRAINS. Exp Cell Res. 1961;25:585–621.

127. Strasser A, Cory S, Adams JM. Deciphering the rules of programmed cell death to improve therapy of cancer and other diseases. EMBO J. 2011;30(18):3667–83.

128. Coller HA. What's taking so long? S-phase entry from quiescence versus proliferation. Mol cell Biol. 2007;8(August):667–70.

129. Ferbeyre G, De Stanchina E, Querido E, Baptiste N, Prives C, Lowe SW. PML is induced

by oncogenic ras and promotes premature senescence. Genes Dev. 2000;14(16):2015–27.

130. Narita M, Nũnez S, Heard E, Narita M, Lin AW, Hearn SA, et al. Rb-mediated heterochromatin formation and silencing of E2F target genes during cellular senescence. Cell. 2003;113(6):703–16.

131. Lemons JMS, Coller HA, Feng XJ, Bennett BD, Legesse-Miller A, Johnson EL, et al. Quiescent fibroblasts exhibit high metabolic activity. PLoS Biol. 2010;8(10).

132. Liyun S, Hilary A. C, James M. R. Control of the Reversibility of Cellular Quiescence by the Transcriptional Repressor HES1. Science (80-). 2008;321:1095–100.

133. Narita M, Young ARJ, Arakawa S, Samarajiwa SA, Nakashima T, Yoshida S, et al. Spatial Coupling of mTOR and Autophagy Augments Secretory Phenotypes. Science (80-). 2012;332(6032):966–70.

134. Romanov SR, Kozakiewicz BK, Holst CR. Normal human mammary epithelial cells spontaneously escape senescence and acquire genomic changes. Nature. 2001;2262(2000):633–7.

135. Benne R, Tabak HF. Senescence comes of age. Trends Genet. 1986;2(C):147–8.

136. Braig M, Lee S, Loddenkemper C, Rudolph C, Peters AHFM, Schlegelberger B, et al. Oncogene-induced senescence as an initial barrier in lymphoma development. Nature. 2005;436(7051):660–5.

137. Collado M, Gil J, Efeyan A, Guerra C, Schuhmacher AJ, Barradas M, et al. Tumour biology: Senescence in premalignant tumours. Nature. 2005;436(7051):642.

138. Childs BG, Durik M, Baker DJ, Van Deursen JM. Cellular senescence in aging and age-related disease: From mechanisms to therapy. Nat Med. 2015;21(12):1424–35.

139. Ovadya Y, Landsberger T, Leins H, Vadai E, Gal H, Biran A, et al. Impaired immune surveillance accelerates accumulation of senescent cells and aging. Nat Commun [Internet]. 2018;9(1). Available from: http://dx.doi.org/10.1038/s41467-018-07825-3

140. Coppé J-P, Desprez P-Y, Krtolica A, Campisi J. The Senescence-Associated Secretory Phenotype: The Dark Side of Tumor Suppression. Annu Rev Pathol. 2010;8(9):99–118.

141. Nelson G, Wordsworth J, Wang C, Jurk D, Lawless C, Martin-Ruiz C, et al. A senescent cell bystander effect: Senescence-induced senescence. Aging Cell. 2012;11(2):345–9.

142. Boskey AL, Coleman R. Aging and Bone. J Dent Res. 2010;89(12):1333–48.

143. Eastell R, O'Neill TW, Hofbauer LC, Langdahl B, Reid IR, Gold DT, et al. Postmenopausal osteoporosis. Nat Rev Dis Prim [Internet]. 2016;2:1–17. Available from: http://dx.doi.org/10.1038/nrdp.2016.69

144. Cowin SC. Wolff's law of trabecular architecture at remodeling equilibrium. J Biomech Eng. 1986;108(1):83–8.

145. Jee WSS. H. M. Frost's Legacy: The Utah Paradigm of Skeletal Physiology. Niigata J Heal Welf. 2004;6(1):1–9.

146. Sugiyama T, Price JS, Lanyon LE. Functional adaptation to mechanical loading in both cortical and cancellous bone is controlled locally and is confined to the loaded bones. Bone [Internet]. 2010;46(2):314–21. Available from: http://dx.doi.org/10.1016/j.bone.2009.08.054

147. Lanyon LE, Sugiyama T, Price JS. Regulation of bone mass: Local control or systemic influence or both? IBMS Bonekey. 2009;6(6):218–26.

148. Reaction of bone to mechanical stimuli. 1. Continuous and intermittent loading of tibia in rabbit - PubMed [Internet]. [cited 2022 Feb 23]. Available from: https://pubmed.ncbi.nlm.nih.gov/5142775/

149. Meakin LB, Price JS, Lanyon LE. The contribution of experimental in vivo models to understanding the mechanisms of adaptation to mechanical loading in bone. Front Endocrinol (Lausanne). 2014;5(OCT).

150. Saxon LK, Jackson BF, Sugiyama T, Lanyon LE, Price JS. Analysis of multiple bone responses to graded strains above functional levels, and to disuse, in mice in vivo show that the human Lrp5 G171V High Bone Mass mutation increases the osteogenic response to loading but that lack of Lrp5 activity reduces it. Bone [Internet]. 2011 Aug [cited 2022 Feb 24];49(2):184. Available from: /pmc/articles/PMC3121951/

151. Sugiyama T, Meakin LB, Browne WJ, Galea GL, Price JS, Lanyon LE. Bones' adaptive

response to mechanical loading is essentially linear between the low strains associated with disuse and the high strains associated with the lamellar/woven bone transition. J Bone Miner Res. 2012;27(8):1784–93.

152. Kumar G, Narayan B. Regulation of Bone Formation by Applied Dynamic Loads. Class Pap Orthop [Internet]. 2014 Jan 1 [cited 2022 Mar 2];511–3. Available from: https://link.springer.com/chapter/10.1007/978-1-4471-5451-8_134

153. O'Connor JA, Lanyon LE, MacFie H. The influence of strain rate on adaptive bone remodelling. J Biomech. 1982;15(10):767–81.

154. Banaszkiewicz PA, Kader DF. Classic Papers in Orthopaedics (Regulation of Bone Formation by Applied Dynamic Loads). Class Pap Orthop. 2014;511–3.

155. Meakin LB, Price JS, Lanyon LE. The contribution of experimental in vivo models to understanding the mechanisms of adaptation to mechanical loading in bone. Front Endocrinol (Lausanne). 2014;5(OCT):1–13.

156. De Souza, R L and Matsuura, M and Eckstein, F and Rawlinson, S C F and Lanyon, L E and Pitsillides AA. Non-invasive axial loading of mouse tibiae increases cortical bone fori-nation and modifies trabecular organization: A new model to study cortical and cancellous compartments in a single loaded element - RVC Research Online. Bone [Internet]. 2005 [cited 2022 Mar 30];12;37(6):810–8. Available from: https://researchonline.rvc.ac.uk/id/eprint/814/

157. Black-6 lab mice and the history of biomedical research [Internet]. [cited 2022 Jul 3]. Available from: http://www.slate.com/articles/health_and_science/the_mouse_trap/2011/11/black_6_lab_mice_and_the_history_of_biomedical_research.html?via=gdpr-consent

158. Poulet B, Hamilton RW, Shefelbine S, Pitsillides AA. Characterizing a novel and adjustable noninvasive murine joint loading model. Arthritis Rheum [Internet]. 2011 Jan [cited 2020 May 6];63(1):137–47. Available from: http://doi.wiley.com/10.1002/art.27765

159. van 't Hof RJ, Rose L, Bassonga E, Daroszewska A. Open source software for semi-automated histomorphometry of bone resorption and formation parameters. Bone.

2017 Jun 1;99:69–79.

160. Stephens AS, Stephens SR, Morrison NA. Internal control genes for quantitative RT-PCR expression analysis in mouse osteoblasts, osteoclasts and macrophages. BMC Res Notes. 2011 Oct;4:410.

161. Klein-Nulend J, Bacabac RG, Bakker AD. Mechanical loading and how it affects bone cells: The role of the osteocyte cytoskeleton in maintaining our skeleton. Eur Cells Mater. 2012;24:278–91.

162. Mizokami A, Kawakubo-yasukochi T, Hirata M. Osteocalcin and its endocrine functions. Biochem Pharmacol [Internet]. 2017;132:1–8. Available from: http://dx.doi.org/10.1016/j.bcp.2017.02.001

163. Bergwitz C, Hospital MG, Unit N, Hospital MG. HHS Public Access. 2016;91–104.

164. Kini U, Nandeesh BN. Physiology of Bone Formation, Remodeling, and Metabolism. 2012;

165. Hauschka P V., Lian JB, Cole DE, Gundberg CM. Osteocalcin and matrix Gla protein: Vitamin K-dependent proteins in bone. Physiol Rev. 1989;69(3):990–1047.

166. Lacombe J, Karsenty G, Ferron M. In vivo analysis of the contribution of bone resorption to the control of glucose metabolism in mice. Mol Metab [Internet]. 2013;2(4):498–504. Available from: http://dx.doi.org/10.1016/j.molmet.2013.08.004

167. Szulc P. Best Practice & Research Clinical Endocrinology & Metabolism Bone turnover : Biology and assessment tools. Best Pract Res Clin Endocrinol Metab [Internet]. 2018;32(5):725–38. Available from: https://doi.org/10.1016/j.beem.2018.05.003

168. Kanazawa I. Osteocalcin as a hormone regulating glucose metabolism. World J Diabetes. 2015;6(18):1345.

169. Koivula MK, Risteli L, Risteli J. Measurement of aminoterminal propeptide of type I procollagen (PINP) in serum. Vol. 45, Clinical Biochemistry. 2012. p. 920–7.

170. Koivula M, Ruotsalainen V, Nurmenniemi S. Difference between total and intact assays for N-terminal pN-collagen rather than denaturation of intact propeptide. Ann

Clin Biochem. 2010;47(pt 1):67–71.

171. Kuo TR, Chen CH. Bone biomarker for the clinical assessment of osteoporosis: Recent developments and future perspectives. Biomark Res. 2017;5(1):5–13.

172. Rosen HN, Moses AC, Garber J, Iloputaife ID, Ross DS, Lee SL, et al. Serum CTX: A New Marker of Bone Resorption That Shows Treatment Effect More Often Than Other Markers Because of Low Coefficient of Variability and Large Changes with Bisphosphonate Therapy. Calcif Tissue Int [Internet]. 2000;66(2):100–3. Available from: https://doi.org/10.1007/PL00005830

173. Garnero P, Borel O, Byrjalsen I, Ferreras M, Drake FH, McQueney MS, et al. The collagenolytic activity of cathepsin K is unique among mammalian proteinases. J Biol Chem. 1999;273(48):32347–52.

174. Nenonen A, Cheng S, Ivaska KK, Alatalo SL, Lehtimäki T, Schmidt-gayk H, et al. Treatment : Comparison With Other Markers of Bone Turnover. 2005;20(8):1804–12.

175. Wang KX, Wang KX. Osteopontin : Role in immune regulation and stress responses by. 2008;

176. Gericke A, Qin C, Spevak L, Fujimoto Y, Butler WT, Sørensen ES, et al. Importance of Phosphorylation for Osteopontin Regulation of Biomineralization. Calcif Tissue Int [Internet]. 2005;77(1):45–54. Available from: https://doi.org/10.1007/s00223-004-1288-1

177. Poundarik AA, Bailey S, Vashishth D. Structural role of osteocalcin and osteopontin in energy dissipation in bone. J Biomech. 2018;80:45–52.

178. Lund SA, Giachelli CM. The role of osteopontin in inflammatory processes. J Cell Commun Signal. 2009;3(3–4):311–22.

179. Klein-Nulend J, van Oers RFM, Bakker AD, Bacabac RG. Bone cell mechanosensitivity, estrogen deficiency, and osteoporosis. J Biomech [Internet]. 2015;48(5):855–65. Available from: http://dx.doi.org/10.1016/j.jbiomech.2014.12.007

180. Klein-Nulend J, Van Der Plas A, Semeins CM, Ajubi NE, Erangos JA, Nijweide PJ, et al. Sensitivity of osteocytes to biomechanical stress in vitro. FASEB J. 1995;9(5):441–5.

181. Lock CA, Lecouturier J, Mason JM, Dickinson HO. Lifestyle interventions to prevent osteoporotic fractures: a systematic review. Osteoporos Int [Internet]. 2006;17(1):20–8. Available from: https://doi.org/10.1007/s00198-005-1942-0

182. Shao J, Zhou S, Qu Y, Liang B, Yu Q, Wu J. Correlation between bone turnover and metabolic markers with age and gender : a cross-sectional study of hospital information system data. 2020;1–10.

183. Yoo J, Park A, Lim YK, Kweon OJ, Choi J, Do JH, et al. Age-related Reference Intervals for Total Collagen-I- N-terminal Propeptide in Healthy Korean Population. JBM. 2018;25(4):235–41.

184. Confavreux CB, Szulc P, Casey R, Varennes A, Goudable J, Chapurlat RD. Lower serum osteocalcin is associated with more severe metabolic syndrome in elderly men from the MINOS cohort. Eur J Endocrinol. 2014;171(2):275–83.

185. Silva MJ, Brodt MD, Lynch MA, Stephens AL, Wood DJ, Civitelli R. Tibial Loading Increases Osteogenic Gene Expression and Cortical Bone Volume in Mature and Middle-Aged Mice. 2012;i(4):1–10.

186. Qvist P, Christgau S, Pedersen BJ, Schlemmer A, Christiansen C. Circadian variation in the serum concentration of C-terminal telopeptide of type I collagen (serum CTx): Effects of gender, age, menopausal status, posture, daylight, serum cortisol, and fasting. Bone [Internet]. 2002;31(1):57–61. Available from: http://dx.doi.org/10.1016/S8756-3282(02)00791-3

187. Meakin LB, Udeh C, Galea GL, Lanyon LE, Price JS. Exercise does not enhance aged bone's impaired response to artificial loading in C57Bl/6 mice. Bone [Internet]. 2015;81:47–52. Available from: http://dx.doi.org/10.1016/j.bone.2015.06.026

188. Leupin O, Piters E, Halleux C, Hu S, Kramer I, Morvan F, et al. Bone overgrowth-associated mutations in the LRP4 gene impair sclerostin facilitator function. J Biol Chem [Internet]. 2011;286(22):19489–500. Available from: http://dx.doi.org/10.1074/jbc.M110.190330

189. Robling AG, Niziolek PJ, Baldridge LA, Condon KW, Allen MR, Alam I, et al. Mechanical stimulation of bone in vivo reduces osteocyte expression of Sost/sclerostin. J Biol

Chem [Internet]. 2008;283(9):5866–75. Available from: http://dx.doi.org/10.1074/jbc.M705092200

190. Bonnet N, Standley KN, Bianchi EN, Stadelmann V, Foti M, Conway SJ, et al. The matricellular protein periostin is required for sost inhibition and the anabolic response to mechanical loading and physical activity. J Biol Chem [Internet]. 2009;284(51):35939–50. Available from: http://dx.doi.org/10.1074/jbc.M109.060335

191. Callewaert F, Bakker A, Schrooten J, Van Meerbeek B, Verhoeven G, Boonen S, et al. Androgen receptor disruption increases the osteogenic response to mechanical loading in male mice. J Bone Miner Res. 2010;25(1):124–31.

192. Tu X, Rhee Y, Condon KW, Bivi N, Allen MR, Dwyer D, et al. Sost downregulation and local Wnt signaling are required for the osteogenic response to mechanical loading. Bone [Internet]. 2012;50(1):209–17. Available from: http://dx.doi.org/10.1016/j.bone.2011.10.025

193. Moustafa A, Sugiyama T, Prasad J, Zaman G, Gross TS, Lanyon LE, et al. Mechanical loading-related changes in osteocyte sclerostin expression in mice are more closely associated with the subsequent osteogenic response than the peak strains engendered. Osteoporos Int. 2012;23(4):1225–34.

194. William Lau KH, Baylink DJ, Zhou XD, Rodriguez D, Bonewald LF, Li Z, et al. Osteocyte-derived insulin-like growth factor I is essential for determining bone mechanosensitivity. Am J Physiol - Endocrinol Metab. 2013;305(2):271–81.

195. Meakin LB, Galea GL, Sugiyama T, Lanyon LE, Price JS. Age-related impairment of bones' adaptive response to loading in mice is associated with sex-related deficiencies in osteoblasts but no change in osteocytes. J Bone Miner Res. 2014;29(8):1859–71.

196. Sinnesael M, Laurent MR, Jardi F, Dubois V, Deboel L, Delisser P, et al. Androgens inhibit the osteogenic response to mechanical loading in adult male mice. Endocrinology. 2015;156(4):1343–53.

197. Galea GL, Lanyon LE, Price JS. Sclerostin ' s role in bone ' s adaptive response to mechanical loading. Bone [Internet]. 2017;96:38–44. Available from:

http://dx.doi.org/10.1016/j.bone.2016.10.008

198. Morse A, McDonald MM, Kelly NH, Melville KM, Schindeler A, Kramer I, et al. Mechanical load increases in bone formation via a Sclerostin-independent pathway. J Bone Miner Res. 2014 Nov 1;29(11):2456–67.

199. Ciarelli MJ, Goldstein SA, Kuhn JL, Cody DD, Brown MB. Evaluation of orthogonal mechanical properties and density of human trabecular bone from the major metaphyseal regions with materials testing and computed tomography. J Orthop Res. 1991;9(5):674–82.

200. Sophocleous A, Huesa C. Osteoarthritis mouse model of destabilization of the medial meniscus. Vol. 1914, Methods in Molecular Biology. 2019. 281–293 p.

201. Uchihashi K, Aoki S, Matsunobu A, Toda S. Osteoblast migration into type I collagen gel and differentiation to osteocyte-like cells within a self-produced mineralized matrix: A novel system for analyzing differentiation from osteoblast to osteocyte. Bone [Internet]. 2013;52(1):102–10. Available from: http://dx.doi.org/10.1016/j.bone.2012.09.001

202. Burger EH, Klein-Nulend J. Mechanotransduction in bone—role of the lacunocanalicular network. FASEB J. 1999;13:s101–12.

203. Bonewald LF, Johnson ML. Osteocytes , mechanosensing and Wnt signaling. Bone. 2008;42:606–15.

204. Miyauchi A, Notoya K, Mikuni-Takagaki Y, Takagi Y, Goto M, Miki Y, et al. Parathyroid hormone-activated volume-sensitive calcium influx pathways in mechanically loaded osteocytes. J Biol Chem [Internet]. 2000;275(5):3335–42. Available from: http://dx.doi.org/10.1074/jbc.275.5.3335

205. Hirose S, Li M, Kojima T, De Freitas PHL, Ubaidus S, Oda K, et al. A histological assessment on the distribution of the osteocytic lacunar canalicular system using silver staining. J Bone Miner Metab. 2007;25(6):374–82.

206. Sugawara Y, Kamioka H, Honjo T, Tezuka KI, Takano-Yamamoto T. Three-dimensional reconstruction of chick calvarial osteocytes and their cell processes using confocal

microscopy. Bone. 2005;36(5):877–83.

207. van Hove RP, Nolte PA, Vatsa A, Semeins CM, Salmon PL, Smit TH, et al. Osteocyte morphology in human tibiae of different bone pathologies with different bone mineral density - Is there a role for mechanosensing? Bone [Internet]. 2009;45(2):321–9. Available from: http://dx.doi.org/10.1016/j.bone.2009.04.238

208. Boyde A, Jones SJ. Scanning electron microscopy of bone: Instrument, specimen, and issues. Microsc Res Tech. 1996;33(2):92–120.

209. Okada S, Yoshida S, Ashrafi SH, Schraufnagel DE. The canalicular structure of compact bone in the rat at different ages. Microsc Microanal. 2002;8(2):104–15.

210. Rubin MA, Rubin J, Jasiuk I. SEM and TEM study of the hierarchical structure of C57BL/6J and C3H/HeJ mice trabecular bone. Bone. 2004;35(1):11–20.

211. You LD, Weinbaum S, Cowin SC, Schaffler MB. Ultrastructure of the osteocyte process and its pericellular matrix. Anat Rec - Part A Discov Mol Cell Evol Biol. 2004;278(2):505–13.

212. Veverka V, Henry AJ, Slocombe PM, Ventom A, Mulloy B, Muskett FW, et al. Characterization of the structural features and interactions of sclerostin. Molecular insight into a key regulator of Wnt-mediated bone formation. J Biol Chem [Internet]. 2009;284(16):10890–900. Available from: http://dx.doi.org/10.1074/jbc.M807994200

213. Murshed M. Mechanism of Bone Mineralization. 2018 [cited 2022 Mar 30];8:1–11. Available from: www.perspectivesinmedicine.org

214. Hagan ML, Yu K, Zhu J, Vinson BN, Roberts RL, Montesinos Cartagena M, et al. Decreased pericellular matrix production and selection for enhanced cell membrane repair may impair osteocyte responses to mechanical loading in the aging skeleton. Aging Cell. 2020;19(1):1–15.

215. Knothe Tate ML, Adamson JR, Tami AE, Bauer TW. The osteocyte. Int J Biochem Cell Biol. 2004;36(1):1–8.

216. Tiede-Lewis LM, Hulbert MA, Campos R, Dallas MR, Bonewald LF, Dallas SL. Degeneration of the osteocyte network in the C57Bl/6 mouse model of aging. Aging

(Albany NY). 2017;9(10):2190–208.

217. Yao W, Dai W, Jiang JX, Lane NE. Glucocorticoids and osteocyte autophagy. Bone [Internet]. 2013;54(2):279–84. Available from: http://dx.doi.org/10.1016/j.bone.2013.01.034

218. Kobayashi K, Nojiri H, Saita Y, Morikawa D, Ozawa Y, Watanabe K, et al. Mitochondrial superoxide in osteocytes perturbs canalicular networks in the setting of age-related osteoporosis. Sci Rep. 2015 Mar 16;5.

219. Farr JN, Fraser DG, Wang H, Jaehn K, Ogrodnik MB, Weivoda MM, et al. Identification of Senescent Cells in the Bone Microenvironment. J Bone Miner Res. 2016;31(11):1920–9.

220. Tatsumi S, Ishii K, Amizuka N, Li M, Kobayashi T, Kohno K, et al. Article Targeted Ablation of Osteocytes Induces Osteoporosis with Defective Mechanotransduction. 2007;

221. Xiong J, Onal M, Jilka RL, Weinstein RS, Manolagas SC, Brien CAO. articles Matrix-embedded cells control osteoclast formation. Nat Med. 2011;i(10):1235–42.

222. Javaheri B, Pitsillides AA. Aging and Mechanoadaptive Responsiveness of Bone. 2019;560–9.

223. Holguin N, Brodt MD, Sanchez ME, Silva MJ. Aging diminishes lamellar and woven bone formation induced by tibial compression in adult C57BL / 6 ☆. Bone [Internet]. 2014;65:83–91. Available from: http://dx.doi.org/10.1016/j.bone.2014.05.006

224. Wang Z, Gerstein M, Snyder M. RNA-Seq: a revolutionary tool for transcriptomics. Nat Rev Genet. 2009;10(1):57–63.

225. Kukurba KR, Montgomery SB. RNA sequencing and analysis. Cold Spring Harb Protoc. 2015;2015(11):951–69.

226. Love MI, Huber W, Anders S. Moderated estimation of fold change and dispersion for RNA-seq data with DESeq2. Genome Biol. 2014;15(12):1–21.

227. Van der Flier A, Sonnenberg A. Structural and functional aspects of filamins. Biochim

Biophys Acta - Mol Cell Res. 2001 Apr 23;1538(2–3):99–117.

228. Bittermann E, Liegel RP, Menke C, Timms A, Beier DR, Kline-Fath B, et al. Differential requirements of tubulin genes in mammalian forebrain development. bioRxiv. 2018;1–28.

229. Zhang A, Yeung PL, Li C, Tsai S, Dinh GK, Wu X, et al. Identification of a Novel Family of Ankyrin Repeats Containing Cofactors for p160 Nuclear Receptor Coactivators *. 2004;279(32):33799–805.

230. Arumugam K, Shin W, Schiavone V, Vlahos L, Tu X, Carnevali D, et al. The Master Regulator protein BAZ2B can reprogram human hematopoietic lineage-committed progenitors into a multipotent state. Cell Rep. 2020;33(10):1–48.

231. Solomon LA, Li JR, Bérubé NG, Beier F. Loss of ATRX in Chondrocytes Has Minimal Effects on Skeletal Development. PLoS One [Internet]. 2009 Sep 23 [cited 2022 Mar 30];4(9):e7106. Available from: https://journals.plos.org/plosone/article?id=10.1371/journal.pone.0007106

232. Guo Y, Wang M, Zhang S, Wu Y, Zhou C, Zheng R, et al. Ubiquitin-specific protease USP 34 controls osteogenic differentiation and bone formation by regulating BMP 2 signaling . EMBO J. 2018 Oct 15;37(20).

233. Li Q, Wang M, Xue H, Liu W, Guo Y, Xu R, et al. Ubiquitin-Specific Protease 34 Inhibits Osteoclast Differentiation by Regulating NF-κB Signaling. 2020;

234. Furushima K, Yamamoto A, Nagano T, Shibata M, Miyachi H, Abe T, et al. Mouse homologues of Shisa antagonistic to Wnt and Fgf signalings. Dev Biol. 2007 Jun 15;306(2):480–92.

235. Murakami K, Zhifeng H, Suzuki T, Kobayashi Y, Nakamura Y. The Shisa3 knockout mouse exhibits normal bone phenotype. J Bone Miner Metab. 2019 Nov 1;37(6):967–75.

236. Ciumas M, Eyries M, Poirier O, Maugenre S, Dierick F, Gambaryan N, et al. Bone morphogenetic proteins protect pulmonary microvascular endothelial cells from apoptosis by upregulating α-b-crystallin. Arterioscler Thromb Vasc Biol.

2013;33(11):2577–84.

237. Javaheri B, Pitsillides AA. Aging and Mechanoadaptive Responsiveness of Bone. Curr Osteoporos Rep. 2019;17(6):560–9.

238. Gimeno EJ. Epidemiology of osteoporotic fractures. Mortality and morbidity. Rev Osteoporos Metab Min. 2010;2:5–9.

239. Burr DB. Changes in bone matrix properties with aging. Bone [Internet]. 2019;120(September 2018):85–93. Available from: https://doi.org/10.1016/j.bone.2018.10.010